

UNIVERSITY OF WARMIA AND MAZURY IN OLSZTYN

# Technical Sciences

21(2) 2018



PUBLISHER UWM

## Editorial Board

Ceslovas Aksamitauskas (Vilnius Gediminas Technical University, Lithuania), Olivier Bock (Institut National de L'Information Géographique et Forestière, France), Stefan Cenkowski (University of Manitoba, Canada), Adam Chrzanowski (University of New Brunswick, Canada), Davide Ciucci (University of Milan-Bicocca, Italy), Sakamon Devahastin (King Mongkut's University of Technology Thonburi in Bangkok, Thailand), German Efremov (Moscow Open State University, Russia), Mariusz Figurski (Military University of Technology, Poland), Maorong Ge (Helmholtz-Zentrum Potsdam Deutsches GeoForschungsZentrum, Germany), Dorota Grejner-Brzezinska (The Ohio State University, USA), Janusz Laskowski (University of Life Sciences in Lublin, Poland), Arnold Norkus (Vilnius Gediminas Technical University, Lithuania), Stanisław Pabis (Warsaw University of Life Sciences-SGGW, Poland), Lech Tadeusz Polkowski (Polish-Japanese Institute of Information Technology, Poland), Arris Tijsseling (Technische Universiteit Eindhoven, Netherlands), Vladimir Tilipalov (Kaliningrad State Technical University, Russia), Alojzy Wasilewski (Koszalin University of Technology, Poland)

## Editorial Committee

Marek Markowski (Editor-in-Chief), Piotr Artiemjew, Kamil Kowalczyk, Wojciech Sobieski, Piotr Srokosz, Magdalena Zielińska (Assistant Editor), Marcin Zieliński

## Features Editors

Piotr Artiemjew (Information Technology), Marcin Dębowski (Environmental Engineering), Zdzisław Kaliniewicz (Biosystems Engineering), Grzegorz Królczyk (Materials Engineering), Marek Mróz (Geodesy and Cartography), Ryszard Myhan (Safety Engineering), Wojciech Sobieski (Mechanical Engineering), Piotr Srokosz (Civil Engineering), Jędrzej Trajer (Production Engineering)

## Statistical Editor

Paweł Drozda

## Executive Editor

Mariola Jezierska

The Technical Sciences is indexed and abstracted in BazTech (<http://baztech.icm.edu.pl>) and in IC Journal Master List (<http://journals.indexcopernicus.com>)

The Journal is available in electronic form on the web sites  
<http://www.uwm.edu.pl/techsci> (subpage Issues)  
<http://wydawnictwo.uwm.edu.pl> (subpage Czytelnia)

The electronic edition is the primary version of the Journal

PL ISSN 1505-4675

e-ISSN 2083-4527

© Copyright by Wydawnictwo UWM • Olsztyn 2018

### Address

ul. Jana Heweliusza 14  
10-718 Olsztyn-Kortowo, Poland  
tel.: +48 89 523 36 61  
fax: +48 89 523 34 38  
e-mail: [wydawca@uwm.edu.pl](mailto:wydawca@uwm.edu.pl)

---

Ark. wyd. 6,7, ark. druk. 5,75, nakład 85 egz.  
Druk – Zakład Poligraficzny UWM  
zam. 327

## Contents

O.S. SHTYKA, Ł. PRZYBYSZ, M. BŁASZCZYK, J. P. SĘK – <i>Analysis of Process of Emulsions Transport in Hydrophilic/Oleophilic Granular Porous Media Driven By Capillary Force</i> .....	85
K. TKACZ, A. WIEK, R. ŻYWICA, J. K. BANACH – <i>The Effects of Beef Carcasses High Voltage Electrical Stimulation and Roasting Methods on Tenderness and Water Retention of Beef</i> .....	103
G. PEŁKA, W. LUBOŃ, D. MALIK – <i>An Analysis of the Power Demand and Electricity Consumption of Automatic Pellet Boiler</i> .....	117
N. KORCZ, E. URBAŃSKA-GALEWSKA <i>Influence of Fasteners and Connections Flexibility on Deflections of Steel Building Including the Stressed Skin Effect</i> .....	131
K. KALINOWSKA-WICHROWSKA – <i>The Use of Fine Waste Material for the Future of Sustainable Construction</i> .....	149
<span style="border: 1px solid black; padding: 2px;">O. YUSHCHYK</span> , B. HAVRYSH, OLEKSANDR TYMCHENKO, K. SZTURO – <i>Design of Modern Tools for Digital Output Raster Scanning</i> .....	157





Quarterly peer-reviewed scientific journal

ISSN 1505-4675  
e-ISSN 2083-4527

**TECHNICAL SCIENCES**

Homepage: [www.uwm.edu.pl/techsci/](http://www.uwm.edu.pl/techsci/)



## ANALYSIS OF PROCESS OF EMULSIONS TRANSPORT IN HYDROPHILIC/OLEOPHILIC GRANULAR POROUS MEDIA DRIVEN BY CAPILLARY FORCE

*Olga S. Shtyka, Łukasz Przybysz,  
Mariola Błaszczuk, Jerzy P. Sęk*

Faculty of Process and Environmental Engineering,  
Lodz University of Technology

Received 1 June 2016; accepted 15 March 2017; available online 22 March 2018.

**Key word:** emulsion, viscosity, imbibition, granular medium, kinetics, concentration.

### Abstract

The research focuses on the issues concerning a process of multiphase liquids transport in granular porous media driven by the capillary pressure. The current publication is meant to introduce the results of experimental research conducted to evaluate the kinetics of imbibition and emulsions behavior inside the porous structures. Moreover, the influence of dispersed phase concentration and granular media structure on the mentioned process was considered. The medium imbibition with emulsifier-stabilized emulsions composed of oil as the dispersed phase in concentrations of 10 vol%, 30 vol%, and 50 vol%, was investigated. The porous media consisted of oleophilic/hydrophilic beads with a fraction of 200–300 and 600–800  $\mu\text{m}$ . The experimental results provided that the emulsions imbibition in such media depended strong on its structure compare to single-phase liquids. The increase of the dispersed phase concentration caused an insignificant mass decreasing of the imbibed emulsions and height of its penetration in a sorptive medium. The concentrations of the imbibed dispersions exceeded their initial values, but reduced with permeants front raise in the granular structures that can be defined as the influential factor for wicking process kinetics.

### Symbols

- $A_s$  – cross-section area of a porous medium,  $\text{m}^2$ ,  
 $D_f$  – pore fractal dimension, –,  
 $d_b$  – average diameter of beads in a granular medium, m,  
 $d_t$  – diameter of a tube, m,  
 $f_n$  – fragment of a porous medium, m,

Correspondence: Olga Shtyka, Wydział Inżynierii Procesowej i Ochrony Środowiska, Politechnika Łódzka, ul. Wólczańska 213, A6, 90-924 Łódź, phone: (42) 631-39-75, e-mail: [olga.shtyka@gmail.com](mailto:olga.shtyka@gmail.com)

- $h_c$  – height of a liquid front in a capillary, m,  
 $h_{im}$  – imbibed liquid height, m,  
 $h_m$  – height of a porous medium, m,  
 $h_{max}$  – maximal height of an imbibed liquid, m,  
 $m_{im}$  – imbibed liquid mass, kg,  
 $L_s$  – distance in the flow direction, m,  
 $K$  – proportionality coefficient,  $m^2$ ,  
 $k_{kc}$  – Kozerny constant, –,  
 $r_{av}$  – average pore radius of the investigated porous medium, m,  
 $r_c$  – radius of a capillary, m,  
 $r_h$  – hydraulic radius, m,  
 $r_{max}$  – maximum pore radius, m,  
 $r_p$  – radius of pore, m,  
 $S_{in}$  – initial saturation, –,  
 $S_{im}$  – medium saturation after imbibition, –,  
 $t_{im}$  – time of imbibition, s,  
 $\varphi_d$  – initial dispersed phase concentration, vol%,  
 $\varphi_{im}$  – dispersed phase concentration of an imbibed emulsion, vol%,  
 $\varepsilon$  – porosity of a medium, –,  
 $\rho$  – density of a wetting liquid,  $kg/m^3$ ,  
 $\delta$  – pore shape parameters, –,  
 $\eta$  – viscosity of permeant, Pa·s, –,  
 $\sigma$  – surface tension, N/m,  
 $\theta$  – contact angle between a penetrating liquid surface and pore surface,  $0^\circ$ ,  
 $\psi$  – angle formed between an inclined tube and free liquid surface,  $0^\circ$ ,  
 $\lambda_e$  – average length of a permeant path, m,  
 $\tau$  – tortuosity of the pores in a medium, –,  
 HLB – hydrophilic-lipophilic balance.

## Introduction

A porous medium consists of a matrix as skeletal portion and an interconnected or unconnected network of capillary channels, which are usually characterized by an irregular shape, the different size and structural organization. One type of porous structures is the granular media, which can be characterized with the different porosities, dimension and shape of particles (KOWALSKI 2004, STRZELECKI et al. 2008, MASOODI, PILLAI 2010). The representatives of such media can be the void systems of soil, sands and sandstones, sorbent composed of silica gel, concrete specimen composed of vermiculite, etc. (CHATTERJEE, GUPTA 2002, MASOODI, PILLAI 2010, CARBAJO et al. 2015). Over the last decades, a lot of researches have focused on the liquids flow through porous structures. The process of liquids transport driven by the capillary pressure and balanced by viscous drag force and gravity acceleration, is known in literature as the spontaneous imbibition or wicking (KOWALSKI 2004, MASOODI et al. 2007, MASOODI, PILLAI 2010). The suction pressure derives as a result of pore walls wetting with a permeant due to interchanging of their surface energies. The imbibition

occurs in case when an adhesion predominates a mutual force of attraction between molecules in a permeating liquid (CHATTERJEE et al. 2002, MASOODI et al. 2007, MASOODI, PILLAI 2010).

The prediction of the imbibition process in porous media is of the practical importance thanks to its relevance as a fundamental phenomenon in numerous industrial technologies and nature. Presently, there has been a continuous discussion concerning the single-phase liquids wicking in the different porous media and its mechanisms (SIEBOLD et al. 2000, ZHMUD et al. 2000, HAMRAOUI, NYLANDER 2002, XUE et al. 2006, MASOODI et al. 2007, MASOODI, PILLAI 2010).

The equation firstly suggested the analytical explanation of a liquid rise in the capillary is known as the Lucas–Washburn equation, but its relevance is extended to describe a process of the porous media imbibition. However, the model application for such a reason has a set of limitations connected with disregard of the influential factors (ZHMUD et al. 2000, FRIES et al. 2008, MAGGI et al. 2012). On the other hand, there are the numerous efforts to modified the mentioned equation due to capturing the constitutive issues such as a mean pore radius (HAMRAOUI, NYLANDER 2002, BENAVENTE et al. 2002, MASOODI et al. 2007), tortuosity and shape of pores (BENAVENTE et al. 2002, YU 2008, ZHAO, LI 2009, CAI et al. 2012, 2014), changes of contact angle (HAMRAOUI, NYLANDER 2002, SIEBOLD et al. 2000, CHEBBI 2007, DIGILOV 2008), roughness of pores wall (MARTIC 2003, LIU 2014), surface tension (HAMRAOUI, NYLANDER 2002), and a permeant viscosity (SIEBOLD et al. 2000, XUE et al. 2006, DIGILOV 2008).

The influence of the dynamic contact angle was studied in the work of SIEBOLD et al. (2000) by means of model experiments with capillary rise of the organic single-phase liquids in a glass cylinder tube and in columns filled with powders.

The experiments concerning water and ethanol rise in the vertical glass capillaries differed with a radius (0.4–1 mm) was performed and analysed in the publication of HAMRAOUI and NYLANDER (2002). The obtained results allowed to represent a model, which considered the energy dissipation caused mainly by gravity and surface tension during a liquid rise. To account these influential factors, the introduction of a retardation coefficient was proposed (HAMRAOUI, NYLANDER 2002).

Another model for description of the single-phase liquid penetration rising in a capillary considered the hydrostatic effects (XUE et al. 2006). The short-time and long-time analytical solutions for the dynamics of a fluid penetration in a capillary was also discussed (CHEBBI 2007). MASOODI et al. (2007) compared the adequacy of capillary and energy balance models with Washburn equation using independently measured parameters. The effect of a permeant viscosity and dynamic contact angle on the liquid rise dynamics in a vertical capillary was investigated experimentally and debated in the work of DIGILOV (2008). To conclude, a majority of the reviewed previously models considered mostly interaction on the border of solid-liquid and gas-liquid phases.

The model initially based of LWE and modified by the correction factors relating to porous media structure such as the pore shape, i.e. roundness, its effective radius, and tortuosity was used to predict the weight rate (BENAVENTE et al. 2002). There is another approach related to the spontaneous imbibition of a wetting permeant into gas-saturated porous media consisting of a complex structure of pores based on their fractal geometry (YU 2008, ZHAO, LI 2009, CAI et al. 2012, 2014). The mentioned models allowed to characterize the imbibition process in a variety of the porous media, i.e. rocks, soil, fibrous material and bio-structures, etc. (BENAVENTE et al. 2002, YU 2008, ZHAO, LI 2009, CAI et al. 2012, 2014).

To conclude spontaneous imbibition in porous media is a complex physical process, which depends on numerous parameters and in the recent publications there is a great deal of the mathematical models to predict this phenomenon. However, the issue regarding the porous structure imbibition with liquids composed with several phases has not yet been fully investigated experimentally and described by theoretical models.

Thus, the present work focuses on a study of the kinetics of granular structures imbibition with two-phase liquids such as oil-in-water emulsions. In the current publication, there is a discussion of the hypothesis that the porous media imbibition with the multiphase permeants differs considerably from the process with single-phase liquids, and its validation using the obtained experimental results. Such a deviation can relate to the obstruction of penetration path by the dispersed phase. The dependence of imbibition rate on the emulsions properties, i.e. the fractional composition, viscosity, and structure of the granular porous media was also currently considered.

## Materials and methods

In these experiments, the object of investigation was a granular medium consisting of spherical hydrophilic/oleophilic grains. The beads were produced and obtained from “Alumetal-Technik” (Lodz, Poland). The porous structures differed by a size of the particles diameter, which was in a range of 200–300 and 600–800  $\mu\text{m}$ . The bulk density was equal to  $1621 \pm 5.2$  and  $1728 \pm 1.2$   $\text{kg/m}^3$ . The porosity of prepared media was  $0.36 \pm 0.011$  and  $0.37 \pm 0.013$ , respectively.

The wicking liquids were oil, distilled water and their stabilized emulsions with the different dispersed phase concentrations, i.e. 10 vol%, 30 vol%, and 50 vol%. The oil-in-water emulsions were prepared by means of mechanical stirring during 600 s. The vegetable oil was produced by EOL Polska Sp. z o.o., Poland. The used non-ionic emulsifier was Rokacet O7 (PCC Exol SA, Poland) composed of ethoxylated oleic acid. The fraction of the emulsifier equalled 2 vol%. The emulsions components properties are given in Table 1.

Table 1

Physicochemical characteristics of the basic liquids ( $T=23\pm 1^\circ\text{C}$ )

Component	Viscosity [mPa·s]	Surface tension [mN/m]	Density [kg/m <sup>3</sup> ]	HLB* [-]	Contact angle [degs]
Dispersed phase	53.2±0.4	32 ±1.7	922±1.6	–	22.4±2.1
Emulsifier	50.2±0.6	36 ±1.8	908±2.7	10.6	24.3±2.7

\* HLB – hydrophilic-lipophilic balance

The density of liquids was measured using the pycnometric method. The prepared dispersions differed from each other by density, thus, for 10% emulsion it was  $990.1\pm 1.31\text{ kg/m}^3$ , in case of 30% one, it was  $973.9\pm 1.43\text{ kg/m}^3$ . For emulsions with the dispersed phase concentration of 50%, density equaled  $959.1\pm 2.18\text{ kg/m}^3$ . The surface tension was defined by means of a tensiometer KRÜSS K100 (KRÜSS GmbH, Germany). The viscosity of permeating liquids was measured by a shear rheometer Bohlin CVO-120 (Malvern Instruments, UK).

The kinetics of the imbibition process evaluated as changes of the imbibed emulsion mass and the height of its front penetration versus time. They were investigated using the classical wicking test, during which the porous medium was directly submerged in a liquid. The used experimental stand is shown schematically in Figure 1.

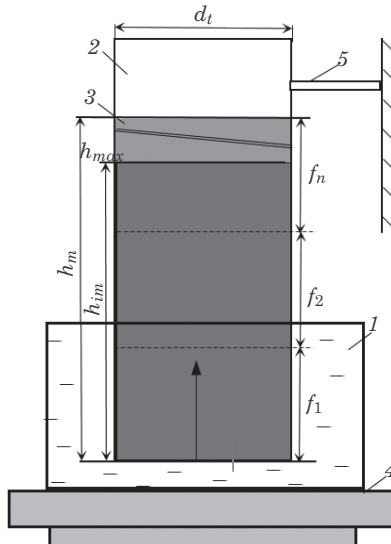


Fig. 1. Scheme of the experimental stand: 1 – reservoir with a liquid, 2 – tube with a diameter  $d_t$ , 3 – dry granular bed in a tube, 4 – balance, 5 – fixator of a tube

The process was observed and followed till the equilibrium state achieving when the mass changes became negligible small, i.e. less than 0.001 g per 300 s. After the imbibition test, in the obtained samples the concentrations of the imbibed emulsions were defined at certain heights of liquids penetration, e.g.  $f_1, f_2 \dots f_n$ , as in Figure 1. The nephelometrical method was used to measure such concentrations by means of the optical analyser Turbiscan<sup>TM</sup> LAB (Formulation, France). The mentioned methods have been reported in details elsewhere (SEK et al. 2015, SHTYKA et al. 2016).

All experiments were performed at the temperature of  $23 \pm 1^\circ\text{C}$  and atmospheric pressure. Three independent replications were conducted for each type of liquids and their mean value was considered as the obtained result.

## Results and Discussion

### Changes of imbibition kinetics versus time

The kinetics of imbibition process as mentioned previously, was characterized as the changes of wicked emulsion mass  $m_{im}$  and height of its penetration  $h_{im}$  as a function of time  $t_{im}$ . The obtained results on the mass variation are represented in Figure 2. The highest mass of the imbibed liquid was observed for water, i.e.  $25.2 \cdot 10^{-3}$  kg. Among the investigated two-phase liquids it was obtained in case of emulsions with the lowest dispersed phase concentration, i.e.  $\varphi_d = 10$  vol% for both granular media (Figs. 2a and 2b). In contrast, the lowest one was derived for oil, i.e.  $\sim 9.5 \cdot 10^{-3}$  kg (Fig. 2). The tendency of imbibition was the similar for both investigated granular media, but higher values of the mass were obtained in case of a bed with particles diameters of 200–300  $\mu\text{m}$ . Consequently, the increase of beads size caused the decrease of imbibed mass. Thus, for emulsions the mass value reduced twice, for water by about 30% and only for oil such difference was negligibly small (Fig. 2).

To summarize, the emulsions imbibition in the granular media considerably differed from the process of their pure components wicking, and depended strongly on the hydraulic radius of pores. The difference between the masses of imbibed emulsions was lower than 1.1 g, thus, the initial concentration of the dispersed phase is considered as a less significant factor.

Figure 3 represents the comparison of the obtained results related to the height changes versus time. In this case, the beads and consequently, pores radius were proved to be the influential parameter. As shown on the graph, the highest values were observed for a bed with smaller particles diameter, i.e. 200–300  $\mu\text{m}$  (Fig. 3). The maximal value of experimental data error was equal to 3.8% for a medium with beads diameter of 200–300  $\mu\text{m}$ , and up to 10% for another type.

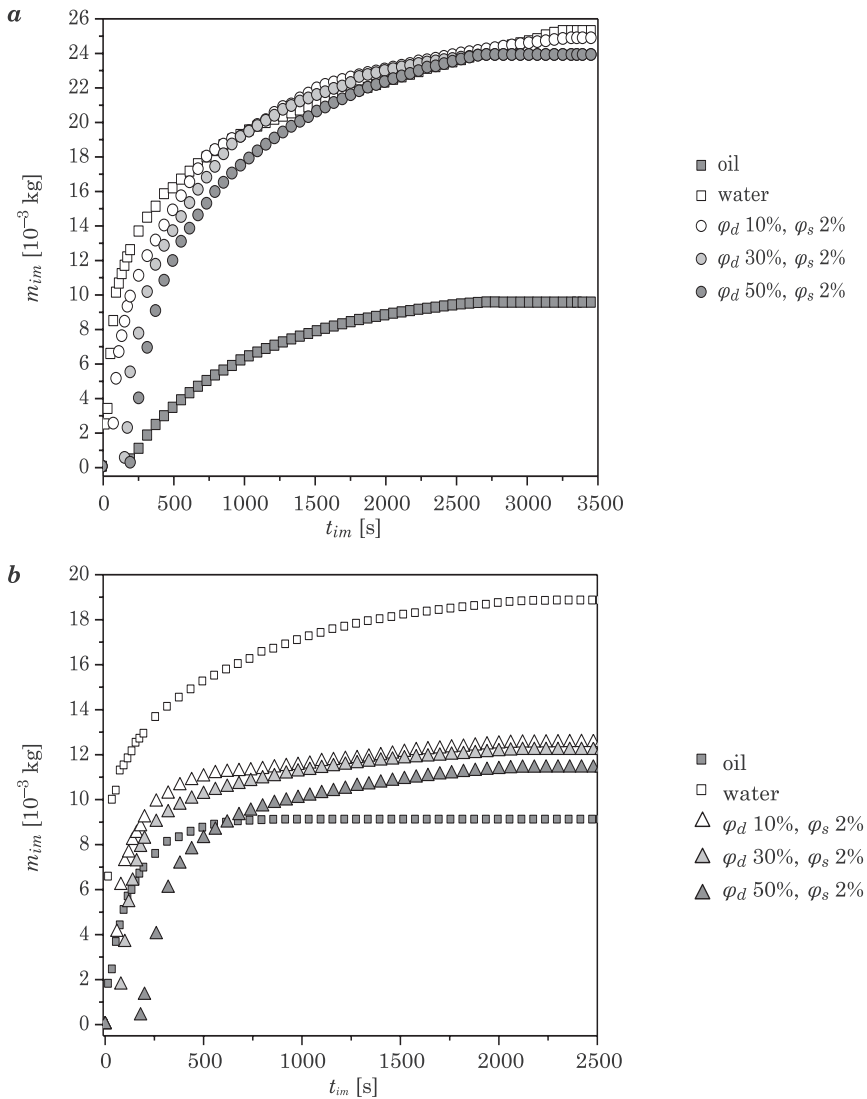


Fig. 2. Changes of wicked liquid mass  $m_{im}$  versus time  $t_{im}$  during emulsions imbibition in granular media with beads diameter of: *a* – 200–300  $\mu\text{m}$ , *b* – 600–800  $\mu\text{m}$

The maximal height of emulsions penetration depended on the initial dispersed phase concentration in case of granular diameter of 200–300  $\mu\text{m}$  ( $d_1$  in Fig. 3). Thus, for 10% emulsion such value was the highest and equalled 0.083 m, for 30% it was about 11% lower, i.e. 0.074 m, and 0.069 m in case of 50% emulsion. The data also showed that for another porous medium with a particles fraction of 600–800  $\mu\text{m}$ , such difference between the heights of emulsions fronts was

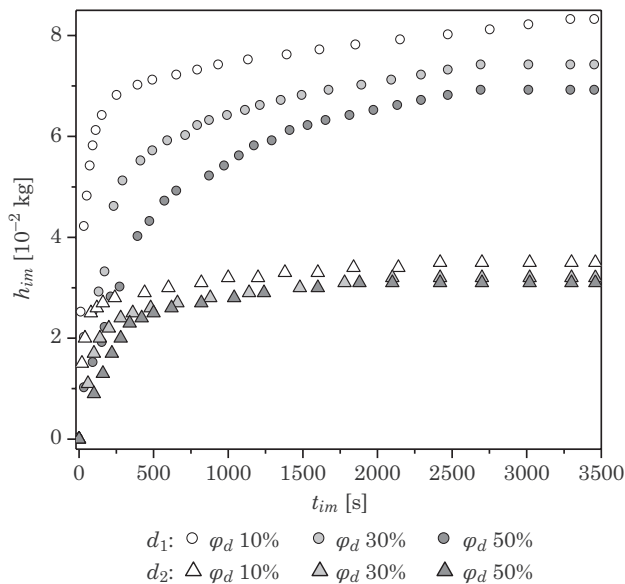


Fig. 3. Changes of an imbibed liquid height  $h_{im}$  versus time  $t_{im}$  during emulsions imbibition in granular media with beads diameter of:  $d_1$  – 200–300  $\mu\text{m}$ ,  $d_2$  – 600–800  $\mu\text{m}$

insignificant, and the imbibition process achieved more quickly the equilibrium state ( $d_2$  in Fig. 3). Analysing the data presented in Figures 2 and 3, it is possible to conclude that the structure of a granular medium can be admitted as one of the main factor defining a trend of the multiphase liquids imbibition.

### Approximation of the experimental data on the emulsion imbibition

The accuracy of the proposed in literature models to describe the liquids wicking in porous structure and possibility of their application to predict the dispersions penetration were also discussed in the current work. The obtained experimental data on emulsions imbibition in the granular media were approximated by equations mentioned previously in introduction.

The classical Lucas-Washburn equation is frequently used to describe the capillary rise in one cylinder or their bundle, but its application is extended to characterize imbibition process in porous structures (KOWALSKI 2004, MASOODI et al. 2007, FRIES, DREYER 2008, MASOODI, PILLAI 2010). In case when the gravity force is small enough to be negligible in comparison with the capillary force ( $p_c \gg \rho g h_c$ ), the equation has the following form (KOWALSKI 2004, MASOODI et al. 2007):

$$h_c^2 = \frac{r_c \sigma \cos \theta}{2\eta} t \tag{1}$$

where:

- $h_c$  – the height of a liquid front in a capillary,
- $t$  – the time of rise,
- $\eta$  – the viscosity of a permeant and  $\sigma$  is its surface tension,
- $r_c$  – the radius of this capillary,
- $\theta$  – the contact angle between a penetrating liquid surface and pores surface.

The expression for a liquid height  $h_f$  rise for the polymer wicks proposed in the publication of MASSODI et al. (2007). This equation considers such peculiarity of a porous medium as the tortuosity of pores in the investigated medium  $\tau$ , and it can be written as:

$$h_f^2 = \frac{r_h \sigma \cos \theta}{2\eta \tau^2} t \tag{2}$$

where:

- $r_h$  – the hydraulic radius.

The hydraulic radius is calculated according to Kozeny-Carman theory. Thus, the hydraulic radius can be calculated as (KOWALSKI 2004):

$$r_h = \frac{1}{6} d_b \left( \frac{\varepsilon}{1-\varepsilon} \right) \tag{3}$$

where:

- $d_b$  – the average diameter of beads in a granular medium.

The tortuosity can be calculated as a ratio of the average length of a permeant path  $\lambda_e$  to the distance in flow direction  $L_s$  (DUDA et al. 2011):

$$\tau = \frac{\lambda_e}{L_s} \tag{4}$$

In the discussed publication, the capillary model was also presented to predict a permeant front height rise considering the porosity  $\varepsilon$ , the proportionality coefficient  $K$ , known also as the permeability or hydraulic conductivity parameter. The represented model neglects the gravity effect, and has the following form as (MASOODI et al. 2007):

$$h_f^2 = \frac{4K \sigma \cos \theta}{\varepsilon \eta r_p} t \tag{5}$$

where:

- $r_p$  – the mean pore radius.

The permeability regarded in this equation can be calculated using Kaviany model which considers the porosity of investigated bed and average diameter of beads. Thus, this parameter is expressed as (KAVIANY 1995):

$$K = \frac{\varepsilon^3}{36k_{kc}(1-\varepsilon)^2} d_b^2 \quad (6)$$

where:

$k_{kc}$  – the Kozerny constant, which is equal to 5 for a bed packed with beads (KAVIANY 1995, KOWALSKI 2004).

The permeability of a granular medium can also be determined according to the following equation (RUMPF, GUPTA 1975):

$$K = \frac{\varepsilon^{5.5}}{5.6} d_b^2 \quad (7)$$

Fries and Dreyer analyzed the capillary rise of a wetting liquid in a cylinder or porous medium considering the gravity term. The equation has the following form (FRIES, DREYER 2008):

$$h(t) = \frac{a}{b} \left( 1 - e^{-(b^2 t/a)} \right) \quad (8)$$

and related to the spontaneous imbibition in porous structures by means of coefficients, which are expressed as:

$$a = \frac{\sigma r_p \cos \theta}{4\eta} \quad (9)$$

$$b = \frac{\rho g r_p^2 \sin \psi}{8\eta} \quad (10)$$

where:

$\psi$  – the angle formed between an inclined tube and free liquid surface.

There is a group of the mathematical models that describe the kinetics of spontaneous imbibition in term of mass changes with time (BENAVENTE et al. 2002, LI, HORNE 2004, MASSODI et al. 2007, CAI et al. 2012, 2014). The increase of an imbibed mass can be represented in relation to the height of liquid front  $h_f$  according to the equation (MASSODI et al. 2007):

$$m = \varepsilon \rho \pi r_p^2 h_f \quad (11)$$

BENAVENTE et al. (2002) derived a model that considers the imbibition weight related to the structural parameters of porous medium, such as tortuosity  $\tau$ ,

pore shape parameters, denoted as  $\delta$ , and the average pore radius  $r_{av}$  of the investigated porous bed. The equation can be represented as:

$$m^2 = \frac{A_s^2 \varepsilon^2 \rho^2 r_{av} \delta \sigma \cos \theta}{2\eta\tau} t \tag{12}$$

where:

$A_s$  – the cross-section area of a porous medium (BENAVENTE et al. 2002).

The tortuosity of a granular medium can be calculated analytically using Du Plessis–Masliyah equation (DU PLESSISS, MASLIYAH 1991):

$$\tau = \varepsilon / \left[ 1 - (1 - \varepsilon)^{2/3} \right] \tag{13}$$

Thus, the tortuosity was equal to 1.4 that was also confirmed experimentally due to microscopic images analysis of porous structure.

The influence of the investigated porous media saturation with a wetting liquid was taken into consideration in Li-Horne equation (LI, HORNE 2004). It is introduced as the difference between the initial saturation  $S_{in}$  and the medium saturation after imbibition,  $S_{im}$ . The equation can be written as follows:

$$m^2 = \frac{2A_s^2 \rho^2 K \varepsilon (S_{im} - S_{in}) \sigma \cos \theta}{\eta r_p} t \tag{14}$$

The porous bed might be not fully saturated by a wetting permeant during the spontaneous wicking due to gas phase entrapment or the partial connectivity of pore voids, i.e. in rocks, soil, building materials, concrete, etc.

CAI et al. (2012, 2014) proposed an approach to predict the spontaneous imbibition of a wetting liquid on the base of fractal geometry. The mass changes versus time is expressed in a form of:

$$m^2 = \frac{A_s^2 \rho^2 \varepsilon^2 r_{max}}{1 - \varepsilon} \frac{\sigma \cos \theta}{2\eta\tau^2} \frac{2 - D_f}{3 - D_f} t \tag{15}$$

where:

$r_{max}$  – the maximum pore radius, which can be calculated as a ratio (YU 2005, CAI et al. 2014):

$$r_{max} = \frac{r_{av}}{(D_f / (4 - D_f))^{1/4}} \tag{16}$$

where:

$D_f$  – the pore fractal dimension (XU, YU 2008, CAI et al. 2012, 2014).

The graphs plotted in Figure 4 introduce the comparisons between the experimental data and the predictions by equations presented in the current work. It can be noted that Equation 1 describes more precisely experimental data on the height changes than others, but till  $t_{im} = 600$  s. Further, a trend towards lower than the equation prediction (Fig. 4a).

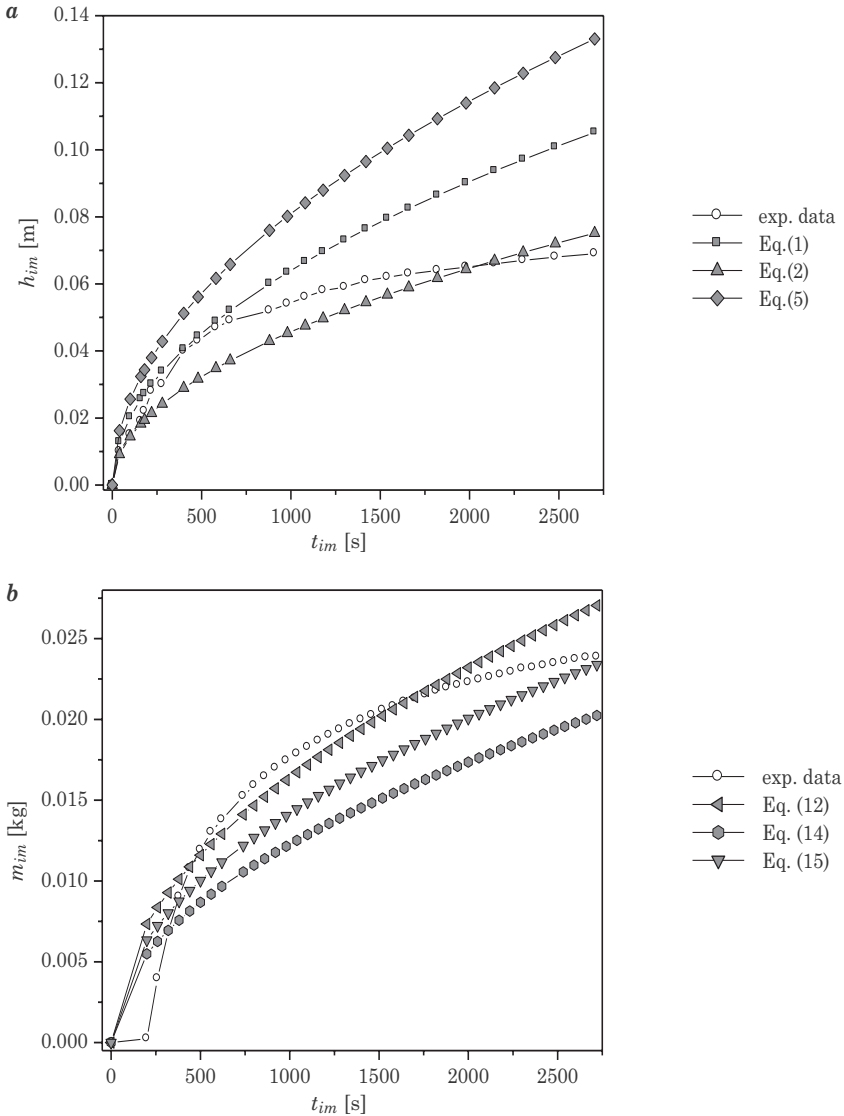


Fig. 4. Comparisons of the emulsion imbibition process predicted by the models and experimental data:  $a$  – height  $h_{im}$  changes versus time  $t_{im}$ ,  $b$  – mass  $m_{im}$  changes versus time  $t_{im}$ . The parameters used are  $A_s = 9.62 \text{ cm}^2$ ,  $\rho = 0.959 \text{ g/cm}^3$ ,  $\sigma = 36 \text{ mN/m}$ ,  $r_h = 22.9 \text{ }\mu\text{m}$ ,  $\eta = 87.35 \text{ mPa}\cdot\text{s}$ , and  $\theta = 30^\circ$

The data in Figure 4b were obtained both experimentally and analytically, and represent the imbibed mass changes versus time. More accurate approximation was observed in case of Equation 12, but till  $t_{im} = 1,800$  s. Thereafter, the mass increase slowed down and the imbibition process achieved the equilibrium state (Fig. 4b). To summarize, the trends of the experimental data differed from those obtained analytically by mean of models.

### Peculiarities of imbibition process in case of emulsions

The results on viscosity changes with increase of the dispersed phase concentration are shown in Figure 5. Its increase caused changes of emulsion viscosity and its behavior at the different shear rates. The investigated disperses behaved as the Newtonian liquids and flow curves are approximated by a straight line if the dispersed phase concentration is less than 30%. Whereas other emulsions with higher concentrations behaved as the non-Newtonian liquids (Fig. 5).

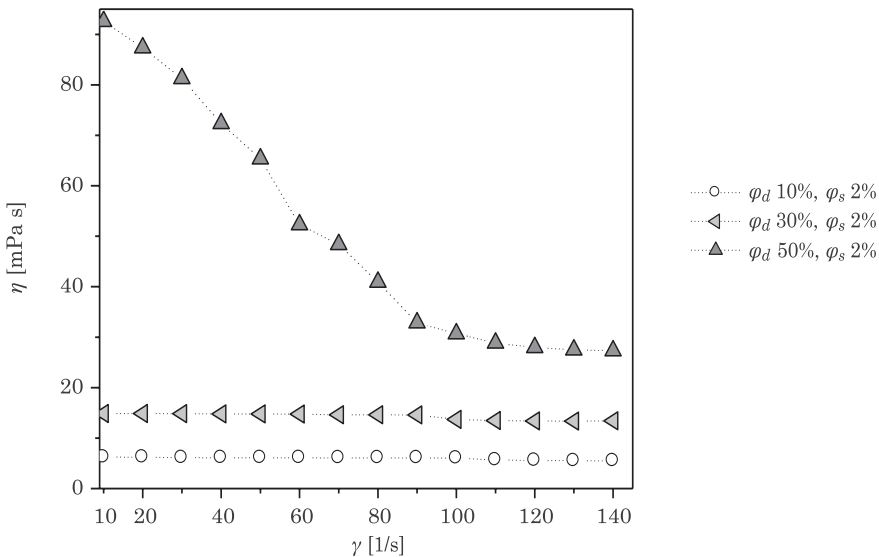


Fig. 5. Viscosity of the investigated emulsions at the different shear rates  $\gamma$

The results of emulsions concentration changes versus the height of their front penetration in the porous media are plotted in Figure 6.

According to the experimental data, the imbibed emulsions revealed a tendency to decrease concentration with the increase of their penetration height in both granular beds. To compare, the highest dispersed phase concentrations were observed for porous media with beads diameter of 600–800  $\mu\text{m}$ , whereas

the height of penetration in this case was the lowest one, i.e. less than 0.04 m (Fig. 6). It related to pores structure, i.e. hydraulic radius, which was wider compared to another type of medium, but it was still enough to induce the capillary forces.

At  $h_{im} \leq 0.02$  m, the concentration of imbibed emulsions was recognized as maximal in both experiments. Furthermore, the concentration of imbibed

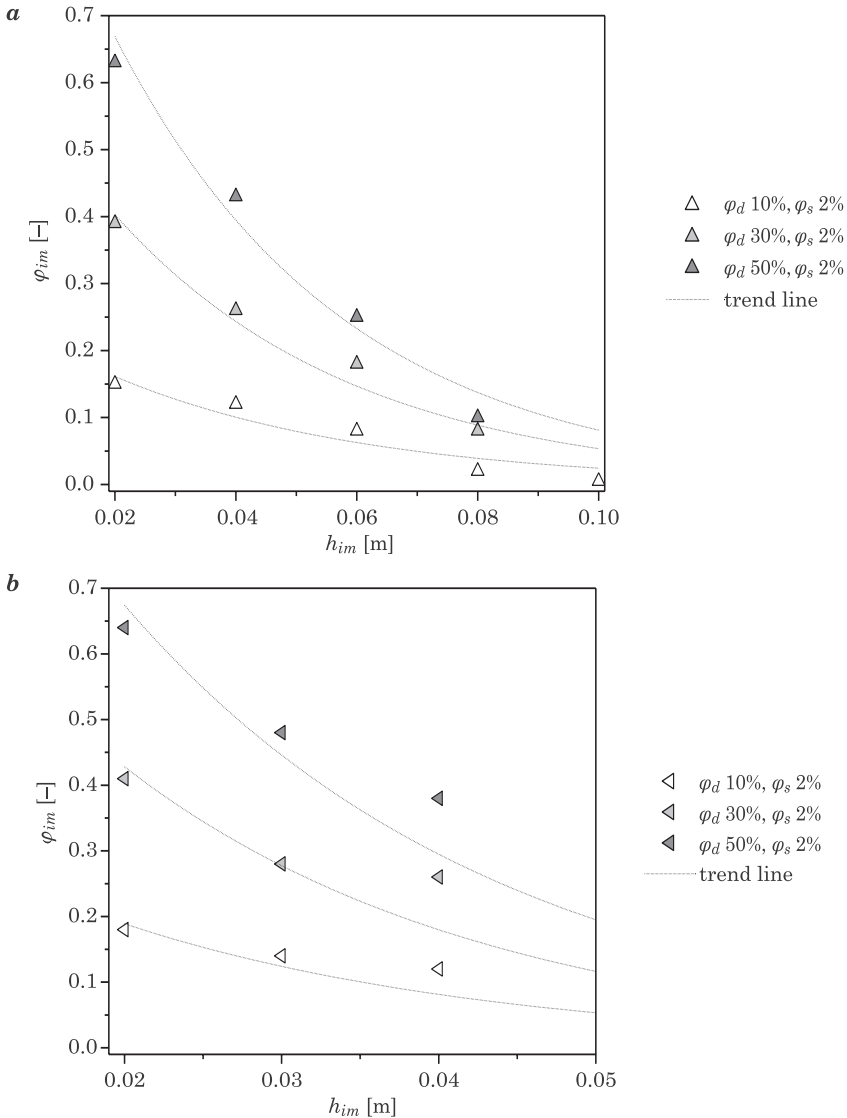


Fig. 6. The dispersed phase concentration  $\phi_{im}$  changes with the height  $h_{im}$  for emulsions penetration in granular media with beads diameter of: *a* – 200–300 μm, *b* – 600–800 μm

emulsions exceeded their initial values  $\varphi_d$ , the exception was observed for 50% emulsions at  $0.03 \text{ m} \leq h_{im}$ . As shown in Figure 6, the obtained concentrations were lower for emulsions with  $\varphi_d$  of 10 vol%.

## Conclusions

The imbibition of multiphase liquids in granular media differs significantly from the same process with single-phase liquids. There was a strong influence of the pores structure on wicking process that revealed the increase of the imbibed mass and penetration height with the decrease of particles diameter in a granular bed. Though such a factor was of less significance for the investigated single-phase liquids, especially for oil.

The highest mass of imbibed emulsion and penetration height were obtained for emulsions with the lowest dispersed phase concentration and consequently, viscosity. The increase of oil content in an emulsion was a reason of the insignificant reduction of the imbibed mass in both investigated media. The difference between the heights of permeant penetration was derived only in case of porous media with beads diameter of 200–300  $\mu\text{m}$ .

The comparisons between the obtained experimental data and those predicted by the equations shown that they disallow to describe the emulsions imbibition in porous structures with the sufficient accuracy. The limitations might be related to the several aspects: i) emulsions are recognized as heterogeneous multiphase systems, consisting of immiscible components with different physicochemical properties, and ii) their composition changes during wicking process.

On the one hand, the concentrations of imbibed emulsions exceeded their initial value at  $h_{im} \leq 0.02 \text{ m}$ . On the other hand, there was a general tendency of concentrations decrease with front raise in both granular media. The highest value of the dispersed phase was observed for a bed composed of 600–800  $\mu\text{m}$  beads. Consequently, higher radius of pores allows to prevent the penetration paths obstruction with emulsion droplets. The effect of permeants concentration increase was the viscosity changes, and as a result, the lowest height of penetration was observed.

The experimental data on the spontaneous imbibition discussed in this publication, can facilitate understanding of two-phase liquids behaviour inside the granular media during their transport by the capillary force. The obtained results can be appropriate to predict and describe the imbibition of multiphase liquids in porous media with different particles sizes, for example sorbents and such structures as soils, sand, rocks, and others.

**Acknowledgment.** The study was funded in framework of the Foundation Program for Young Scientists in Lodz University of Technology (Grant No. 501/10-34-2-1015).

## References

- BENAVENTE D., LOCK P., ÁNGELES GARCÍA DEL CURA M., ORDÓÑEZ S. 2002. *Predicting the capillary imbibition of porous rocks from microstructure*. Transport in Porous Media, 49: 59–76.
- CAI J., PERFECT E., CHENG C.-L., HU X. 2014. *Generalized modelling of spontaneous imbibition based on Hagen–Poiseuille flow in tortuous capillaries with variably shaped apertures*. Langmuir, 30: 5142–5151.
- CAI J., HU X., STANDNES D.C., YOU L. 2012. *An analytical model for spontaneous imbibition in fractal porous media including gravity*. Colloids and Surfaces A: Physicochemical and Engineering Aspects, 414: 228–233.
- CARBAJO J., ESQUERDO-LLORET T.V., RAMIS J., NADAL-GISBERT A.V., DENIA F.D. 2015. *Acoustic properties of porous concrete made from arlite and vermiculite lightweight aggregates*. Materiales de Construcción, 65(320) : e072.
- CHATTERJEE P.K., GUPTA B.S. 2002. *Absorbent Technology*. 1th ed. Elsevier, Netherlands, p. 7–45.
- CHEBBI R. 2007. *Dynamics of liquid penetration into capillary tubes*. Journal of Colloid and Interface Science, 315(1): 255–260.
- DIGILOV R.M. 2008. *Capillary rise of a non-Newtonian power law liquid: impact of the fluid rheology and dynamic contact angle*. Langmuir, 24(23): 13663–13667.
- DU PLESSISS J.P., MASLIYAH J.H. 1991. *Flow through isotropic granular porous media*. Transport in Porous Media, 6(3): 207–221.
- DUDA A., KOZA Z., MATYKA M. 2011. *Hydraulic tortuosity in arbitrary porous media flow*. Physical Review E, 84(84): 036319-1-8.
- FRIES N., DREYER M. 2008. *An analytic solution of capillary rise restrained by gravity*. Journal of Colloid and Interface Science, 320: 259–263.
- HAMRAOUI A., NYLANDER T. 2002. *Analytical Approach for the Lucas–Washburn Equation*. Journal of Colloid and Interface Science, 250(2): 415–421.
- KAVIANY M. 1995. *Principles of Heat Transfer in Porous Media*. 2nd ed. Springer, New York, p. 17–45.
- KOWALSKI J.S. 2004. *Inżynieria materiałów porowatych*. Wydawnictwo Politechniki Poznańskiej, Poznań.
- LI K.W., HORNE R.N. 2004. *An analytical scaling method for spontaneous imbibition in gas-water-rock systems*. SPE Journal, 9: 322–329.
- LIU G., ZHANG M., RIDGWAY C., GANE P. 2014. *Pore wall rugosity: The role of extended wetting contact line length during spontaneous liquid imbibition in porous media*. Colloids and Surfaces A: Physicochemical and Engineering Aspects, 443: 286–295.
- MAGGI F., ALONSO-MARROQUIN F. 2012. *Multiphase capillary flows*. International Journal of Multiphase Flow, 42: 62–73.
- MARTIC G., DE CONINCK G., BLAKE T.D.J. 2003. *Influence of the dynamic contact angle on the characterization of porous media*. Journal of Colloid and Interface Science, 263: 213–216.
- MASOODI R., PILLAI K.M., VARANASI P.P. 2007. *Darcy's law based models for liquid absorption in polymer wicks*. AIChE Journal, 53(11): 2769–2782.
- MASOODI R., PILLAI K. M. 2010. *Darcy's law-based model for wicking in paper-like swelling porous media*. AIChE Journal, 56(9), 2257–2267.
- RUMPF H., GUPTA A.R. 1975. *The influence of porosity and grain size distribution on the permeability equation of porous flow*. Chemie Ingenieur Technik, 43(6): 367–375.
- SEK J., SHTYKA O.S., SZYMCAK K. 2015. *Modelling of the spontaneous polypropylene sorbents imbibition with emulsions*. Journal of Environmental Engineering and Landscape Management, 23(2): 83–93.
- SHTYKA O.S., SEK J., BŁASZCZYK M., KACPRZAK S. 2016. *Investigation into hydro- and oleophilic porous medium saturation with two-phase liquids during the imbibition process*. Inżynieria i Aparatura Chemiczna, 55(1): 36–37.
- SIEBOLD A., NARDIN M., SCHULTZ J., WALLISER A., OPPLIGER M. 2000. *Effect of dynamic contact angle on capillary rise phenomena*. Colloids and Surfaces A: Physicochemical and Engineering Aspects Flow, 161(1): 81–87.

- STRZELECKI T., KOSTECKI S., ŻAK S. 2008. *Modelowanie przepływów przez ośrodki porowate*. Dolnośląskie Wyd. Edu, Wrocław.
- XU P., YU B.M. 2008. *Developing a new form of permeability and Kozeny-Carman constant for homogeneous porous media by means of fractal geometry*. *Water Resources Research*, 31: 74–81.
- XUE H.T., FANG Z.N., YANG Y., HUANG J.P., ZHOU L. W. 2006. *Contact Angle Determined by Spontaneous Dynamic Capillary Rises with Hydrostatic Effects: Experiment and Theory*. *Chemical Physics Letters*, 432(1–3): 326–330.
- YU B.M. 2005. *Fractal character for tortuous streamtubes in porous media*. *Chinese Physics Letters*, 22: 158–160.
- YU B.M. 2008. *Analysis of flow in fractal porous media*. *Applied Mechanics Reviews*, 61: 050801(19).
- ZHAO H.Y., LI K.W. 2009. *A fractal model of production by spontaneous water imbibition*. Society of Petroleum Engineers. Latin American and Caribbean Petroleum Engineering Conference, 31 May-3 June, Cartagena de Indias, Colombia.
- ZHMUD B.V., TIBERG F., HALLSTENSSON K. 2000. *Dynamics of Capillary Rise*. *Journal of Colloid and Interface Science*, 228: 263–269.





## THE EFFECTS OF BEEF CARCASSES HIGH VOLTAGE ELECTRICAL STIMULATION AND ROASTING METHODS ON TENDERNESS AND WATER RETENTION OF BEEF

*Katarzyna Tkacz*<sup>1</sup>, *Adam Więk*<sup>1</sup>,  
*Ryszard Żywica*<sup>2</sup>, *Joanna K. Banach*<sup>2</sup>

<sup>1</sup> Department of Meat Technology and Chemistry

<sup>2</sup> Department of Commodity

University of Warmia and Mazury in Olsztyn

Received 22 September 2017; accepted 15 March 2018; available online 22 March 2018.

**Key words:** electrical stimulation, beef, roasting, tenderness, WHC, cooking loss.

### Abstract

The aim of the study was to determine the effect of high voltage electrical stimulation (330 V, 17 Hz, 120 s) of beef half-carcass and heat treatment on tenderness and water holding capacity of meat. The experimental material was a *semimembranosus* muscle derived from Polish Holstein-Friesian heifers ( $n=12$ ). In the experiment, a forced and natural air circulation ovens were used; the raw material was heated at 170°C to obtain a final temperature from 55 to 80°C inside the beef. Results showed that electrical stimulation improved tenderness of roasted beef, which was demonstrated in the decrease in the maximum shear force from 39% to 26%. The electrical stimulation had a negative effect on cooking losses during roasting and water content in the final product. It has also been shown that studied quality attributes of beef depends on the type of heat treatment. Beef prepared in forced air circulation oven, were characterized by lower water content and higher values of maximum shear and compression forces than those heated in natural air circulation oven.

### Subscripts

ES – electrically stimulated sample,

C – control sample,

NC – heat treated in natural air circulation oven,

FC – heat treated in forced air circulation oven.

Correspondence: Katarzyna Tkacz, Katedra Technologii i Chemii Mięsa, Uniwersytet Warmińsko-Mazurski, Plac Cieszyński 1/3, 10-719 Olsztyn, phone: +48 89 523 47 11, e-mail: [ktkacz@uwm.edu.pl](mailto:ktkacz@uwm.edu.pl)

## Introduction

Electrical stimulation of carcasses of slaughter animals is one of the technological treatments that are aimed at improving the sensory attributes of meat, in particular tenderness (FERGUSON et al. 2000, HWANG et al. 2003, KIM et al. 2013). This method consists in carcass muscle tissue exposure to the impact of an electric current imitating nervous impulses, within the first hour after slaughter (RING, TAYLOR 1988, ROGOW, MOJSENKO 1981, ŻYWICA 1998). Endogenous biochemical and ultrastructural transformations induced by electrical stimulation effect a change in post-slaughter properties of the muscle tissue. This change is manifested by increased tenderness, elongated stability, as well as improved flavor, juiciness, and color of the tissue (DEVINE et al. 1999, GEESINK et al. 1994, PALEARI et al. 1991, RASHID et al. 1983).

The improvement of these traits of meat increases its eating and processing usability. For this reason, electrical stimulation is applied to process of beef and lamb meat (BOUTON et al. 1980, EIKELENBOOM et al. 1985, HWANG et al. 2003, JONES et al. 1991, TOOHEY et al. 2008), and also to improve quality attributes of meat from such animals as alpacas (SMITH et al. 2016), donkeys (POLIDORI et al. 2016), and goats (KADIM et al. 2014).

Based on long-standing investigations, the improvement of tenderness of electrically stimulated meat is believed to result from:

- activating the calpain enzymes, specifically  $\mu$ -calpain, has been found to be responsible for the majority of postmortem proteolysis of muscle proteins associated with tenderness in the first 72 h postmortem (ANDERSON et al. 2012, FERGUSON et al. 2000, GEESINK et al. 1994, GEESINK et al. 2006, HUFF-LONERGAN et al. 2010),

- prevention of cold shortening through reducing the concentration of ATP and other high-energy phosphatides and through rapidly reduced pH owing to enhanced glycolysis (CHRYSTALL and DEVINE 1978, GARIEPY et al. 1995, HWANG et al. 2003, SOARES, AREAS 1995),

- physical damages inside the stimulated tissue (SORINMADE et al. 1982, ŻYWICA et al. 1998),

- increased activity of lysosomal enzymes, probably, the rapid decrease of pH accelerates the disruption of lysosomes, thereby causing release of proteases (cathepsin-C and  $\beta$ -glucuronidase) to the intra- and inter-cellular compartments at still high temperature (DUTSON, 1980, GEESINK et al. 1994, SOARES, AREAS 1995, SONAIYA et al. 1982),

- destabilization of collagen fibers (GEESINK et al. 1994, LESIÓW 1993).

Earlier studies demonstrated the highest rate of post-slaughter transformations of beef, accelerated by the electric current, to occur in the first 24 h post slaughter (GEESINK et al. 1994, POLIDORI et al. 1996, SOARES, AREAS 1995).

The non-stimulated beef needs to undergo the ageing process (lasting from 9 to 14 days) to develop all desirable sensory traits.

To get the full picture of the effect of electrical stimulation on the culinary quality of beef, a study was undertaken to analyze the dynamics of changes in the electrically stimulated muscle tissue after the first 48 h of carcass ageing under chill conditions in a meat processing plant. This objective was accomplished by determining the effect of high-voltage electrical stimulation of beef carcasses and the effect heat treatment under conditions of forced and natural air circulation on the tenderness and water holding capacity of roasted beef.

## Materials and methods

The experimental material consisted on *semimembranosus* muscle from half-carcasses of heifers of Polish Holstein-Friesian breed of the Black-and-White variety ( $n=12$ ) aged ca. 18 months and mean final body weight of  $340\pm 22$  kg. Animals were slaughtered according with the technology used in meat processing plants (ŻYWICA, BANACH 2014). Left half-carcasses, 40 min after slaughter, were subjected to electrical high voltage stimulation using a device of own construction applying 330 V AC, 17 Hz, for 120 s. Right half-carcasses were the controls. After ca. 48 h of storage in the cooling conditions ( $\pm 4^\circ\text{C}$ ,  $0.5\text{ m s}^{-1}$ ), from the electrically stimulated (ES) and non-stimulated (C) half-carcasses *semimembranosus* muscles were cut, divided into a samples of ca. 300 g and dimensions  $90\times 60\times 60$  mm ( $n=72$ ). The samples were analysed without any further ageing. The pH of the samples was measured using a pH-meter type HI 8314 C equipped with a stiletto electrode FC 200. The samples were then heat-treated (temp.  $170^\circ\text{C}$ ) in ovens: with natural (NC) and forced air convection (FC) to obtain in its geometrical center temperature: 55; 60; 65; 70; 75 and  $80^\circ\text{C}$  (monitored with thermocouples). Roasts were cooled to room temperature ( $22^\circ\text{C}$ ) for 60 min.

Texture of the analyzed material was evaluated with two types of tests performed using the INSTRON 45942 apparatus:

**A.** shear force test – a Warner-Bratzler single-knife system 2830-013 type. Ten cuboids with the cross-section area equal to  $1\text{ cm}^2$  were cut out (at  $200\text{ mm/min}$ ) from each sample perpendicular the muscle fibers. Peak or maximum shear force across the fibres was expressed in N.

**B.** compression test – a 2830-011 type piston, 30 mm in diameter and 10 mm in thickness. This test consisted in one-time compression of the samples to 50% of their initial height; with the direction of applied force being perpendicular to the direction of muscle fiber arrangement. Peak or maximum shear force across the fibres was expressed in N.

To determine water-holding capacity (WHC) of the samples, they were weighed before and after the compression test. Whatman No. 1 filter paper (Whatman

Laboratory Division, Maidstone, England) was placed under each sample, into which the drip caused by compression absorbed. The expressible water content was calculated from the formula:

$$\text{Expressible water content} = \frac{m_1 - m_2}{m_2} \cdot 100 [\%]$$

where:

$m_1$  – weight of meat sample [g],

$m_2$  – weight of filter paper without meat sample before pressing [g],

$m_3$  – weight of filter paper with meat juice after pressing [g].

The surface area of the trace of drip on the filter paper was measured using a computer system for image analysis with JAVA and MOCHA software (JANDEL SCIENTIFIC, SAN RAFAEL CA, USA).

Cooking losses were calculated as the percent in weight differences between the raw and roasted beef based on the raw weight. After thermal treatment, the samples were first left until reach the room temperature and then weighted. Water content in raw and roasted beef was determined using the oven drying method (drying at  $103 \pm 2^\circ\text{C}$  to a constant weight, PN-ISO1442, 2000),

Data was first carefully examined to eliminate outliers. A general linear model (one-way ANOVA) was used to determine significant differences ( $p < 0.05$ ) among samples with different temperatures and roasting conditions used in the experiments. Multiple comparisons were done by the Tukey's test. All statistical analyses were done using STATISTICA.10 software (StatSoft, Inc., Tulsa, OK, USA).

## Results

The raw material collected for analyses was characterized by water content of 75%; no significant differences were demonstrated between the samples in this respect. Also, the samples did not differ in the pH value which reached  $5.64 \pm 0.05$  (C) and  $5.68 \pm 0.07$  (ES).

### **Effect of electrical stimulation and heating methods on cooking losses and water content in roasted beef**

Regardless of raw material preparation method or type of the oven, the cooking losses and water content in the roasted beef depended on the final temperature inside the roast. Roasting temperature increase caused an increase in cooking losses and a decrease in water content in the products.

Table 1

Effects of electrical stimulation on cooking loss, water content and surface area of drip (mean values ± standard deviation) in roasted beef heated with natural air circulation

Final temperature [°C]	Cooking loss [%]			Water content [%]			Area of drip [cm <sup>2</sup> ]		
	C	ES	signifi-cance	C	ES	signifi-cance	C	ES	signifi-cance
55	14.95±0.38 <sup>A</sup>	18.40±0.47 <sup>A</sup>	**	71.11±0.21 <sup>E</sup>	70.76±0.24 <sup>E</sup>	NS	18.73±1.09 <sup>F</sup>	13.47±0.19 <sup>F</sup>	**
60	22.64±0.07 <sup>B</sup>	23.07±0.12 <sup>B</sup>	**	70.05±0.11 <sup>D</sup>	70.21±0.05 <sup>E</sup>	NS	13.22±0.01 <sup>E</sup>	12.00±0.10 <sup>E</sup>	**
65	24.04±0.44 <sup>C</sup>	29.87±0.47 <sup>C</sup>	**	68.95±0.01 <sup>C</sup>	67.40±0.05 <sup>D</sup>	**	10.94±0.45 <sup>D</sup>	7.79±0.52 <sup>D</sup>	**
70	30.80±0.05 <sup>D</sup>	31.77±0.02 <sup>D</sup>	**	67.64±0.05 <sup>B</sup>	67.28±0.12 <sup>D</sup>	NS	9.28±0.35 <sup>C</sup>	5.77±0.13 <sup>C</sup>	**
75	33.71±0.28 <sup>E</sup>	35.89±0.14 <sup>E</sup>	**	67.46±0.08 <sup>B</sup>	65.12±0.02 <sup>C</sup>	**	6.69±0.31 <sup>B</sup>	3.61±0.14 <sup>B</sup>	**
80	41.35±0.30 <sup>F</sup>	38.53±0.09 <sup>F</sup>	**	63.38±0.07 <sup>A</sup>	64.17±0.35 <sup>A</sup>	*	3.71±0.31 <sup>A</sup>	2.82±0.05 <sup>A</sup>	**

A-F – mean values in columns with different letters differ significantly at  $P < 0.05$ ;  
 \*\* – significance level  $P < 0.01$ ; \* – significance level  $P < 0.05$ ; NS – non significant  
 C – control sample  
 ES – electrical stimulation sample

Table 2

Effects of electrical stimulation on cooking loss, water content and surface area of drip (mean values ± standard deviation) in roasted beef heated with forced air circulation

Final temperature [°C]	Cooking loss [%]			Water content [%]			Area of drip [cm <sup>2</sup> ]		
	C	ES	signifi-cance	C	ES	signifi-cance	C	ES	signifi-cance
55	25.71±0.39 <sup>A</sup>	26.50±0.47 <sup>A</sup>	NS	68.62±0.29 <sup>E</sup>	67.51±0.23 <sup>E</sup>	**	10.84±0.80 <sup>D</sup>	9.56±0.47 <sup>D</sup>	NS
60	32.28±0.58 <sup>B</sup>	33.72±0.21 <sup>B</sup>	*	68.58±0.38 <sup>E</sup>	65.96±0.02 <sup>D</sup>	**	9.30±0.63 <sup>D</sup>	8.57±0.24 <sup>D</sup>	NS
65	33.61±0.51 <sup>C</sup>	35.34±0.42 <sup>C</sup>	**	66.59±0.23 <sup>D</sup>	65.85±0.09 <sup>D</sup>	**	6.86±0.07 <sup>C</sup>	4.48±0.11 <sup>C</sup>	**
70	37.14±0.16 <sup>D</sup>	38.74±0.07 <sup>D</sup>	**	65.04±0.15 <sup>C</sup>	64.38±0.27 <sup>C</sup>	*	5.94±0.62 <sup>C</sup>	4.10±0.27 <sup>C</sup>	**
75	38.56±0.44 <sup>E</sup>	39.27±0.28 <sup>E</sup>	NS	64.10±0.09 <sup>B</sup>	63.51±0.12 <sup>B</sup>	**	3.79±0.09 <sup>B</sup>	3.15±0.13 <sup>B</sup>	**
80	39.12±0.23 <sup>E</sup>	39.95±0.43 <sup>E</sup>	NS	64.02±0.08 <sup>D</sup>	62.91±0.17 <sup>A</sup>	**	3.10±0.29 <sup>A</sup>	2.75±0.07 <sup>A</sup>	NS

A-E – mean values in columns with different letters differ significantly at  $P < 0.05$ ;  
 \*\* – significance level  $P < 0.01$ ; \* – significance level  $P < 0.05$ ; NS – non significant  
 C – control sample  
 ES – electrical stimulation sample

Weight losses caused by NC treatment in the analyzed range of final temperatures were as follows: from 14.95% to 41.35% in the control samples, and from 18.40% to 38.53% in the stimulated samples (Tab. 1). The FC treatment caused higher than NC losses which ranged from 25.71% to 38.56% (C) and from 26,50% to 39,27% (ES) at temperatures between 55 °C and 75°C (Tab. 2). The samples heated to the internal temperature of 80°C were characterized by weight loss of 39% (C and ES). A similar value of weight loss (38.53%) was noted during the treatment of ES samples in the oven with natural air circulation. The electrical stimulation had a negative effect on weight losses during heat treatment. At each analyzed temperature, the NC treatment caused significantly higher weight losses in the ES samples ( $p < 0.05$ ). Such a dependency was also noticed during FC treatment, but only at temperatures of 60°C, 65°C, and 70°C. The weight losses had a strong effect on water content of the samples. A higher water content was determined in the NC (71.11%–63.38%) than in the FC (68.62%–62.91%) roasted beef (Tab. 1, 2). The electrical stimulation had a negative effect on water content in the roasted beef; and this effect was particularly noticeable in FC roasted beef (Tab. 2). Regardless of the final temperature the samples were heated to, the content of water was significantly lower ( $p < 0.05$ ) in the ES than in the C samples.

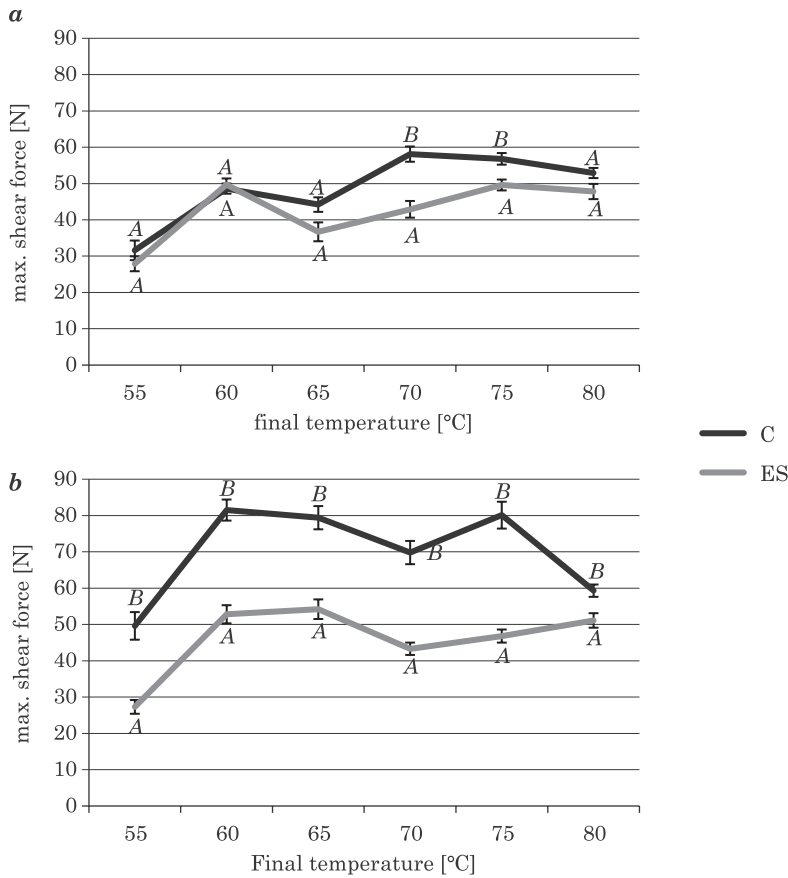
### **Effect of electrical stimulation and heating methods on tenderness and WHC of roasted beef**

The value of the maximum shear force, used to evaluate meat tenderness, depended on the final temperature the meat was heated to and on the method of its preparation (C and ES). Regardless of the treatment method, the ES samples were characterized by a significantly lower ( $p < 0.05$ ) value of the maximum shear force which was similar for both NC (27.9 N–49.7 N) and FC (27.3 N–54.2 N) samples – Figure 1.

The roasted beef made of non-stimulated meat, roasted in FC, was characterized by the maximum shear forces ranging from 49.6 N to 81.5 N, whereas shear force of the NC samples ranged from 31.6 N to 58.0 N (Fig. 1).

Results showed that ES improved meat tenderness, decreasing the maximum shear force from 39% (55–75°C FC) to 26% (70°C NC).

The force needed to induce 50% compression of the samples, as well as meat WHC, and drip area were influenced by both the final temperature of meat and the usage of electrical stimulation. Regardless of the heating method, the samples from the stimulated carcasses were characterized by a lower compression force compared to the control samples. The greatest impact of electrical stimulation on roasted beef compression force decrease was observed during

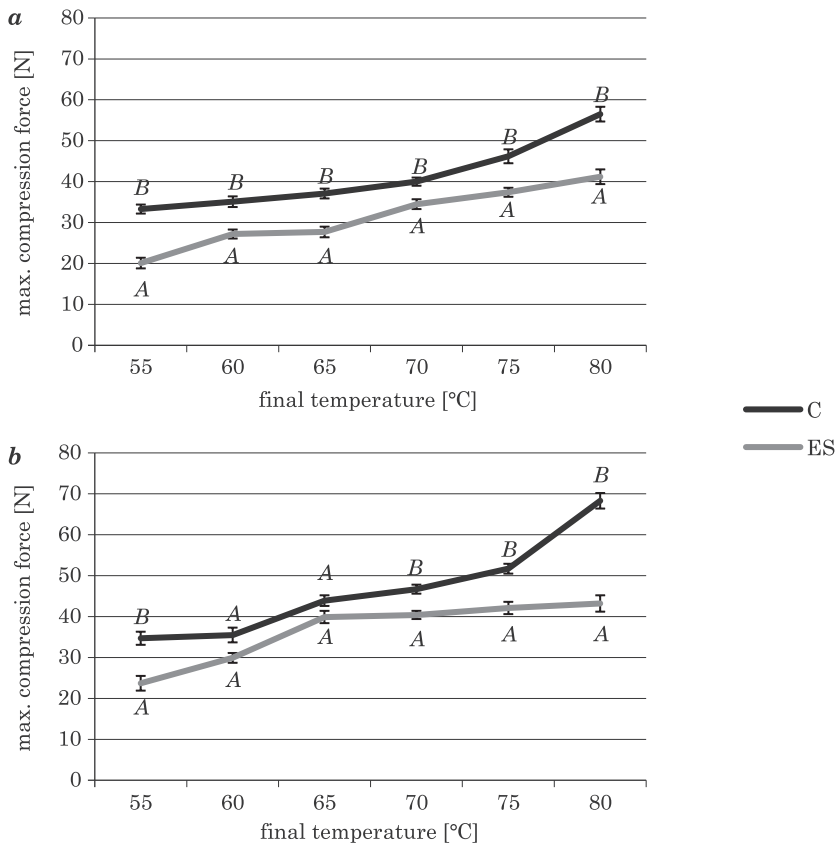


ES – electrically stimulated sample  
 C – control sample  
 NC – heat treated in natural air convection oven  
 FC – heat treated in forced air convection oven  
 A, B – means in each temperature with different letters differ significantly at  $P < 0.05$

Fig. 1. Maximum shear force of the roasted beef depending on the final temperature: a – NC, b – FC

compression of the samples heated to 80°C. The maximum compression force of the ES roasted beef was lower by 27% (NC) and by 37% (FC) than that of the control samples (Fig. 2).

Higher values of the maximum compression force were determined in the FC (from 34.7 N to 68.3 N for C samples; from 23.7 N to 43.2 N for ES samples) than in the NC (from 33.3 N to 56.5 N for C samples; from 20.1 N to 41.2 N for ES samples) roasted beef (Fig. 2). An increase in the final temperature of samples caused a decrease in roasted beef WHC. The electrical stimulation diminished WHC of roasted beef in all analyzed variants.



ES – electrically stimulated sample

C – control sample

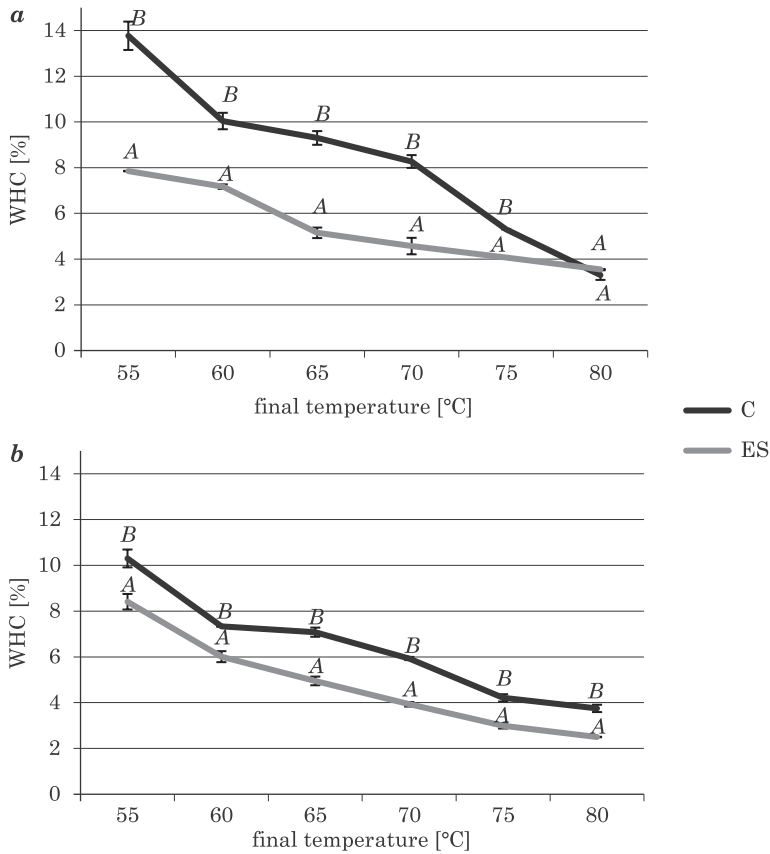
NC – heat treated in natural air convection oven

FC – heat treated in forced air convection oven

A, B – means in each temperature with different letters differ significantly at  $P < 0.05$

Fig. 2. Maximum compression force of the roasted beef depending on the final temperature: a – NC, b – FC

Result showed that ES samples, both heated in NC and FC, were characterized by lower WHC compared to the control samples. For the NC-heated samples, the difference in WHC between the C and ES samples decreased along with an increase of the final temperature. This difference reached 5.52% in the roasted beef heated to 55°C, 4.15% in those heated to 65°C, 1.24% to 75°C, whereas no significant differences were noted in the roasted beef heated to 80°C (Fig. 3).



ES – electrically stimulated sample  
 C – control sample  
 NC – heat treated in natural air convection oven  
 FC – heat treated in forced air convection oven  
 A, B – means in each temperature with different letters differ significantly at  $P < 0.05$

Fig. 3. Water-holding capacity (WHC) of the roasted beef depending on the final temperature: a – NC, b – FC

During FC heating, WHC of C samples was significantly higher ( $p < 0.05$ ) than that of the ES samples in the whole range of the analyzed temperatures. This difference reached 1.89% in the samples heated to 55°C, 2.13% in those heated to 65°C, and 1.25% in the samples heated to 80°C (Fig. 3).

The one-way analysis of variance indicated a significant effect of both of factors: the final temperature and electrical stimulation on the studied quality attributes of the roasted beef.

## Discussion

### Effect of electrical stimulation and heating method on cooking losses, water content and WHC of roasted beef

Total cooking losses caused by the heat treatment depended primarily on the final temperature, rate of heating, and electrical stimulation treatment. Higher cooking losses in the FC samples may be attributed to the forced circulation of air which, apart from creating more favorable conditions for heat penetration, facilitates more intensive evaporation of water. In all samples, the increase of the losses was the fastest in a temperature range from 55°C to 70°C. This may be due to the fact that in this range of temperatures changes occur in two main structural proteins of meat: actomyosin complex and collagen. The extent of losses had a great effect upon WHC of the roasted beef. An increase in the final temperature inside the heated product was accompanied by a decrease in water content and WHC of the roasted beef, and in drip surface during compression.

Investigations addressing the effect of electrical stimulation on cooking losses indicate both a negative effect of this treatment on the analyzed trait (BOUTON et al. 1980, GEESINK et al. 1994), a lack of its effect on water holding capacity (BOWLES et al. 1983, POSPIECH et al. 1992, RASHID et al. 1983, SHIVAS et al. 1985) as well as its positive influence on the extent of losses (HOSTETLER et al. 1982, POWELL 1991, ROGOW, MOJSENKO 1981). HOSTETLER et al. (1982), who obtained a lesser by 6% drip during heating ES samples compared with C samples, pointed to the feasibility of increasing the number of water-binding sites in proteins as a result of structural changes induced by the flow of electric current. BOUTON et al. (1980), who compared C and ES samples (voltage from 45 V to 1,100 V), achieved higher scores for WHC in the case of the stimulated samples despite greater losses noted for these samples during heat treatment. On the other hand, SAVELL et al. (1981) demonstrated that WHC of the ES samples not to differ significantly from that of the C samples after 24 h of chill storage. But as the ripening time extended the difference between the C and ES samples was increasing, i.e. WHC of the ES samples decreased. In turn, POWELL (1991) and OLSSON et al. (1994) concluded that electrical stimulation contributes to a significant ( $p < 0.05$ ) improvement of WHC, regardless of the age of animals and ripening duration. Some other authors indicate no effect of electrical stimulation on WHC of the products (BOWLES et al. 1983, SHIVAS et al. 1985).

A lower water content, WHC, and drip surface were demonstrated for the FC than for the NC heated samples. Alike results were published by other authors dealing with similar research issues who showed increased losses, decreased water content and WHC of roasted beef along with temperature increase (EIKELLENBOOM et al. 1998, NAEWBANIJ et al. 1983, PALKA et al. 1999).

### **Effect of electrical stimulation and heating method on tenderness of roasted beef**

Results of the experiment allow concluding the electrical stimulation treatment improved tenderness of all samples and caused lesser differences between the maximum shear forces in the ES samples heated to temperatures from 55 to 80°C in both NC and FC. The FC-treated control samples were characterized by higher maximum shear forces than these heated in NC.

Changes in the maximum shear force are associated with transformations of proteins that are determined by temperature of the roasting process. The increase in the maximum shear forces at temperatures ranging between 55 and 60°C may be induced by denaturation of myofibrillar proteins of meat, myosin and  $\alpha$ -actinin in particular, and by granulation of the epimysium. A decrease in the maximum shear force at 65°C, followed by its increase may be explained by the fact that at a temperature of ca. 65°C the denaturation process begins in muscle collagen, whereas changes observed at a temperature of ca. 70°C include fragmentation of myofibrils in the Z line coupled with denaturation of titins, and shrinkage of collagen fibers in the endomysium (FRITZ et al. 1992, MARTENS et al. 1982, PALKA, DAUN 1999). According to ZALEWSKI (1995), once the temperature of ca. 65°C is reached inside the muscle, there occurs a respective, small denaturation of muscle fiber proteins, which contributes to softness and WHC of a dish. PALKA and DAUN (1999) concluded that analyzed texture parameters, such as springiness, cohesiveness, chewiness, modulus of elasticity, initial stress, and hardness, changed during heating independently and their values increased along with temperature increase reaching their maxima in a temperature range from 70 to 100°C. EIKELENBOOM et al. (1998) also obtained the lowest value of the shear force for the samples heated at a temperature of 65°C. The course of values of the maximum compression force, presented by these author, is very similar to that shown in this paper.

Temperature increase during roasting caused an increase in the value of the maximum compression force in all analyzed samples. Results showed also the FC treatment to induce an increase in the maximum force during compression compared to the NC-heated samples. Presumably, this increase may be linked with structural changes of meat proteins and a lower water content in the FC-heated beef. This method of roasting makes meat more dry and more resistant during compression. It is generally accepted (PALKA, DAUN 1999) that heat-induced changes evoke a softening effect in the connective tissues and that denaturation of myofibrillar proteins causes the hardening effect. The culinary cut used in the study has very little collagen, hence the effect of hardening as a result of denaturation of myofibrillar proteins is especially tangible and is manifested by the increased maximum forces of shear and compression.

CONTRERAS-CASTILLO et al. (2016) found that the direct application of low-voltage electrical stimulation (104 V) on muscle did not significantly affect the rate of meat tenderisation or degradation of myofibrillar proteins in beef evaluated during post mortem ageing (up to 28 days pm).

The improvement of tenderness, presented in this paper, may be explained by the fact that electric current flow through a carcass causes physical damages inside the stimulated tissues, destabilization of collagen fibers, enhanced activity of lysosomal enzymes, as well as accelerated decrease in the activity of  $\mu$ -calpains, and proteolysis of myofibrillar proteins (GEESINK et al. 1994, OSTOJA, KORZENIOWSKI 1992, SOARES, AREAS 1995, SONAIYA et al. 1982, ŻYWICA et al. 1998).

The positive effect of electrical stimulation on beef tenderness was also demonstrated by other authors who unanimously reported about its improvement as a result of this treatment (BOUTON et al. 1980, HOSTETLER et al. 1982, PALEARI et al. 1991, POWELL 1991, SAVELL et al. 1981, RASHID et al. 1983, ROGOW, MOJSENKO 1981, SONAIYA et al. 1982).

## Conclusions

Results of the study presented in this paper indicate a positive effect of electrical stimulation on tenderness of roasted beef. In most of the analyzed samples, regardless of the final temperature and heating method, lower shear and compression forces were achieved after the electrical stimulation.

It was shown also that investigated quality attributes of roasted beef depended on heating method. The beef obtained as a result of roasting in forced air circulation oven, were characterized by lower water content and higher shear and compression forces than those roasted in natural air circulation oven. Quality attributes varied depending on final temperature inside the beef cuts. The roasts prepared from electrical stimulation beef heated to 65 and 70°C in natural air circulation oven, had the best quality.

## References

- ANDERSON M.J., LONERGAN S.M., FEDLER C.A., PRUSA K.J., BINNING J.M., HUFF-LONERGAN E. 2012. *Profile of biochemical traits influencing tenderness of muscles from the beef round*. Meat Science, 91: 247–254.
- BOUTON P.E., FORD A.L., HARRIS P.V., SHAW F.D. 1980. *Electrical stimulation of beef sides*. Meat Science, 4: 145–155.
- BOWLES AXE J.E., KASTNER C.L., DIKEMAN M.E., HUNT M.C., KROPF D.H., MILLIKEN G.A. 1983. *Effect of beef carcass electrical stimulation, hot boning, and aging on unfrozen and frozen longissimus dorsi and semimembranosus steaks*. Journal of Food Science, 48: 332.
- CHRYSTALL B.B., DEVINE C.E. 1978. *Electrical stimulation, muscle tension and glycolysis in bovine sternomandibularis*. Meat Science, 2: 49–58.

- CONTRERAS-CASTILLO C.J., LOMIWES D., WU G., FROST D., FAROUK M.M. 2016. *The effect of electrical stimulation on post mortem myofibrillar protein degradation and small heat shock protein kinetics in bull beef*. Meat Science, 113: 65–72.
- DEVINE C.E., WAHLGREN N.M., TORNBORG E. 1999. *Effect of rigor temperature on muscle shortening and tenderisation of restrained and unrestrained beef m. longissimus thoracicus et lumborum*. Meat Science, 51: 61–72.
- DUTSON T.R., SMITH G.C., CARPENTER Z.L. 1980. *Lysosomal enzyme distribution in electrically stimulated bovine muscle*. Journal of Food Science, 45: 1097–1098.
- EIKELENBOOM G., SMULDERS F.J.M., RUDÉRUS H. 1985. *The effect of high and low voltage electrical stimulation on beef quality*. Meat Science, 15: 247–254.
- EIKELENBOOM G., BARNIER V.M.H., HOVING-BOLINK A.H., SMULDERS F.J.M., CULIOLI J. 1998. *Effects of pelvic suspension and cooking temperature on the tenderness of electrically stimulated and aged beef, assessed with shear and compression tests*. Meat Science, 49: 89–99.
- FERGUSON D.M., JIANG S.T., HEARNshaw H., RYMILL S.R., THOMPSON J.M. 2000. *Effect of electrical stimulation on protease activity and tenderness of M. longissimus from cattle with different proportions of Bos indicus content*. Meat Science, 55: 265–272.
- FRITZ J.D., DIETRICH L.J., GREASER M.L. 1992. *Cooking effects on titin in fresh and processed beef products*. Journal of Muscle Foods, 3: 133–140.
- GARIEPY C., DELAQUIS P.J., AALHUS J.L., ROBERTSON M., LEBLANC C., RODRIGUE N. 1995. *Functionality of high and low voltage electrically stimulated beef chilled under moderate and rapid chilling regimes*. Meat Science, 39: 301–310.
- GEESINK G.H., VAN LAACK R.L.J.M., BARNIER V.M.H., SMULDERS F.J.M. 1994. *Does electrical stimulation affect the speed of ageing or ageing response?* Sciences des Aliments, 14 : 409–421.
- GEESINK G.H., KUCHAY S., CHISHTI A.H., KOOHMARAIE M. 2006. *Mu-calpain is essential for post-mortem proteolysis of muscle proteins*. Journal of Animal Science, 84(10): 2834–2840.
- HOSTETLER R.L., DUTSON T.R., SMITH G.C. 1982. *Effect of electrical stimulation and steak temperature at the beginning of cooking on meat tenderness and cooking loss*. Journal of Food Science, 47: 687–688.
- HUFF-LONERGAN E., ZHANG, W.G., LONERGAN S.M. 2010. *Biochemistry of postmortem muscle – Lessons on mechanisms of meat tenderization*. Meat Science, 86: 184–195.
- HWANG I.H., DEVINE C.E., HOPKINS D.L. 2003. *The biochemical and physical effects of electrical stimulation on beef and sheep meat tenderness*. Meat Science, 65: 677–691.
- JONES S.D.M., JEREMIAH L.E., TONG A.K.W., LUTZ S., ROBERTSON W.M. 1991. *The effects of marbling level, electrical stimulation, and post – mortem aging on the cooking and palatability properties of beef rib – eye steaks*. Journal of Animal Science, 71: 1037–1043.
- KADIM I.T., MAHGOUB O., KHALAF S. 2014. *Effects of the transportation during hot season and electrical stimulation on meat quality characteristics of goat Longissimus dorsi muscle*. Meat Science, 121: 120–124.
- KIM Y.H., LONERGAN S.M., GRUBBS J.K., CRUZEN S.M., FRITCHEN A.N., DELLA MALVA A, MARINO R., HUFF-LONERGAN E. 2013. *Effect of low voltage electrical stimulation on protein and quality changes in bovine muscles during postmortem aging*. Meat Science, 94: 289–296.
- LESIÓW T. 1993. *Zastosowanie elektrostymulacji w przetwórstwie mięsa bydłęcego*. Gospodarka Mięsna, 2: 22–25.
- MARTENS H., STABURVIK E., MARTENS M. 1982. *Texture and colour changes in meat during cooking related to thermal denaturation of muscle proteins*. Journal of Texture Studies, 13: 291–309.
- NAEWBANJ J.O., HARRISON D.L., STONE M.B. 1983. *Roasting vs cooking in a model system: tenderness of bull adductor muscle, conventionally chilled or electrically stimulated – hot boned*. Journal of Food Science, 48: 337–342.
- OLSSON U., HERTZMAN C., TORNBORG E. 1994. *The influence of low temperature, type of muscle and electrical stimulation on the course of rigor mortis, ageing and tenderness of beef muscles*. Meat Science, 37: 115–131.

- OSTOJA H., KORZENIOWSKI W. 1992. *Wpływ elektrostymulacji na niektóre cechy fizyczne wołowej tkanki mięśniowej*. Postępy Techniki Przetwórstwa Spożywczego, 1: 15–18.
- PALEARI M.A., BERETTA G., PANUNZI F., PARINI M., RASI M., CRIVELLI G., BERTOLO G. 1991. *Effect of extra low voltage on the carcass quality of cows*. Fleischwirtschaft, 5: 553–554.
- PALKA K., DAUN H. 1999. *Changes in texture, cooking losses, and myofibrillar structure of bovine m. semitendinosus during heating*. Meat Science, 51: 237–243.
- PN-ISO1442 (2000). *Meat and meat products. Determination of water content (reference method)*. Polish Committee for Standardization, Warsaw, Poland.
- POLIDORI P., KAUFFMAN R.G., VALFRE F. 1996. *The effects of electrical stimulation on meat quality*. Italian Journal of Food Science, 3: 183–193.
- POLIDORI P., ARIANI A., MICOZZI D., VINCENZETTI S. 2016. *The effects of low voltage electrical stimulation on donkey meat*. Meat Science, 119: 160–164.
- POSPIECH E., DZIERŻYŃSKA-CYBULKO B., ZUBIELIK P. 1992. *Analiza zmian glikolitycznych i kruchości mięśni bydlęcych poddanych elektrostymulacji niskonapięciowej*. Roczniki AR Poznań. Technologia Żywności, 17: 75–83.
- POWELL V.H. 1991. *Quality of beef loin steaks as influenced by animal age, electrical stimulation and ageing*. Meat Science, 30: 195–205.
- RASHID N.H., HENRICKSON R.L., ASGHAR A., CLAYPOOL P.L. 1983. *Biochemical and quality characteristics of ovine muscles as affected by electrical stimulation, hot boning, and mode of chilling*. Journal Food Science, 48: 136–140.
- RING C., TAYLOR A.A. 1988. *Electrical stimulation of slaughtered cattle*. Fleischwirtschaft, 9: 1157–1158.
- ROGOW I.A., MOJSENKO E.H. 1981. *Elektrostymulacja myszowej tkani gowjadyny*. Mjasno Industri, 2: 31–33.
- SAVELL J.W., MCKEITH F.K., SMITH G.C. 1981. *Reducing postmortem ageing time of beef with electrical stimulation*. Journal of Food Science, 46: 1777–1781.
- SHIVAS S.D., KASTNER C.L., DIKEMAN M.E., HUNT M.C., KROPF D.H. 1985. *Effects of electrical stimulation, hot boning and chilling on bull semimembranosus muscle*. Journal of Food Science, 50: 36–38.
- SMITH M.A., BUSH R.D., VAN DE VEN R.J., HOPKINS D.L. 2016. *Effect of electrical stimulation and ageing period on alpaca (Vicugna pacos) meat and eating quality*. Meat Science, 111: 38–46.
- SOARES G.J.D., AREAS J. A. G. 1995. *Effect of electrical stimulation on post mortem biochemical characteristics and quality of longissimus dorsi thoracis muscle from buffalo (Bubalus bubalis)*. Meat Science, 41: 369–379.
- SONAIYA E.B., STOFFER J.R., BEERMAN D.H. 1982. *Electrical stimulation of mature cow carcasses and its effect on tenderness, myofibril protein degradation and fragmentation*. Journal of Food Science, 47: 889–891.
- SORINMADE S.O., CROSS H.R., ONO K., WERGIN W.P. 1982. *Mechanisms of ultrastructural changes in electrically stimulated beef longissimus muscle*. Meat Science, 6: 71–77.
- StatSoft, Inc. 2011. STATISTICA (data analysis software system), version 10. www.statsoft.com.
- TOOHEY E.S., HOPKINS D.L., STANLEY D.F., NIELSEN S.G. 2008. *The impact of new generation pre-dressing medium-voltage electrical stimulation on tenderness and colour stability in lamb meat*. Meat Science, 79: 683–691.
- ZALEWSKI S. 1995. *Przemiany składników odżywczych w procesach kulinarnych*. Przegląd Gastro-nomiczny, 3: 3–7.
- ŻYWICA R., BUDNY J., CIERACH M. 1998. *Influence of high-voltage electrical stimulation on the structure of beef meat*. Polish Journal of Food and Nutrition Sciences, 2: 172–177.
- ŻYWICA R., BANACH J. K. 2014. *Device for electrostimulation of beef carcasses*. PL Patent No. 216791, Polish Patent Office, Warsaw.



Quarterly peer-reviewed scientific journal

ISSN 1505-4675  
e-ISSN 2083-4527

**TECHNICAL SCIENCES**

Homepage: [www.uwm.edu.pl/techsci/](http://www.uwm.edu.pl/techsci/)



## AN ANALYSIS OF THE POWER DEMAND AND ELECTRICITY CONSUMPTION OF AUTOMATIC PELLET BOILER

*Grzegorz Pełka, Wojciech Luboń, Daniel Malik*

Department of Fossil Fuels  
Faculty of Geology, Geophysics and Environmental Protection  
AGH University of Science and Technology

Received 5 July 2017; accepted 8 November 2017; available online 22 March 2018.

**Key words:** automatic pellet boiler, electricity consumption, power demand.

### Abstract

Pellet boilers are increasingly popular on the market, largely due to the fact that their use does not demand constant control by the user, but is reduced only to replenishing fuel and cleaning the combustion chamber and heat exchanger every few days. However, this functionality creates additional costs in terms of power consumption due to the work of boiler components, such as the pellet igniter, screw conveyors motors, fan, pump and controller. The purpose of this research was the analysis of the power demand and energy consumption of the electricity devices installed on the automatic pellet boiler in two operating modes, determining the total energy consumption and costs of electricity due to heating seasons in each mode. In the first mode, the boiler worked with modulated power, and in the second the boiler was working with nominal power. To carry out the mentioned research, a pellet boiler installed in the AGH UST Laboratory of Renewable Energy Sources in Miękinia was used. All the data obtained was used to simulate the total electricity consumption during one standard heating season and the costs involved. In the first case the boiler consumed 623,195 kWh of electricity per heating season and in the second the boiler consumed 304,503 kWh electricity per heating season. Although electricity consumption in the modulated mode is higher, the total cost of heating is lower, due to lower fuel consumption.

## Introduction

Today, when sustainable energy usage is a key element of the modern world and the EU has set itself the 3×20 target to achieve, the growth in renewable energy usage and improvements of energy efficiency is so important (RUOKAMO 2016), the pellet boilers can help to achieve each of the three goals, which emphasize the reduction of greenhouse gas emissions, growth in renewable energy usage and improvements of energy efficiency.

In recent years, pellets have become an important fuel for heat and electricity production in Europe. Pellets have a higher fuel density and hence demand less transportation and storage surface. In comparison with unprocessed biomass, pellets present a lower moisture content, higher effective heating value, uniform shape, clear burning and reduction of ashes (MOLA-YUDEGO et al. 2014). An increase in the Polish market of pellet boilers has also been observed. In 2014, 26,000 units of biomass boilers were sold and 14% of the total amount were pellet boilers (IEO 2015). Automatic solid fuel boilers need electricity to work, and the amount of the electricity is rarely stated by producers. Due to their fully automatic workings, the ease of boiler use, the small amount of ash and lack of pollution in the boiler room, all combine to make the pellet boiler increasingly popular (GÓRECKI et al. 2015).

Pellet boilers are devices which produce the lowest emissions of air pollutants compared to other solid fuel boilers, but the problem of hazardous substances in flue gas cannot be eliminated (BIERANOWSKI, OLKOWSKI 2009, MUSIL-SCHLÄFFER et al. 2010). Most pellet boilers offered on the market are of the fifth best class according to PN-EN 303-5:2012 standard (KACZMARCZYK et al. 2015). The nominal heating power efficiency currently produced pellet boilers is over 90% (SCHWARZ et al. 2011). According to CARLON et al. (2015) the annual efficiency (measured as a quotient heat produced by the boiler and energy consumed in the fuel) for standard house from 2004 was 83%, when efficiency during the standard testing conditions in nominal load was 93.2% and during the part load was 90.9%. The boiler work in modulating power mode.

The electricity demand of pellet boilers depends on the thermal power and equipment of the boiler. From 1<sup>st</sup> April 2017 energy labeling for solid fuels boilers has become obligatory. According to EU Commission Regulation No. 2015/1187 solid fuel boilers may exist in the class from G to A++, and from 26<sup>th</sup> September 2019 the energy labels will be from class D to A+++.

The electricity consumed by the boiler has a large influence on the final result of the energy label. Defining real electricity consumption is important to demonstrate the impact on the total costs caused by the consumption of energy by a pellet boiler. Data obtained are necessary to check real power and electricity consumption. The knowledge about power and electricity consumption is necessary for designing a self-supplying electricity system for a pellet boiler.

The main aim of the investigation was to determine the electricity consumption and power demand by a pellet boiler in the various operating modes of the boiler. The values are important for further research and the construction of a prototype of an energy generator for supplying the boiler. Furthermore, the total energy consumed by a pellet boiler and the costs of electricity was investigated. The costs generated by a pellet boiler are important for users. The results were discussed and the cheapest mode of pellet boiler operation was indicated.

## **Material and methods**

### **Description of pellet boiler**

The measurements were conducted in 2016 in the educational boiler room in the AGH UST Laboratory of Energy Sources and Energy Saving in Miękinia. The fully automatic pellet boiler with a nominal power 25 kW was used to carry out the research. It is a high-performance device (89–92%) and fulfills the requirements of a fifth-class boiler according to the PN EN 303-5:2012 standard. In the pellet boiler, there is a burner with modulated power ranging from 5 to 25 kW. The burner has an electric resistance igniter for the automatic ignition of pellets, a stoker feeding system to fuel supply to the grate and a moving grate for improving deash. The ash is removed from the burner by the air stream and the moving grate, which moves every five minutes. The ash is collected in the ash box and must be removed manually about every two weeks. The functionality of the pellet boiler is controlled by an electronic controller (technical documentation of pellet boiler, on-line).

The electric devices contained in a boiler are:

- pellet igniter,
- screw conveyors motors,
- fan,
- pump,
- controller.

The working parameters of particular components were set by the boiler installer.

The pellet boiler has four working stages. The first stage is ignition. It starts with switching on the fan, which removes ash from the burner. Then a starting dose of fuel is supplied to the burner, and the igniter is activated. The purpose of this step is to warm up the fuel to ignition temperature. The igniter works until a signal from the light sensor appears and the fan in this operating mode is in constant operation. The fuel is transported from hopper to burner using two different screw conveyors and these devices work periodically.

After ignition, the boiler goes into the heating operation mode. During the heating operation mode, the screw conveyor motor, fan and stoker are working. The circulation pumps are activated when the boiler obtain the expected temperature (in the analyzed case, only the central heating pump). The burner can work at four power levels. While working at nominal power, parameters such as time of fuel supply and airflow power are set by the user. In case of lower power usage etc.  $\frac{1}{2}$ ;  $\frac{1}{4}$ ;  $\frac{1}{8}$ , the time of fuel supply and fan power are properly reduced. The burner works with nominal power as long as the boiler water temperature remains at 7°C below the expected temperature. Above this temperature, the controller modulates the burner power.

When the expected temperature is reached, the boiler switches to extinguishing mode. During this stage, fuel is not supplied and the fan begins working at full power to finish burning the last fuel and to blow ash from the burner.

After extinguishing mode, the burner goes over to standby mode, while the controller measures the temperature of the water supply. When the temperature is lower than the expected temperature minus the modulation temperature, the boiler starts the ignition process again.

A simplified algorithm for the operation of the pellet boiler is shown on Figure 1. When the process starts, a controller measures the light intensity on the burner. If the measurement is higher than 200 [-] the boiler runs, otherwise an outflow water temperature measurement is conducted. The controller starts the ignition mode when the outlet water temperature is lower than the set temperature minus the outflow water hysteresis, otherwise the controller is on standby. Ignition end when the light intensity on the burner is higher than 200 [-] and then the heating mode operation is initiated. Heating power in this mode is independent of the current temperature of water exiting from the boiler. When this temperature exceeds a set temperature, the extinguishing mode begins. The last stage is standby mode where the controller measures light intensity on the burner and the temperature of outflow water. The working stage depends on the settings of the device parameters and current heat power demands of the building.

### **Description of measurements**

Power demand and energy consumption were measured by a single-phase electricity meter using the RS485 communication protocol to send data to a computer. Measurements of power demand were made separately for each device and in every mode of the operation of the pellet boiler.

Electricity consumption measurements were also conducted during every operating mode: initiating the burner, working with modulated power, extinguishing and standing by. The received values were read for ten minutes and recorded automatically every five seconds. In later considerations, averaged values were used.

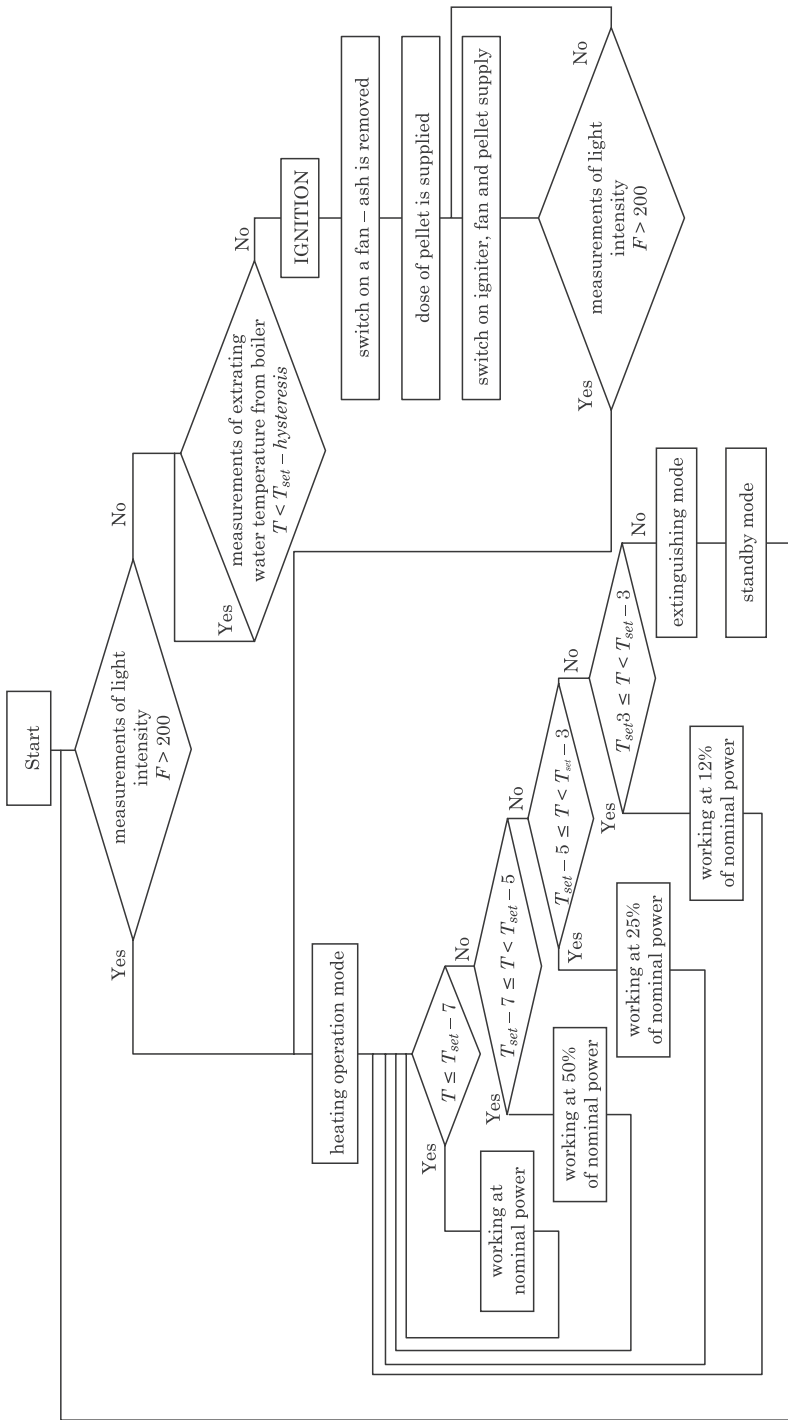


Fig. 1. Pellet boiler's work algorithm. F is a value of light intensity readied by photoresistor,  $F \in <0,1000>$ .  $T_{set}$  is a value of set temperature. T is a current temperature

## Simulation

The calculations of the energy consumption under the two different operation systems (modulated and constant power) of the boiler were conducted.

The data presenting the typical yearly weather and statistical climate information for Krakow to calculate energy consumption was collected from the Ministry of Infrastructure and Construction website ([www.miib.pl](http://www.miib.pl), on-line).

Simulations were conducted in a developed spreadsheet for a theoretical single family detached home. All parameters of the building were assumed, internal gains were 20 kWh/m<sup>2</sup>a and external (solar) gains were 50 kWh/m<sup>2</sup>a. The heat energy demand is 25 kW and heating area is 250 m<sup>2</sup>. The location is in the third climate zone (according to standard PN-EN 12831) with an external design temperature equaling -20°C. The analysis was performed with the assumption that the heating season lasts for nine months – from September to May.

In the first scenario the controller modulates the power of boiler to maintain a constant temperature inside the building (20°C). The burner can work at full-power or with reduced power (50%, 25%, 12,5%). The controller chooses the intervals of work with appropriate power to cover the temporary heating power demands of the building. The temperature inside the building can increase above 20°C only when the temperature outside is higher than 20°C. The boiler switches on when the risk of an inside temperature reduction below 20°C occurs.

The second scenario assumes the boiler working with nominal power (25 kW), in order to maintain a temperature inside the building between 20°C and 22°C. This scenario also assumes that heat will be accumulated in the building's construction. An established range of temperature changes are dictated by thermal comfort inside the building. The boiler is turned on when temperature inside the building drops below 20°C and it is turned off when the temperature inside the building increases above 22°C.

The assumption of different temperatures for both scenarios is deliberate. In a scenario with modulating power the indoor temperature is possible to achieve by choosing boiler power properly while in a scenario with constant power it is necessary to assume that the temperature range inside of the building is changing. It is due to the building's construction acting as an accumulator of energy produced by the boiler and it is a disadvantage of this solution.

## Results and discussion

### Results of laboratory tests

The results of the measurements of power demand are shown in Table 1. The igniter has the highest power consumption among the all components of boiler. The pump can work with three different power values, depending on flow resistances occurring in central heating installation. The measurement of the grate's motor and controller's monitor did not result in any power consumption, due to their small power demands. For this reason, the controller's monitor power demand was not taken into consideration in further calculations and the grate's motor power demand was taken from technical documentation. The average values of power demand are presented in Table 1.

Table 1  
Results of measurements of power demand (average values)

Device	Power [W]	
Fan	25	
Pellet igniter	215	
Fuel hopper conveyor motor	31	
Mechanical stoker	32	
Grate motor	2	
Pump	speed III	78
	speed II	62
	speed I	55

During measurement the pellet boiler worked continuously with a nominal heating power (25 kW) for 85 minutes and consumed 0.13 kWh of energy. Minimal power demand was 23 W (when only the fan was working) and maximal power demand was 362 W (when creating an ignition, the fan and screw conveyor motors are working). The average power demand of the pellet boiler was 91 W. According to research conducted in the Austrian Bioenergy Centre GmbH, different pellet boilers at full load and under electrical demand give results ranging from 0.2 to 1.8% nominal heat capacity (MOSER et al. 2006). According to LAICANE et al. (2015), for a 15 kW pellet boiler, the electricity power demand is 150 W. During winter the boiler works 24 hours per day to ensure continuous operation. The electricity demand in pellet boilers also depends on the operation mode. For example, a 10 kW boiler in the on/off mode can consume as much as 172 W, but in modulating power mode, when the same boiler can work with constant heating power at 3 kW, the power demand can be reduced to 95 W (HALLER, KONERSMANN 2008). The tested boiler showed a lower power demand than quoted examples.

## Simulation results

The results of calculations from both scenarios are presented in Table 2 and Table 3. A simulation of a scenario in which the boiler is working with modulated power showed that the boiler would work for 6,134 hours and would be switched off 356 times. In this time it would consume 623,195 kWh energy at a cost of 405.08 PLN (0.65 PLN for 1 kWh). The highest power consumption during the heating season was caused by the central heating pump (more than 402 kWh). Energy consumption by the circulating pump alone represented 64.57 percent of the total energy consumption by the heating installation.

In the second case (working at only 25 kW heating power) the pellet boiler would work 2,596 hours and be switched off 143 times. During the operation, the boiler would consume 304,503 kWh of energy, at a cost of 197.93 PLN. As before, the highest consumer of energy was the circulating pump. It represents 53 percent of the total energy consumption in this mode.

Due to the hysteresis of the internal temperature of 2 K, in the nominal operating mode, the number of boiler launches was lower than in the modulated mode. In the case of lowering the internal temperature hysteresis, the number of boiler outputs for nominal power would far exceed that of a boiler with modulated power.

In fact, the amount of energy and cost of electricity consumption depends on many factors. The first one is the climatic zone in which the building is located. The colder the climate, the higher the heat demand and the resulting longer working of the boiler and higher costs. The second factor are the applied sets of devices which are installed in the boiler and their individual parameters (the number of pumps, an additional mechanism to remove ash and soot, etc.). The mentioned simulations assumed two extreme ways of using the boiler while the real energy consumption would depend on user habits and expected thermal comfort.

The analysis of the total cost of heating has also been conducted. Pellet boiler a seasonal efficiency in the first scenario is assumed as 75% and in the second case is assumed as 83% (according similar conditions as the CARLON et al. 2015). In the first scenario efficiency is reduced by reason of part load working and twice more ignitions. To assume more detailed efficiencies for the considered boiler there are need conduct experimental tests of the system (CARLON et al. 2016). The cost of the pellets would be 8,847.30 PLN if the boiler would work with modulated power and 8,474.20 PLN if the boiler would work with constant power. In the scenario with modulated power, the total cost would be 9,252.38 PLN. In the second scenario, the total cost would be 8,672.13 PLN and lower by 6.67% than the first scenario. Although maintaining a higher temperature in the building (from 20°C to 22°C instead a constant 20°C), the total costs of heating would be lower, because the boiler efficiency is higher and thus cause lower fuel consumption. All costs are presented in Table 4.

Table 2

Energy consumption of a particular electric devices during a heating season  
where the controller modulates the boiler power

Phase	Device	Function	Power [W]	Time [s]	Energy consumption [kWh]	Cost [PLN]	Share [%]	
Ignition	fan	scavenge	28	10,680	0.083	0.05	0.01	
		working	24	32,040	0.214	0.14	0.03	
	fuel hopper conveyor motor	fuel supply	31	10,680	0.092	0.06	0.01	
	mechanical stoker	fuel supply	32	10,680	0.095	0.06	0.02	
	pellet igniter	ignition	215	32,040	1.914	1.24	0.31	
Operating mode	fan	working at 100% of power	29	1,296,142	10.441	6.79	1.68	
		working at 50% of power	27	10,648,838	79.866	51.91	12.82	
		working at 25% of power	26	7,386,292	53.345	34.67	8.56	
		working at 12.5% of power	24	2,752,085	18.347	11.93	2.94	
	fuel hopper conveyor motor	fuel supply	31	25 kW	457,623	8.008	5.21	1.29
			31	12.5 kW	1,879,868	32.898	21.38	5.28
	mechanical stoker		32	6.25 kW	651,961	11.409	7.42	1.83
			32	3.125 kW	121,458	2.126	1.38	0.34
	grate motor	cleaning the burner	2	1,752,647	0.974	0.63	0.16	
	pump	speed III	78	–	–	–	–	
speed II		62	22,083,358	380.324	247.21	61.03		
speed I		55	–	–	–	–		
Extinguishing	mechanical stoker	exhaustion of stoker	32	14,240	0.127	0.08	0.02	
	fan	scavenge	29	106,800	0.860	0.56	0.14	
		speed III	78	–	–	–	–	
	pump	speed II	62	1,281,600	22.072	14.35	3.54	
		speed I	55	–	–	–	–	
SUM				25,194,269	623.195	405.08	100.00	

Table 3

Energy consumption of a particular electric devices during a heating season where the boiler is working with nominal power

Phase	Device	Function	Power [W]	Time [s]	Energy consumption [kWh]	Cost [PLN]	Share [%]	
Ignition	fan	scavenge	28	4,290	0.033	0.02	0.01	
		working	24	12,870	0.086	0.06	0.03	
	fuel hopper conveyor motor	fuel supply	31	4,290	0.037	0.02	0.01	
	mechanical stoker	fuel supply	32	4,290	0.038	0.02	0.01	
	pellet igniter	ignition	215	12,870	0.769	0.50	0.25	
Operating mode	fan	working at 100% of power	29	9,342,000	75.255	48.92	24.71	
		working at 50% of power	27	–	–	–	–	
		working at 250% of power	26	–	–	–	–	
		working at 12.5% of power	24	–	–	–	–	
	fuel hopper conveyor motor	fuel supply	31	3,298,337	57.721	37.52	18.96	
	mechanical stoker	fuel supply	32				0.00	
	grate motor	cleaning the burner	2	741,429	0.412	0.27	0.14	
	pump	speed III	78	–	–	–	–	
		speed II	62	9,342,000	160.890	104.58	52.84	
		speed I	55	–	–	–	–	
Extinguishing	mechanical stoker	exhaustion of stoker	32	5,720	0.051	0.03	0.02	
	fan	scavenge	29	42,900	0.346	0.22	0.11	
		speed III	78	–	–	–	–	
		pump	speed II	62	514,800	8.866	5.76	2.91
			speed I	55	–	–	–	–
SUM			23,325,796	304.503	197.93	100.00		

Table 4

Results of the analysis of the total cost of heating, including the cost of fuel

Scenario	Heat demand [kWh]	The boiler efficiency [-]	The amount of energy supplied as pellets [kWh]	The energy value of pellets [kWh/kg]	The weight of pellets [t]	The price of pellets [PLN/t]	The cost of pellets [PLN]	The cost of electricity [PLN]	The share of electricity in costs [%]	Total costs [PLN]
Constant power 25 kW	50,241	0.83	60,531	5	12.106	700	8,474.20	197.93	2.34	8,672.13
Modulated power	47,397	0.75	63,196		12.639		8,847.30	405.08	4.58	9,252.38

## Conclusions

In this paper the power demand of particular devices of a pellet boiler and an average power demand of the whole boiler are specified, amounting to 91 W. The highest electricity consumption from all of the electric devices installed in the pellet boiler comes from the circulating pump. Circulating pumps working in an installation should be high-quality pumps of the highest energy class and thus low power consumption.

The cost of the power consumption of a pellet boiler is strongly dependent on its manner of usage. The paper presents the electricity consumption of a pellet boiler in two extremely different ways of using boilers. The foregoing calculations have shown that the cost of electricity in a scenario where the boiler works at nominal power is half as cheap. Unfortunately, it is associated with a lower level of comfort, due to the temperature fluctuations of 2°C a few hours. Despite the fluctuations of temperature occurs, the final energy consumption and the costs are lower when the boiler works with constant power and this is caused by burning less fuel connected with higher boiler efficiency. Modulating power boiler increase thermal comfort inside the building but raises costs of exploitation. Buffer tank usage could be solve the problem with lower thermal comfort connected with using constant power pellet boiler. But it could increase the pellet consumption due to decrease overall system efficiency.

The analysis of power demand and energy consumption of particular pellet boilers devices will be used to conduct further investigations about alternative power supplies for these kinds of boilers.

### Acknowledgments

The paper was prepared under AGH-UST statutory research grant No. 11.11.140.031.

## References

- BIERANOWSKI J., OLKOWSKI T. 2009. *Comparison of combustion gas emission by low power boilers fired by biomass obtained from wood-pellets*. Technical Sciences, 12.
- CARLON E., SCHWARZ M., GOLICZA L., VERMA V.K., PRADA A., BARATIERI M., HASLINGER W., SCHMIDL CH. 2015. *Efficiency operational behavior of small-scale pellet boilers installed in residential buildings*. Applied Energy, 155: 854–865.
- CARLON E., SCHWARZ M., PRADA A., GOLICZA L., VERMA V.K., BARATIERI M., GASPARELLA A., HASLINGER W., SCHMIDL CH. 2016. *On-site monitoring and dynamic simulation of low energy house heated by a pellet boiler*. Energy and Buildings, 116: 296–306.
- Commission Delegated Regulation (EU) 2015/1187 of 27 April 2015 supplementing Directive 2010/30/EU of the European Parliament and of the Council with regard to energy labelling of solid fuel boilers and packages of a solid fuel boiler, supplementary heaters, temperature controls and solar devices.

- GÓRECKI W., HAŁAJ E., KOTYZA J., SOWIŹDŹAŁ A., LUBOŃ W., PELKA G., WOŚ D., KACZMARCZYK M., HAJTO M., KACZMARCZYK M., LACHMAN P. 2015. *Efficient use of renewable energy sources*. SOLGEN Sp. z o.o., Kraków.
- HALLER M., KONERSMANN L. 2008. *Energy efficiency of combined pellets and solar heating systems for single family houses*. World Bioenergy 2008, Conference and Exhibition on Biomass for Energy, 27–29 May 2008, Jönköping, Sweden.
- Raporty 2015 z sektorów energetyki odnawialnej. Kolektory słoneczne, fotowoltaika i kotły na biomasę*. 2015. Instytut Energetyki Odnawialnej. InstalReporter, 10: 23–26.
- KACZMARCZYK M., KACZMARCZYK M., PELKA G., LUBOŃ W., BĘDKOWSKA A., PIECHOWICZ Ł., CIAPAŁA B., BLOK M. 2015. *Niska emisja. Od przyczyn występowania do sposobów eliminacji*. Geosystem Burek Kotyza s.c., Kraków.
- LAICANE I., BLUMBERGA D., BLUMBERGA A., ROSA M. 2014. *Evaluation of household electricity savings. Analysis of household electricity demand profile and user activities*. International Scientific Conference “Environmental and Climate Technologies – CONNECT 2014”, Energy Procedia, 72: 285–292.
- Ministry of Infrastructure, Statistical Climate Information for Krakow, online: <http://mib.gov.pl/2-567022e59f3f6.htm> (access: April 2016).
- MOLA-YUDEGO B., SELKIMAKI M., GONZALES-OLABARRIA J.R. 2014. *Spatial analysis of the Wood Pellet production for energy in Europe*. Renewable Energy, 63: 76–83.
- MOSER W., FRIEDL G., HASLINGER W., HOFBAUER H. 2006. *Small-scale pellets boiler with thermoelectric generator*. International Conference on Thermoelectrics, Vienna.
- MUSIL-SCHLÄFFER B., MCCARRY A., SCHMIDL C., HASLINGER W. 2010. *European wood-heating technology survey: an overview of combustion principles and the energy and emissions performance characteristics of commercially available systems in Austria, Germany, Denmark, Norway and Sweden*. New York State Energy Research And Development Authority.
- PN-EN 303-5:2012: Heating boilers. Heating boilers for solid fuels, manually and automatically stoked, nominal heat output of up to 500 kW. Terminology, requirements, testing and marking.
- PN-EN 12831:2006: Heating systems in buildings. Method for calculation of the design heat load.
- RUOKAMO E. 2016. *Household preferences of hybrid home heating systems – A choice experiment application*. Energy Policy, 95.
- SCHWARZ M., HECKMANN M., LASSELSBERGER L., HASLINGER W. 2011. *Determination of annual efficiency and emission factors of small-scale biomass boiler*. Central European Biomass Conference 2011.
- Technical documentation of pellet boiler Kolton Pellmax 25, on-line: [http://www.kolton.pl/\\_pliki/instrukcja-pellmax-012014,41092.pdf](http://www.kolton.pl/_pliki/instrukcja-pellmax-012014,41092.pdf) (access: April 2016).





Quarterly peer-reviewed scientific journal

ISSN 1505-4675  
e-ISSN 2083-4527

**TECHNICAL SCIENCES**

Homepage: [www.uwm.edu.pl/techsci/](http://www.uwm.edu.pl/techsci/)



## INFLUENCE OF FASTENERS AND CONNECTIONS FLEXIBILITY ON DEFLECTIONS OF STEEL BUILDING INCLUDING THE STRESSED SKIN EFFECT

*Natalia Korcz, Elżbieta Urbańska-Galewska*

Department of Metal Structures and Construction Management  
Faculty of Civil and Environmental Engineering  
Gdańsk University of Technology

Received 8 May 2017; accepted 22 January 2018; available online 14 March 2018.

**Key words:** steel structures, diaphragm design, trapezoidal sheeting, orthotropic plate model, structure displacement, fastener flexibility.

### Abstract

The paper presents the analysis of the influence of fasteners and connections flexibility on displacements of symmetrical single-bay pitched-roof steel building, including trapezoidal cladding acting as a diaphragm. The purpose of the article was to compare numerical models with and without taking into consideration fasteners and connections flexibility in order to observe the differences in transverse stiffness of the building during modifying model from the simple one to more complex and precise. The analyses were carried out for the 3D structure. Fasteners and connections were substituted by equivalent beam finite elements. Corrugated sheets were replaced by three types of equivalent orthotropic shell models and the influence of the choice of the model on the stiffness of the building was observed. The results showed that in the analysed structure the flexibility of fasteners and connections has negligible effect on transverse displacements of the building in the case of four sides fastening of the sheeting, however in the case of two sides fastening the influence significantly increases.

### Abbreviations

- ARSA – Autodesk Robot Structural Analysis Professional 2015
- ER – European Recommendations for the Application of Metal Sheeting Acting as a Diaphragm. Stressed Skin Design. 1995. ECCS – TC7, TWG 7.5
- P1 – structural models without cladding
- T1, T2, T3 – structural models with the stressed skin effect included; without fasteners and connectors (T1), with purlin/rafter connections and shear connector fasteners (T2), with purlin/rafter connections, shear connector fasteners and sheet/purlin fasteners (T3)

Correspondence: Natalia Korcz, Katedra Konstrukcji Metalowych i Zarządzania w Budownictwie, Wydział Inżynierii Lądowej i Środowiska, Politechnika Gdańska, ul. G. Narutowicza 11/12, 80-233 Gdańsk, e-mail: [natkorc1@pg.edu.pl](mailto:natkorc1@pg.edu.pl)

- M0, MA, MB – types of sheeting model used in structural models: infinitely rigid plate (M0), pre-defined orthotropic plate with the trapezoid plate geometry selected by user (MA), orthotropic plate with orthotropic matrix calculated and defined by user (MB)
- 2K/4K – two/four sides fastening of the shear panel
- $\Delta$  – displacement measured in mm
- $c$  – in-plane shear flexibility of panel measured in mm/kN

## Introduction

Trapezoidal cladding of the steel building has an undeniable effect on the stiffness and spatial character of work of the structure and, by extension, on deflections and cross-sectional forces of particular structural members. Although the idea of stressed skin design (diaphragm design) has been widely known for many years, in traditional design it is usually omitted. It seems that the biggest obstacle which hinders the popularity of diaphragm design in engineering practice is the lack of enough universal, verified and simple to apply procedures. More and more effective methods of including the stressed skin effect in structural calculations are still being searched and developed. Examples can be found in BRÓDKA et al. (1999), EN-1993-1-3:2006, European Recommendations (ER) (1995) provided by European Convention for Constructional Steelwork (ECCS), GRYNIEWICZ and SZLENDAK (2016a, 2016b), JOÓ and DUNAI (2015), LENDVAI and JOÓ (2016), NAGY et al. (2015, 2016). The development of numerical tools which support engineers in static and dynamic analysis of the structure brings new capabilities to take into account the diaphragm effect, which seems to be more and more economy-reasonable approach.

The basis of the work on the stressed skin effect is ER (1995) whereby the definition of the diaphragm (shear panel) depends on the orientation of the sheeting spanning in regard to the length of the diaphragm: perpendicular – typical for purlin systems (Fig. 1) or parallel – typical for non-purlin systems. The dimension  $a$  of the panel is always perpendicular and the dimension  $b$  – parallel to corrugation (Fig. 1). Moreover, the procedures differentiate two static

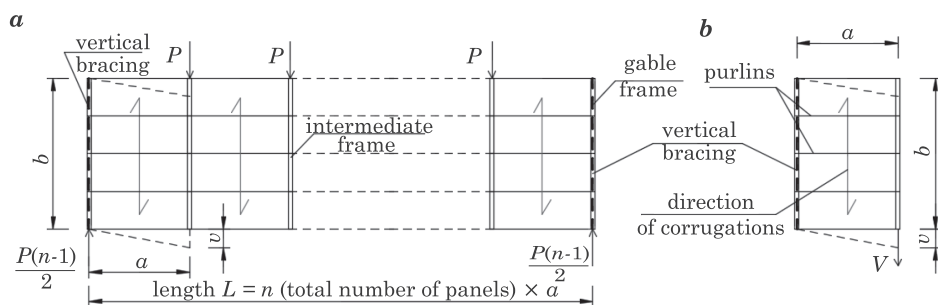


Fig. 1. Static schemes of the diaphragm:  $a$  – panel assembly,  $b$  – cantilevered diaphragm

schemes of the diaphragm, depending on the arrangement of vertical bracings (the elements, which bring forces to the foundation, for instance bracings of gable wall). According to this classification „panel assembly” („diaphragm beam”) and „cantilevered diaphragm” can be recognised (see Fig. 1).

The diaphragm is characterised not only by the cross-section of the trapezoidal sheeting, but also by fasteners: sheet/purlin fasteners, seam fasteners (sheet/sheet fasteners) and sheet/shear connector fasteners. According to ER (1995), shear flexibility of the diaphragm  $c$  is the sum of a series of components. The origins of the shear flexibility are demonstrated in the axonometric view in Figure 2. Shear flexibility of the diaphragm is due to:

- sheet deformation: profile distortion ( $c_{1,1}$ ) and shear strain ( $c_{1,2}$ ),
- fasteners deformation: sheet/purlin fasteners ( $c_{2,1}$ ), seam fasteners ( $c_{2,2}$ ) and connections to rafters ( $c_{2,3}$ ),
- flange forces: axial strain in purlins ( $c_3$ ).

Therefore, there are two main aspects of including the diaphragm effect in 3D numerical analysis of the structure – consideration of the flexibility of:

- steel trapezoidal sheets,
- fasteners and connections.

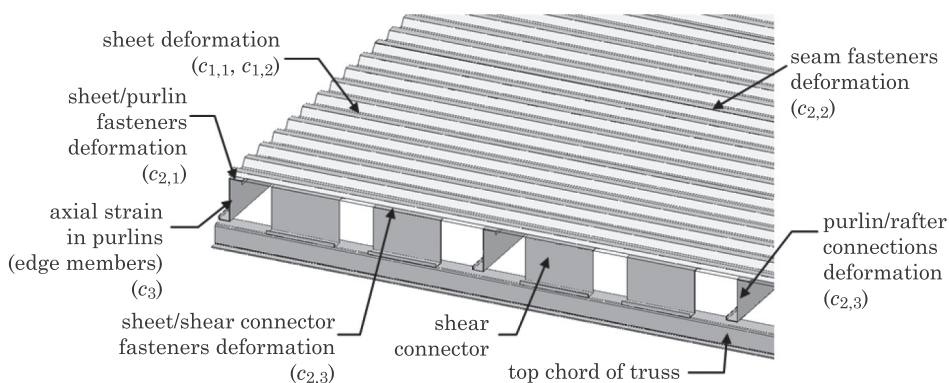


Fig. 2. Components of shear flexibility

The conventional ways of including the stressed skin effect, proposed in ER (1995), consider both of these aspects in one tool. According to ER (1995), the flexibility of diaphragm can be substituted by springs located in the plane of the roof, whose stiffness corresponds with the analytically-calculated shear flexibility  $c$  of the panel (Fig. 3a, c), what is described for instance by KOWALCZYK and NOWICKI (2003). The diaphragm effect in 3D numerical model of the structure can be also included using diagonal bracing model of the roof panel (X type bracing). Then the analytically-calculated shear flexibility  $c$  of the diaphragm is implemented in the computational model of the structure by appropriate EA

stiffness of the equivalent braces (Fig. 3a, b), which is introduced for example by NIEWIADOMSKI (2011), GOCZEK (2013). Nonetheless, more accurate model using more advanced and simultaneously more and more available computational tools are still being searched. Wide-ranging analyses using link elements which connect structural members in order to include the stressed skin effect are submitted by NAGY et al. (2016).

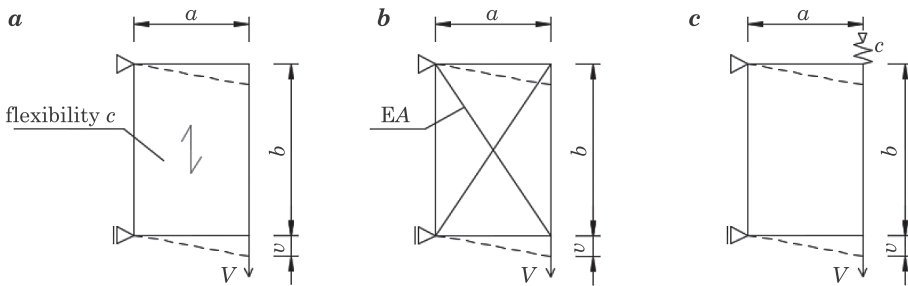


Fig. 3. Shear panel models: *a* – with sheeting, *b* – with braces (equivalent longitudinal stiffness *EA*), *c* – with lateral spring (equivalent flexibility)

Other way to include the stressed skin effect in 3D numerical model of the structure is to substitute trapezoidal sheeting by an orthotropic 2D shell model, which is schematically shown in Figure 4. The idea of this process is to find the equivalent stiffness matrix of orthotropic shell which reflects different stiffness of steel trapezoidal sheeting in perpendicular directions. Obviously this approach is only an approximation, assuming for example the symmetrical cross-section of the cladding and that the dimension of one period of corrugation is small in comparison to the dimension of the sheet. What is more, local changes of stiffness are not recognised.

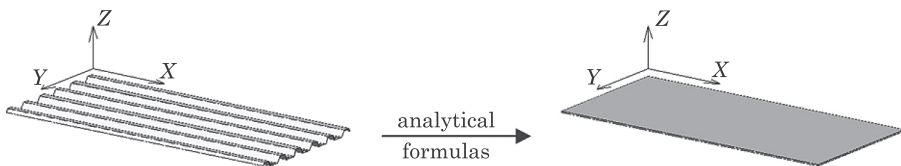


Fig. 4. The idea of substitution the fully 3D-modelled trapezoidal sheeting by the orthotropic 2D shell model according to WENBERG et al. (2011)

Different analytical expressions for stiffness matrix of equivalent orthotropic shell for trapezoidal sheeting are known (BRÓDKA et al. 1999, GRYNIEWICZ, SZLENDAK 2016a, 2016b, WENBERG et al. 2011, XIA et al. 2012). What is more, in computational programs for numerical 3D analysis of the structures

(for instance ARSA, RFEM) the tools (predefined orthotropic shells/plates), which allow the user to select the trapezoidal plate geometry instead of define stiffness matrix of equivalent orthotropic shell, are implemented. Matrix values are calculated by the program on the basis of the geometrical parameters and the user is no longer obliged to calculate the matrix values himself (Autodesk Robot Structural Analysis Professional 2015). It is necessary to emphasize that the analytical procedures for the stiffness matrix of equivalent orthotropic plate for trapezoidal sheeting, both known from the literature and implemented in numerical programs, diverge considerably.

In the article KORCZ (2017) the comparison and evaluation of numerical models of trapezoidal sheeting, by example of cantilevered diaphragm, is presented. Analyses are run in ARSA. Due to the way of definition, two groups of models are distinguished:

- predefined orthotropic shell with trapezoidal geometry selected by user (MA),
- orthotropic shell with orthotropic matrix calculated and defined by user (MB).

Analysed models are built by trapezoidal sheeting, purlins, top chords of truss girders, fasteners and connections. Models (MB) are built using analytical formulas for stiffness matrix of equivalent orthotropic plate for trapezoidal sheeting chosen based on WENBERG et al. (2011), XIA et al. (2012), GRYNIEWICZ and SZLENDAK (2016a, 2016b). Selected procedures, with all used expressions and the convention of orthotropic directions, are introduced precisely by KORCZ (2017). In particular, membrane stiffness matrix  $D$  value is calculated in compliance with formulas (1–6):

$$D = \frac{t}{1 - \nu_{xy} \cdot \nu_{yx}} \begin{bmatrix} E_x & \nu_{yx} \cdot E_x & 0 \\ \nu_{xy} \cdot E_y & E_y & 0 \\ 0 & 0 & (1 - \nu_{xy} \cdot \nu_{yx}) \cdot G_{xy} \end{bmatrix} \quad (1)$$

$$E_x = E \cdot \frac{l_p}{d} \quad (2)$$

$$E_y = E \cdot \frac{I_y^0}{I_y} \quad (3)$$

$$\nu_{yx} = \nu \cdot \frac{E_y}{E_x} \quad (4)$$

$$\nu_{xy} = \nu \quad (5)$$

$$G_{xy} = \frac{a}{b \cdot t \cdot (c_{1,1} + c_{1,2})} \quad (6)$$

where:

- $t$  – thickness of trapezoidal sheeting = thickness of equivalent orthotropic plate,
- $\nu, E$  – Poisson's ratio and elasticity modulus of steel material,
- $I_y^0$  – equivalent plate moment of inertia,
- $I_y$  – trapezoidal plate section moment of inertia,
- $l_p$  – the developed width of one corrugation,
- $d$  – width of one corrugation,
- $a, b$  – dimensions of the shear panel (Fig. 1),
- $c_{1,1}, c_{1,2}$  – flexibility components according to ER (1995).

The most important factor, which distinguishes (MA) and (MB) models, is  $D_{33}$  element of the membrane stiffness matrix  $\mathbf{D}$  (circa 5 times difference). In ARSA-implemented procedures (MA) this element is dependent on cross-section geometry and material properties only, according to formula (7). In model (MB) formula (8) is used – much more data are taken into account: dimensions of the shear panel ( $a, b$ ) and flexibility components  $c_{1,1}$  and  $c_{1,2}$  according to ER (1995). In particular, flexible component  $c_{1,1}$  (the result of profile distortion) depends not only on the sheet geometry but also among others on the way of sheet/purlin fastening (in every corrugation/in every double corrugation) and on the number of sheets in the width of the panel assembly.

$$D_{33}(\text{MA}) = \frac{E}{2(1 + \nu)} \cdot t \cdot \frac{d}{l_p} \quad (7)$$

$$D_{33}(\text{MB}) = \frac{a}{b \cdot (c_{1,1} + c_{1,2})} \quad (8)$$

The evaluation of numerical models of trapezoidal sheeting depends on the degree of the agreement between the numerical and analytical results calculated according to ER (1995). In compliance with this criterion, better accuracy characterised model (MB), so this model should be used in numerical calculations of the whole structure instead of model (MA).

Likewise, the flexibility of connections and fasteners used in the roof panels has strong effect on the flexibility of the whole roof diaphragm. It can be modelled by two perpendicular springs connected to two nodes with zero distance and with stiffness corresponding to the force-displacement relationship of connector (usually linear approximation is used in practice), what is described by BRÓDKA et al. (1999).

Another approach is to take into consideration not only theoretical slip  $s$  of fasteners and other connections, but also their placement, using equivalent cantilever finite beam elements (Fig. 5), introduced by GRYNIEWICZ and SZLENDAK (2016a, 2016b). Knowing theoretical slip  $s$  and expression for maximum displacement of the cantilever under the concentrated force applied at the free end,

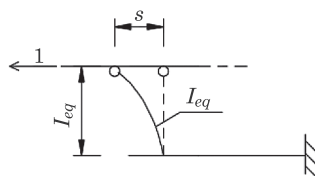


Fig. 5. Model of the fastener or connection – general concept according to GRYNIEWICZ and SZLENDAK (2016b)

for chosen length  $l_{eq}$ , moment of inertia  $I_{eq}$  of equivalent finite element can be calculated using formula (9). This method is implemented in the analyses of cantilevered diaphragm carried out by KORCZ (2017).

$$I_{eq} = \frac{l_{eq}^3}{3sE} \quad (9)$$

The aim of the analysis described in this article was to make an assessment of the influence of including in numerical model fasteners and connections flexibilities and placement of them (which are the component of diaphragm flexibility), on transverse deflections of the steel building. Moreover, the comparison between two types of models of trapezoidal sheeting (MA) and (MB), presented by KORCZ (2017) was continuing. In order to make analyses more complete, third model of trapezoidal sheeting (M0) – the infinitely rigid plate – was added.

The transition between cantilevered diaphragm and panel assembly as a part of the whole structure showed how the choice of the model (M0/MA/MB) effects on the displacements of the structure. Two main aspects of including the diaphragm effect in 3D numerical analysis of the structure (consideration of the flexibility of steel trapezoidal sheets and fasteners and connections flexibility) were accomplished using procedures presented by KORCZ (2017). The structure was built patterned on the building analysed by DENIZIAK et al. (2015). Both the structure model and numerical methods are described in further chapters.

## Material and methods

### Numerical model of the structure – general description

3D numerical model of the steel structure of the single-bay pitched-roof building was built following the single-storey building analysed by DENIZIAK et al. (2015). The geometry of the building in axonometric view presents Figure 6. Axial dimensions were: 12.0 m (width), 30.0 m (length), 10.0 m (eave height), 10.53 m (ridge height). The roof structure of intermediate frames was a truss girder. Top and bottom chords of the trusses, main rafters of gable frames and

purlins were made with IPE section, diagonals of the trusses, beams and columns of gable wall with RHS section, bracings with  $\phi$ -bars. Two variants of columns of the main frames were used (HEB300 and HEB200). The other sections were invariable in all models. Specification of the applied elements is presented in Figure 6. The cladding of the roof was made with trapezoidal sheeting shown in Figure 7.

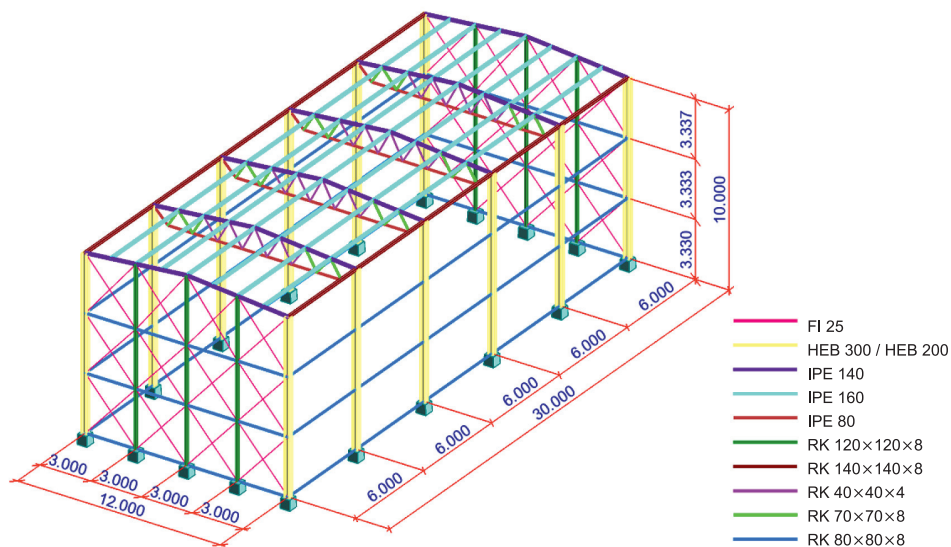


Fig. 6. Geometry and cross-sections of the analysed 3D steel structure

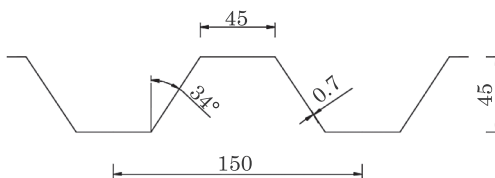


Fig. 7. Trapezoidal sheeting geometry [mm]

Maximal values of deflection of the single-storey building structure in transverse direction was observed, so only the wind blowing perpendicular to the length of the building was taken into consideration. Following load cases were considered:

- G – dead loads (generated automatically);
- S1 – symmetric snow load; according to EN-1991-1-3:2003; characteristic value:  $s=0.96 \text{ kN/m}^2$ ;
- W1 – wind load in the perpendicular direction to the length of the building with suction on downwind surface and no pressure on upwind surface

of the roof; according to EN-1991-1-4:2004 and National Annex PN-EN-1991-1-4:2008; characteristic values of loads for particular areas:  $w_{e,A} = -0.97 \text{ kN/m}^2$ ,  $w_{e,B} = -0.65 \text{ kN/m}^2$ ,  $w_{e,D} = 0.63 \text{ kN/m}^2$ ,  $w_{e,E} = -0.38 \text{ kN/m}^2$ ,  $w_{e,F} = w_{e,G} = w_{e,H} = 0 \text{ kN/m}^2$ ,  $w_{e,I} = w_{e,J} = -0.49 \text{ kN/m}^2$ ;

– W2 – wind in the perpendicular direction to the length of the building with suction on downwind and upwind surface of the roof; according to EN-1991-1-4:2004 and National Annex PN-EN-1991-1-4:2008; characteristic values the same as in case W1, except for:  $w_{e,F} = -1.38 \text{ kN/m}^2$  and  $w_{e,G} = -0.97 \text{ kN/m}^2$ .

In order to gain clear results and limit the number of variables, the analyses were conducted for one load combination:  $\text{KOMB1} = 1.35 \cdot \text{G} + 1.5 \cdot 0.5 \cdot \text{S1} + 1.5 \cdot 0.6 \cdot \text{W1}$ , which was built according to EN-1990:2002 and PN-EN 1990:2004 – *National Annex*. The same load combination as in DENIZIAK et al. (2015) was chosen, which allowed to use the same cross sections of the profiles and to compare the results of both analyses.

In the structure with the stressed skin effect included, the gable walls, as the support for the diaphragm, need to be stiff-braced. Simultaneously roof and longitudinal walls no longer need to be braced (bracing role is undertaken by the diaphragm). Essential elements of the structure are trapezoidal sheets and purlins, as subdivisions of the diaphragm. As it was proved by DENIZIAK et al. (2015), the stressed skin effect of wall's cladding is negligible for this particular building, loads and deflection observations. Therefore, in numerical models only roof diaphragms were included and wall's diaphragms were omitted. Due to the direction of wind load, also in model P1 (without cladding included) it was not necessary to use bracings in longitudinal walls – stability in this direction was achieved by purlins and eave beams.

Numerical analyses were run in ARSA. The main structure was applied as 3D beam finite elements (with real cross-sections). Corrugated sheets were replaced by two types of equivalent orthotropic shell models (chapter *Equivalent models of trapezoidal sheeting*). Fasteners and connections were substituted by equivalent beam finite elements (chapter *Connections and fasteners in numerical model*).

Columns were fix-supported in foundations and hinge-joined with truss girders. In diagonals of the trusses only axial forces acted and in bracings of the gable wall – only axial tensional forces. Other bars had neither advanced properties nor releases declared.

### Equivalent models of trapezoidal sheeting

The flexibility of steel trapezoidal sheeting was accomplished using procedures presented by KORCZ (2017) (chapter *Introduction*). Conclusions of that article cannot be generalized to the wider range of structures (not enough analyses were carried out). However the similarity of geometry of diaphragms analysed by KORCZ (2017) and in this article (the same dimensions  $a$  and  $b$  of the panel

– Fig. 1, the same cross section geometry of the sheeting – Fig. 7) allows to use models and observations introduced by KORCZ (2017) to present analysis. It is important to realise, that in KORCZ (2017) cantilever diaphragms were analysed, whereas in this paper panel assembly was applied. This fact was reflected in calculations of flexibility components  $c_{1,1}$  and  $c_{1,2}$ , so also in the stiffness matrix defined by user in model (MB), according to formulas (1) and (6).

In order to answer the question: how the differences in equivalent models (M0/MA/MB) of trapezoidal sheeting (chapter *Introduction*) translates into deflection's behaviour of the whole structure, analyses of the whole building were carried out, using (M0/MA/MB) model. Results were compared in chapter *Results and Discussion*.

### Connections and fasteners in numerical model

Equivalent numerical model of fasteners and other connections should take into consideration (with satisfactory accuracy) fasteners and connections flexibility with simultaneously slight complication of numerical model of the whole structure and slight increase of the file size. The approach introduced by GRYNIEWICZ and SZLENDAK (2016a) and implemented by KORCZ (2017) was adopted. Theoretical slip  $s$  of fasteners and other connections and their placement were modelled using equivalent cantilever finite beam elements (Fig. 5). The values of theoretical slip  $s$  were adopted from ER (1995). The exception was the flexibility of purlin/rafter connection in the direction parallel to purlin axis, which was assumed by GRYNIEWICZ and SZLENDAK (2016a). Knowing theoretical slip  $s$ , for element length  $l_{eq}$  (Fig. 5) adopted according to GRYNIEWICZ and SZLENDAK (2016a), using formula (9), moment of inertia  $I_{eq}$  and cross sections of equivalent finite element were assessed (Tab. 1).

Table 1

Calculations of equivalent cross sections of diaphragm fasteners and connections according to KORCZ (2017)

Fastener or connection type	Element length $l_{eq}$ [mm]	Theoretical slip $s$ [mm/kN]	Moment of inertia $I_{eq}$ [mm <sup>4</sup> ]	Equivalent cross section
Purlin/sheet fastener	1	0.35	0.00454	Bar $\phi=0.55$ mm
Purlin/rafter connection y-y	10	0.005	317.46032	Plate 17.17×0.75 mm
Purlin/rafter connection z-z	10	2.6	0.61050	length 10 mm
Shear connector fastener	11	0.35	6.03628	Bar $\phi=3.32$ mm

As it was done by KORCZ (2017), the location and flexibility of sheet/purlin fasteners, shear connector/girder fasteners and purlin/girder connections were taken into account. In order to decrease the number of variables, on which the results and their correctness depend, seam fasteners were omitted in the analyses.

## Groups of numerical models

In order to observe the influence of including in numerical model of the structure fasteners and connections flexibilities (which are the components of diaphragm flexibility) on transverse deflections of the steel building, 4 groups of models (P1, T1, T2, T3) were built. They are characterised in Table 2.

Table 2

Characteristic of the analysed groups of models

Symbol of model	Trapezoidal sheeting	Purlin/rafter connections	Shear connector fasteners	Purlin/sheet fasteners	Seam fasteners	2K	4K
P1	–	–	–	–	–	–	–
T1	+	–	–	–	–	–	+
T2	+	+	+	–	–	+	+
T3	+	+	+	+	–	+	+

In model P1 cladding was not included and purlins were defined in the axis plane of the top chords of the truss girders.

Model T1 was built by adding the roof diaphragm substituted by equivalent orthotropic shell in the axis plane of the top chords of the truss girders to model P1. The sheeting was four sides fastened (4K). The stressed skin effect was taken into consideration, but in simplified way, viz. including trapezoidal sheeting, but omitting flexibility of fasteners and connections of the diaphragm. This model is analogical to model used in the analyses performed by DENIZIAK et al. (2015).

In the next step model T2 was built – shear connector fasteners and purlin/girder connections were included by using equivalent cantilever finite beam elements (chapter *Connections and fasteners in numerical model*). As a result, purlins and equivalent orthotropic shell of trapezoidal sheeting were set off from the axis plane of the top chords of the truss girders in the distance equal to the equivalent element length. Both two and four sides fastening of the sheeting (2K, 4K) were taken into account. What is more, the simulation of the shear panel on two parallel layers allowed for shear connectors, which enable to connect sheeting with the truss top chords (rafters) in purlin systems (Fig. 2). According to ER (1995), in purlin systems shear connectors are absolutely required in the case of four sides fastening (4K). In the case of two sides fastening (2K) sheeting is fastened only to purlins, except for the gable diaphragms, which have to be fastened to gable rafters (using shear connectors) in order to transfer forces from the roof diaphragm through wall bracings to the foundations.

Model T3 was built on the basis of model T2 by adding sheet/purlin fasteners using again equivalent cantilever finite beam elements (chapter *Connections and fasteners in numerical model*). Three parallel layers of the diaphragm were

defined: plane of the top chords of the truss girders, plane of the purlins and plane of the trapezoidal sheeting replaced by the orthotropic shell model.

According to ER (1995), in the case of pitched roofs, the roof diaphragms are calculated for two surfaces separately. As a consequence, in models (T2, T3) there was a gap in the ridge between orthotropic shell elements (finite elements of two diaphragms did not have joint nodes).

## Results and Discussion

Numerical models P1, T1, T2, T3 (chapter *Groups of numerical models*) were built, calculations for three equivalent models of trapezoidal sheeting (M0/MA/MB) were run (chapter *Connections and fasteners in numerical model*) and two variants of columns (HEB300 and HEB200) were taken into account. The values of maximum deflection  $\Delta$  at the top of the column in the middle frame were observed as a representative of transverse displacements of the building. Results are presented in Table 3 and Table 4.

Table 3

Maximum deflection  $\Delta$  at the top of HEB300-column in the middle frame

Model	Deflection $\Delta$ of the column [mm]					
	2K			4K		
	M0	MA	MB	M0	MA	MB
P1 <sup>a</sup>	72.1	72.1	72.1	72.1	72.1	72.1
T1	–	–	–	4.0	5.8	8.1
T2	9.5	10.2	12.3	4.6	5.7 <sup>b</sup>	8.1
T3	12.8	14.9	16.9	4.7	6.2	8.5

<sup>a</sup> In model P1 types of model: M0/MA/MB and 2K/4K don't occur (there is only one value of maximum deflection at the top of the column in the middle frame)

<sup>b</sup> Disturbance of the result (described in the text)

According to DENIZIAK et al. (2015), for analysed load combination the ultimate limit state (ULS) conditions of the structure elements were fulfilled for both variants of columns (HEB300 and HEB200) regardless of including the diaphragm effect or not. Simultaneously current analyses showed that in the case of model P1 even cross section HEB300 of columns minimally (8%) does not fulfil the serviceability limit state (SLS) condition (deflection of the column) according to EN-1993-1-1:2005, viz.  $\Delta \leq H/150 = 10,000/150 = 66.6$  mm. By contrast, in models with the stressed skin effect included, the SLS condition is fulfilled by far, even for HEB200. In this situation, crucial in the design of the structure begins to be not SLS, but ULS, which means more economical design.

Interesting phenomenon is the change of the columns' behaviour, observed after including the diaphragm effect. The in-plane behaviour of more stiff columns (HEB300) in all models were cantilever-like while for less stiff columns (HEB200) in some models cantilever-beam behaviour was observed. It arose from the fact that the roof diaphragm blocked the deflection of the ends of the columns and simultaneously the stiffness  $EI$  of the columns was so small that the suction on the longitudinal wall caused bigger columns deflection in the mid-span than at the top. Maximum values of deflections of the middle column are provided in Table 4 in brackets. Exemplary comparison of HEB200 and HEB300 columns deformation is shown in Figure 8.

Table 4  
Maximum deflection  $\Delta$  at the top of HEB200-column in the middle frame

Model	Deflection $\Delta$ of the column [mm]					
	2K			4K		
	M0	MA	MB	M0	MA	MB
P1 <sup>a</sup>	258.3	258.3	258.3	258.3	258.3	258.3
T1 <sup>c</sup>	–	–	–	4.7 (10.7)	6.4 (11.6)	9.0 (13.0)
T2 <sup>c</sup>	10.8 (14.0)	11.7 (14.4)	14.4 (15.8)	5.1 (11.0)	6.3 <sup>b</sup> (11.6)	9.0 (13.0)
T3 <sup>c</sup>	15.1 (16.2)	18.0	20.8	5.2 (11.0)	6.8 (11.9)	9.5 (13.3)

<sup>a</sup> In model P1 types of model: M0/MA/MB and 2K/4K don't occur (there is only one value of maximum deflection at the top of the column in the middle frame).

<sup>b</sup> Disturbance of the result (described in the text).

<sup>c</sup> In brackets maximum values of deflections were provided, if the extreme value occurred not at the top of the column (described in the text).

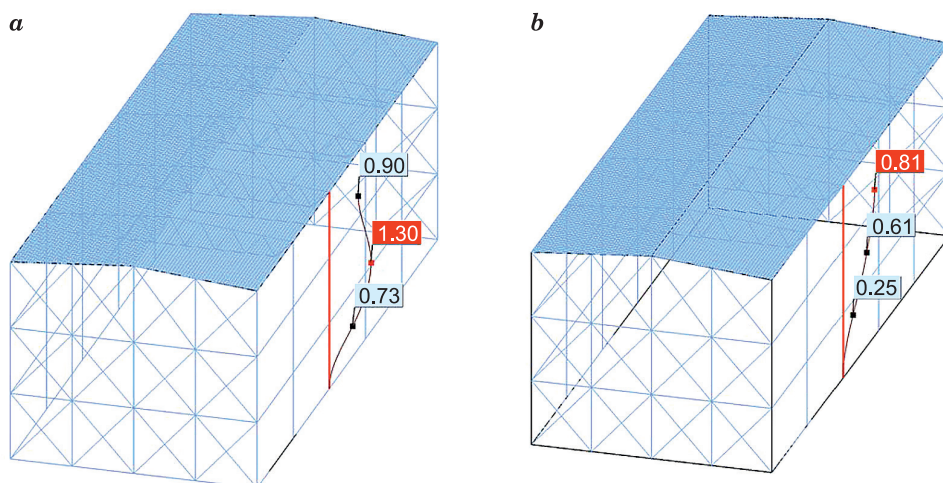


Fig. 8. Forms of deformation of columns – model T2\_MB\_4K: a – HEB200, b – HEB300

Values of maximum deflections were analysed paying special attention to the influence of including in numerical model fasteners and connections flexibilities on transverse displacements of the building. To that end, the percentile quotients of deflection values obtained in models T1÷T3 to values obtained in model T1 were calculated. Results are presented in Tables 5÷7.

Table 5

Percentile quotients of maximum deflection  $\Delta$  at the top of HEB300-column in the middle frame to the value obtained in model T1

Model	$\frac{\Delta_{Ti}}{\Delta_{T1}} \cdot 100\%$ , $i = 1, 2, 3$					
	2K			4K		
	M0	MA	MB	M0	MA	MB
T1	–	–	–	100	100	100
T2	238	176	152	115	98a	100
T3	320	257	209	118	107	105

<sup>a</sup> Disturbance of the result (described in the text).

Table 6

Percentile quotients of maximum deflection  $\Delta$  at the top of HEB200-column in the middle frame to the value obtained in model T1

Model	$\frac{\Delta_{Ti}}{\Delta_{T1}} \cdot 100\%$ , $i = 1, 2, 3$					
	2K			4K		
	M0	MA	MB	M0	MA	MB
T1	–	–	–	100	100	100
T2	230	183	160	109	98 <sup>a</sup>	100
T3	321	281	231	110	106	106

<sup>a</sup> Disturbance of the result (described in the text)

Table 7

Percentile quotients of maximum deflection  $\Delta$  of HEB200-column in the middle frame to the value obtained in model T1<sup>a</sup>

Model	$\frac{\Delta_{Ti}}{\Delta_{T1}} \cdot 100\%$ , $i = 1, 2, 3$					
	2K			4K		
	M0	MA	MB	M0	MA	MB
T1	–	–	–	100	100	100
T2	131	124	122	103	100	100
T3	151	155	160	103	103	102

<sup>a</sup> The maximum values of deflections, which occurred not necessarily at the top of the column, were included in calculations (described in the text, see also Tab. 4 and Fig. 8a)

As it was predicted, including in the numerical model fasteners and connections flexibilities increases the transverse deflection values of the building. In the case of two sides fastening (2K) the increase is much larger than in the case of four sides fastening (4K). Disturbance of the result appeared in model MA in the case of 4K (Tabs. 3–6): change from model T1 to model T2 caused minimal (0.2 mm) decrease of the deflection value. It seems that adding equivalent beam elements to the model resulted in the increase of the stiffness of the roof, because model was no longer two dimensional one and started to work as a spatial structure. In model MA and case 4K, the flexibility of the connectors added to the model was so small that it didn't compensate the increase of the "spatial" stiffness of the roof structure. The problem didn't appear in the case of 2K. It is recommended to analyse this disturbance deeper in order to improve the method of modelling the fasteners and connectors.

In the case (4K) maximally 18% increase in the column deformation value was observed. Keeping in mind that the absolute difference between deformation values obtained in models T1–T3 did not exceed 0.7 mm, in the analysed instance of the structure the omission of fasteners and connections flexibilities in numerical 3D analysis seems to be circumstantiated.

The situation in the case (2K) is different. The increase up to 221% in the column deformation value was observed and the absolute difference amounted to dozen of millimeters. In the analysed instance of the structure this difference did not influence the accomplishment of SLS condition for the column (even in model T2 and HEB200 column it is fulfilled by far), however the difference between models T1 and T3 is significant. It seems to be justified to diversify the analyses for two sides fastening (2K).

As it was emphasized in the chapter *Introducion*, the analytical procedures for the stiffness matrix of equivalent orthotropic plate for trapezoidal sheeting, both known from the literature and implemented in numerical programs, can diverge considerably. Also procedures implemented in ARSA – used in model (MA) and in RFEM – used in analyses performed by DENIZIAK et al. (2015) are different. However, the values of the stiffness matrix obtained in ARSA and in RFEM vary so little that in this case it has not significant effect on the deflection of the analysed structure. Results of the analyses showed that from practical point of view both models are the same. It means that model (MA-T1) performed in this article corresponds to model used in DENIZIAK et al. (2015). Comparing to analyses carried out in DENIZIAK et al. (2015), in this article two more models of trapezoidal sheeting (M0/MB) were analysed and the aspect of including in the calculations the fasteners and connections flexibility was considered (models T2, T3).

Results reconfirmed the observations of DENIZIAK et al. (2015), i.e. that including in numerical model the stressed skin effect reduces the order of magnitude of column deflections. For instance in the case of 4K, HEB300 columns

and model (MA) twelve times reduction in the value of deflection obtained for model T1 in comparison to model P1 was observed and for HEB200 column – circa twenty times. For model (MB) the effect is slightly smaller. It indicates that the more flexible the column is (so also the whole structure of the building), the more susceptible is the structure to the fact of including the diaphragm effect. This observation is in agreement with ER (1995). According to ER (1995) the stiffening effect depends on the relative flexibility, which for rectangular frames is defined as  $r=c/k$ , where  $c$  is the shear flexibility of a panel of sheeting and  $k$  is the frame flexibility (the eaves deflection per unit horizontal eaves load). For pitched roof frames the procedure is slightly different however, for this purpose (evaluation), procedure for rectangular frame is sufficient. In the case of 2K for column HEB300 the value  $r=0.172$  and for column HEB200 the value  $r=0.040$  were obtained. In the case of 4K for column HEB300 the value  $r=0.063$  and for column HEB200 the value  $r=0.014$  were obtained. If  $r$  is large (case of flexible sheeting or stiff frames, for instance HEB300 columns and 2K case), the stiffening effect is smaller. If  $r$  is small (case of stiff sheeting or flexible frames, for instance HEB200 columns and 4K case), the diaphragms have larger stiffening effect on the structure (Tabs. 3 and 4).

As it was said in chapter *Equivalent models of trapezoidal sheeting*, it can be assumed, based on article KORCZ (2017), that in the analysed instance of the structure model (MB) of trapezoidal sheeting is more accurate than model (MA). Justified is the question: how the difference in models (M0/MA/MB) translates to the behaviour of the whole structure. Percentile quotients of maximum deflection of the middle frame column in model (MB) to values obtained in model (MA) are presented in Table 8. Additionally percentile quotients of maximum deflection of the middle frame column in model (MB) to values obtained in model (M0) are presented in Table 9. Results reconfirmed the anticipation, that using models (M0) and (MA) causes increase in the global stiffness of the structure in comparison to model (MB). Percentile values correspond to about 6 mm difference in transverse displacements of the building between models.

Table 8

Percentile quotients of maximum deflection  $\Delta$  of the column in the middle frame in model MB to values obtained in model MA

Model	$\frac{\Delta_{MB}}{\Delta_{M0}} \cdot 100\%$					
	2K			4K		
	HEB300	HEB200 (end node)	HEB200 (max)	HEB300	HEB200 (end node)	HEB200 (max)
T1	–	–	–	140	141	112
T2	121	123	110	142	143	112
T3	113	116	116	137	140	112

Table 9

Percentile quotients of maximum deflection  $\Delta$  of the column in the middle frame in model MB to values obtained in model M0

Model	$\frac{\Delta_{MB}}{\Delta_{M0}} \cdot 100\%$					
	2K			4K		
	HEB300	HEB200 (end node)	HEB200 (max)	HEB300	HEB200 (end node)	HEB200 (max)
T1	–	–	–	203	191	121
T2	129	133	113	176	176	118
T3	132	138	128	181	183	121

In this particular instance of the structure the difference is negligible, so using (M0) model (infinitely rigid diaphragm) or (MA) model instead of more precise one in order to reduce the calculation effort is justified.

Model (MB-T3) in the case of 2K gives circa 4÷5 times bigger transverse displacements of the structure than model (M0-T1), which corresponds to about 13÷16 mm (see Tabs. 3 and 4). Comparing these results to deflection values obtained for model P1 and taking into consideration the calculation and model-building effort lead to conclusion that using model (M0-T1) instead of model (MB-T3) is reasonable for quick design estimations. However, the answer is not clear for precise design. It seems that it can strongly depend on the particular structure.

## Conclusions

There are two main aspects of including the diaphragm effect in 3D numerical analysis of the structure: steel trapezoidal sheets flexibility and fasteners and connections flexibility. Results showed that including fasteners and connections flexibilities in numerical model of the structure leads to the increase of the transverse deflection values of the building. As it was presented, in some cases this effect is negligible, which means that the simple model could be used for analysis instead of more precise one. Similar tendency was observed when choosing of the equivalent model of trapezoidal sheeting (M0/MA/MB). However, identification for which cases this influence is negligible and for which is significant (from engineering point of view) and formulation of all-purpose claims requires wider range of analyses and verification by experimental laboratory researches.

## References

- Autodesk Robot Structural Analysis Professional 2015. Help for users, <http://help.autodesk.com/view/RSAPRO/2015/ENU/>.
- BRÓDKA J., GARNCAREK R., MIŁACZEWSKI K. 1999. *Blachy fałdowe w budownictwie stalowym*. Arkady, Warszawa.
- DENIZIAK P., URBAŃSKA-GALEWSKA E., MIGDA W. 2015. *Analizy wpływu współpracy blach poszycia z konstrukcją nośną na wartości sił wewnętrznych i przemieszczeń hali stalowej*. Czasopismo Inżynierii Lądowej, Środowiska i Architektury – Journal of Civil Engineering, Environment and Architecture, JCEEA, XXXII, 62(4/15): 43–53. DOI: 10.7862/rb.2015.177.
- EN-1990:2002. *Eurocode 0. Basis of structural design*. PN-EN 1990: 2004 – *National Annex*.
- EN 1991-1-3:2003. *Eurocode 1. Actions on structures*. Part 1–3: *General actions. Snow loads*.
- EN 1991-1-4:2004. *Eurocode 1. Actions on structures*. Part 1–4: *General actions. Wind actions*. PN-EN 1991-1-4: 2008 – *National Annex*.
- EN 1993-1-1:2005. *Eurocode 3. Design of steel structures*. Part 1–1: *General rules and rules for the buildings*.
- EN 1993-1-3:2006. *Eurocode 3. Design of steel structures*. Part 1–3: *General rules. Supplementary rules for cold-formed members and sheeting*.
- European Recommendations for the Application of Metal Sheeting Acting as a Diaphragm. Stressed Skin Design*. 1995. ECCS – TC7, TWG 7.5.
- GOCZEK J. 2013. *Belki z kształtowników giętych stężone poszyciem z blach fałdowych*. Wyd. Politechniki Łódzkiej, Łódź.
- GRYNIEWICZ M., SZLENDAK J.K. 2016a. *FEM model of the steel building roof includes stressed skin diaphragm action effects*. In: *Recent Progress in Steel and Composite Structures: Proceedings of The XIII International Conference on Metal Structures*. Eds. M.A. Gizejowski, J. Marcinowski, A. Kozłowski, J. Ziółko. CRC Press, Zielona Góra, Poland.
- GRYNIEWICZ M., SZLENDAK J.K. 2016b. *Wpływ współpracy pokrycia dachowego na przemieszczenia konstrukcji hali stalowej*. Inżynieria i Budownictwo, 8.
- JOÓ A. L., DUNAI L. 2015. *Full-scale experimental tests on steel frames with various claddings*. In *Proceedings of The Eighth International Conference on Advances in Steel Structures*. Lisbon, Portugal.
- KORCZ N. 2017. *Modele numeryczne uwzględniające tarczową pracę pokrycia dachowego z blach trapezowych*. Czasopismo Inżynierii Lądowej, Środowiska i Architektury – Journal of Civil Engineering, Environment and Architecture, JCEEA, XXXIV, 64 (4/I/17). DOI: 10.7862/rb.2017.207.
- KOWALCZYK K., NOWICKI M. 2003. *O wykorzystaniu tarczowego charakteru pracy pokrycia z blach fałdowych*. Inżynieria i Budownictwo, 1.
- LENDVAI A., JOÓ A.L. 2016. *Test based finite element development for diaphragm action*. In *Proceedings of the International Colloquium on Stability and Ductility of Steel Structures*. Timisoara, Romania.
- NAGY ZS., POP A., MOIS I., BALLOK R. 2015. *Stressed Skin Effect on the Elastic Buckling of Pitched Roof Portal Frames*. In *Proceedings of the Eighth International Conference on Advances in Steel Structures*. Lisbon, Portugal.
- NAGY ZS., POP A., MOIS I., BALLOK R. 2016. *Stressed Skin Effect on the Elastic Buckling of Pitched Roof Portal Frames*. *Structures*, 8: 227–244.
- NIEWIADOMSKI L. 2011. *Tarcza dachowa z blachy trapezowej w modelu obliczeniowym konstrukcji dachu hali przemysłowej*. In *Proceedings of the XII International Conference on Metal Structures – ICMS*. Wrocław, Poland.
- WENNBERG D., WENNHAGE P., STICHEL S. 2011. *Orthotropic Models of Corrugated Sheets in Finite Element Analysis*. *ISRN Mechanical Engineering*, 2011, ID 979532, DOI:10.5402/2011/979532.
- XIA Y., FRISWELL M.I., SAAVEDRA FLORES E.I. 2012. *Equivalent models of corrugated panels*. *International Journal of Solids and Structures*, 49: 1453–1462.



Quarterly peer-reviewed scientific journal

ISSN 1505-4675  
e-ISSN 2083-4527

**TECHNICAL SCIENCES**

Homepage: [www.uwm.edu.pl/techsci/](http://www.uwm.edu.pl/techsci/)



## THE USE OF FINE WASTE MATERIAL FOR THE FUTURE OF SUSTAINABLE CONSTRUCTION

*Katarzyna Kalinowska-Wichrowska*

Department of Construction and Road Engineering  
Białystok University of Technology

Received 11 March 2018, accepted 11 May 2018, available online 18 May 2018.

**Key words:** cement composites, recycling binder, physical and mechanical properties of concretes.

### Abstract

The article presents data regarding scale of current production of cement and its future of sustainable construction. In the time of sustainability and Union Directives which rightly impose the reduction of emission of greenhouse gases the solution has been proposed that may in some extent contribute to reducing the cement consumption by using properly prepared recycling binder as its substitute. Some results of own research have been presented, connected with the possibility of using the waste material in form of properly processed cement grout as a partial substitute of cement in the cement composites. Due to high content of contaminants in the industrial secondary binder, which might interfere with the uniformity of results, it has been decided to obtain the recycling binder in the laboratory conditions. The secondary mineral material has been obtained in the process of multi-stage disintegration of prepared laboratory samples, made from cement grouts. The prepared material has been analysed for content of dust fraction and pozzolana activity. The obtained results have revealed that in assumed conditions of recycling binder processing it may be successfully used as cement substitute in the cement composites.

### Introduction

Higher number of people and economic growth imposes an additional load on already limited natural resources and will require maintaining of actions aimed for neutralization of influence on the climate changes. As a key component

---

Correspondence: Katarzyna Kalinowska-Wichrowska, Katedra Budownictwa i Inżynierii Drogowej, Wydział Budownictwa i Inżynierii Środowiskowej, Politechnika Białostocka, ul. Wiejska 45A, 15-351 Białystok, e-mail: [k.kalinowska@pb.edu.pl](mailto:k.kalinowska@pb.edu.pl)

of concrete, the cement plays crucial role in the resource management, therefore the problem of reuse of old grout is an object of research of many scientists due to concrete recycling and recycled materials in the context of their efficient management and environment protection (BOLTRYK, KALINOWSKA-WICHROWSKA 2016, KALINOWSKA-WICHROWSKA 2017b, DUAN, POON 2014).

With increasing use of concrete, the demand for cement and aggregates rises. Earth resources protection and high energy consumption while cement production imposes need to re-use concrete components through recycling. It is estimated that the concrete industry consumes about 11 billion tons of natural aggregate per year (JIN, CHEN 2015) and the cement industry is responsible for about 5% of anthropogenic CO<sub>2</sub> emissions in the world (*Rola cementu...* 2016). Construction waste represent around 25–30% of all waste generated in the European Union. They consist of many materials, including: brick debris, concrete, gypsum, etc., which can be subjected to the recovery process (ZAJĄC, GOŁĘBIEWSKA 2014). The percentage of recycling and re-use varies greatly across Member States. In Spain, for example, only 14% of rubbish waste is recycled. Other countries with a very high level of recycling, such as: the Netherlands, Denmark, Estonia, Germany, for which recycling rates are respectively 92%, 86%, 80% and 75% (Eurostat, online 2016).

The goal of research undertaken in this article is to demonstrate the possibility of reuse of binder obtained from concrete recycling as the cement substitute in the cement composites. Reduction of amount of used cement coming from the factory (where most of CO<sub>2</sub> is emitted to the atmosphere during clinker baking) limits emission of that gas (KALINOWSKA-WICHROWSKA 2017a).

BRAGA et al. (2012) analysed the behaviour of cement mortars using small recycled particles as a substitute for natural sand. In these studies, 15% of the necessary natural sand was replaced with recycled sand. An increase in compressive strength was observed, with a simultaneous decrease in the modulus of elasticity and increased water absorption, as compared to traditional cement mortars.

ZENGFENG et al. (2015) observed the effect of saturation of the fine fraction of recycling aggregates on mechanical properties, properties of fresh mortar and the material transition zone. The results showed that mortars made with dry aggregate from recycled materials show better compressive properties than saturated recycled aggregates due to the thinner transition zone. An increase in compressive strength of composites with dry fine aggregate was also observed from recycling.

## **Object and methodology of own research**

### **Characteristics of raw materials**

Cement CEM I 42,5R and corresponding to the requirements of standard PN-EN 197-1 Cement – Part 1: Composition, specifications and conformity criteria for common cements. Only the fine aggregate in form of standardized sand has been used for the tests.

### **Recycling binder**

The experiment has been realized with use of secondary binder obtained as a result of processing of previously prepared laboratory samples of cement mortars. The recycling mortars have been prepared from cement, sand and water in moulds 40×40×160 mm (according to PN-EN 196-7: 2009 Methods of testing cement – Part 7: Methods of taking and preparing samples of cement, where w/c ratio equalled 0.5). After 28 days of curing in the water conditions the samples of cement mortars have waited for another 6 months in air-dry conditions. Then they have been crushed in the jaw crusher to dimensions of approx. 10–20 mm. In such form they have been placed in the thermal furnace to be subjected to baking in temperatures defined in the experiment plan. After that process the material has been remilled for approx. 20 minutes in micro Deval drum to obtained as high specific surface as possible. During another milling the whole charge consisted of fraction <0.125 cm and the specific surface oscillated in range of 3,800–4,000 cm<sup>2</sup>/g.

In the next step, the recipe of cement composites has been assumed as for standard mortars according to PN-EN 196-7: 2009 Methods of testing cement – Part 7: Methods of taking and preparing samples of cement, where w/c ratio = 0.5. For forming of beams 40×40×160 mm the Portland cement CEM I 42.5R has been used, which 25% of cement has been replaced with recycling material. After 28 days of curing in water conditions the samples have been subjected to compression tests. The test results are presented in section 4.

### **Test methodology**

- Compression strength of cement composites with recycling material:

The compression strength testing has been realized for 6 randomly selected beams 4×4×16 cm from each batch according to standard PN-EN 196-1:2006 Methods of testing cement – Part 1: Determination of strength.

- The pozzolana activity has been determined according to standard PN-EN 450-1:2009. Fly ash for concrete. Part 1: Definition, specifications and conformity criteria.

- The percent content of individual sizes of particles in the recycling material after the thermal and mechanical processing has been determined with use of set of sieves.

## Research experiment

### Experiment plan

In order to determine the influence of thermal processing of recycling mortar on selected properties of cement composites the research experiment has been planned, consisting of 3 basic batches and 1 control batch (no. 4 – not consisting the recycling mortar binder). In the experiment factor ( $X_1$ ) have been taken into consideration, each of three variation levels:

- $X_1$  – baking temperature of recycling binder (400, 650, 800°C).

The baking time of material has been assumed as constant and it amounted to 60 minutes.

The experiment plan including coded values of variables is presented in Table 1.

Table 1

Plan of research experiment		
Batch no.	$X_1$ – baking temperature [°C]	
1	-1	400
	-1	400
	-1	400
2	0	650
	0	650
	0	650
3	+1	800
	+1	800
	+1	800
4	control batch	

### Realization and curing of samples

Batches have been realized with use of automatic laboratory mixer. First the loose components have been weighed and mixed for 5 minutes, then water has been added and mixing lasted another 10 minutes. Such prepared amount of

material has been placed in the steel mould allowing for simultaneous forming of three samples of dimensions 40×40×160 mm. Then the samples in the mould have been consolidated on the vibration table. After removing from the mould the samples have been placed in the water basin of temperature of 20°C until realization of proper tests.

### Results of tests and discussion

As described above, the recycling material after the baking process has been subjected to remilling in the planetary mill down to the specific surface similar to that of cement 42.5 R, and those processes might have with temperature had the significant impact on pozzolana effect. The Figure 1 shows grading curve for the recycling material baked in 650°C and subjected to remilling.

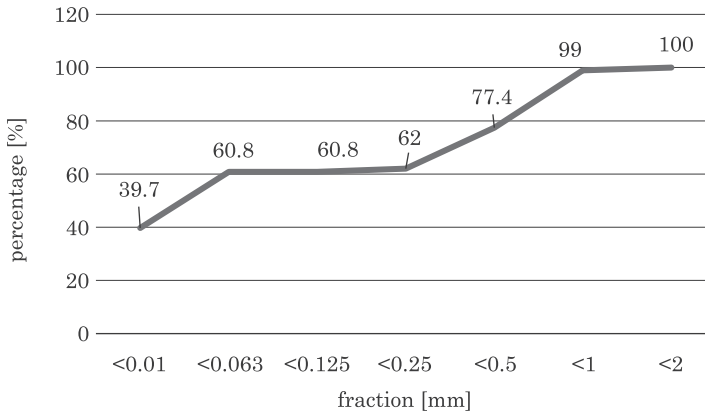


Fig. 1. Percentage content of individual particle sizes in recycling mortar binder (650°C)

Diversification of particle sizes in old grout (as proven by the strength results) does not impair the properties of composites. About 61% of the material have fraction less than 0.125 mm and 0.063 mm. High content of silty fractions indicates the effectiveness of the milling process. It should be noted that with the material's baked in temperature at 800°C and further milling, it became compacting material and deposited on the walls of the grinder. From the point of view of using technology in the industry it would be a disqualifying factor. The photos of the recycled mortar resulting from roasting debris at 650°C taken using the scanning technique are showed below (Fig. 2).

The results of compressive strength and pozzolana shown in Figure 3. The highest results of compression strength have been obtained for the composites including the recycling additive subjected to thermal processing in 650°C (batches 2).

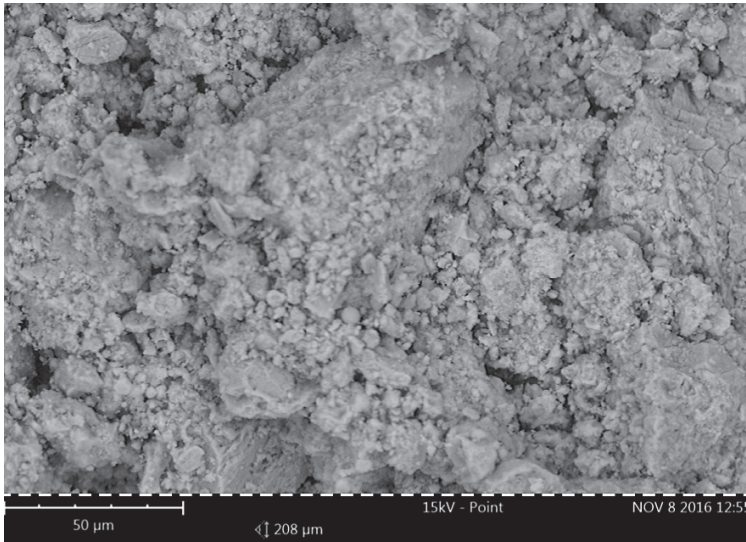


Fig. 2. SEM photo of recycling mortar (after thermal process in 650°C)

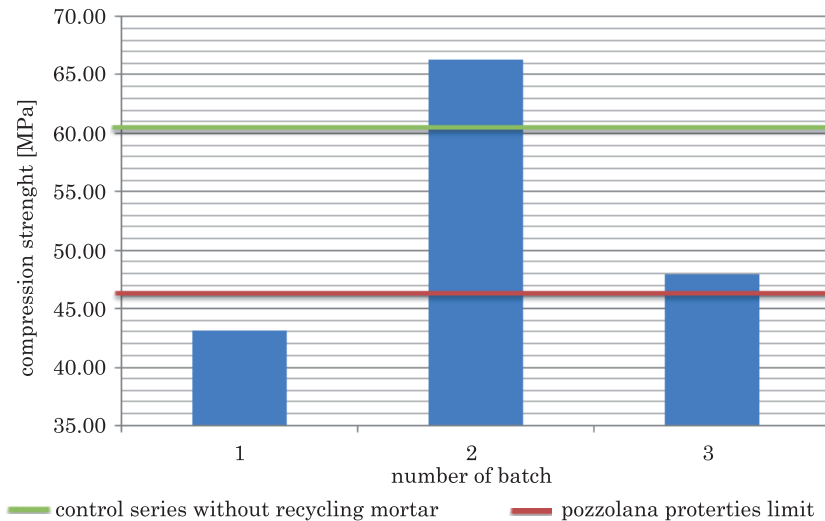


Fig. 3. The results of compression strength for cement composites with addition of recycling binder mortar

The values of obtained strength in those batches are higher results for the control batch (4) without the recycling additive, increased by 10%. According to test method described in PN-EN 450-1:2009 the tested material reveals the pozzolana properties when the compression strength of composite containing 25% of material substituting the cement is 75% of control sample.

In tested composites all strength results for batches, where the recycling material has been subjected to baking in 650°C, had revealed the pozzolana properties (in figure red line shows pozzolana veneer). Only in batches where the thermal processing of recycling material was 400°C (batch 1) and 800°C (batch 3) the pozzolana properties have not been activated. It is assumed that in such range of temperatures 300–500°C there is still significant amount of not decomposed portlandite present and in range 750–800°C there is a breakdown of calcium carbonate into carbon dioxide and a significant amount of inactive calcium oxide (KRZYWOBŁOCKA-LAURÓW 1998). As results shows applying too high temperature of baking decreases pozzolana activity in recycled binder mortars.

Figure 4 shows a composite scanning photo using a recyclable mortar as a cement substitute. The structure of the cement matrix is identical to that of a classic composite made exclusively on cement. The portlandit clusters were not observed, which could indicate an incomplete pozzolanic reaction. The C-S-H phase which fills the structure of the composite is visible in the Figure 4.

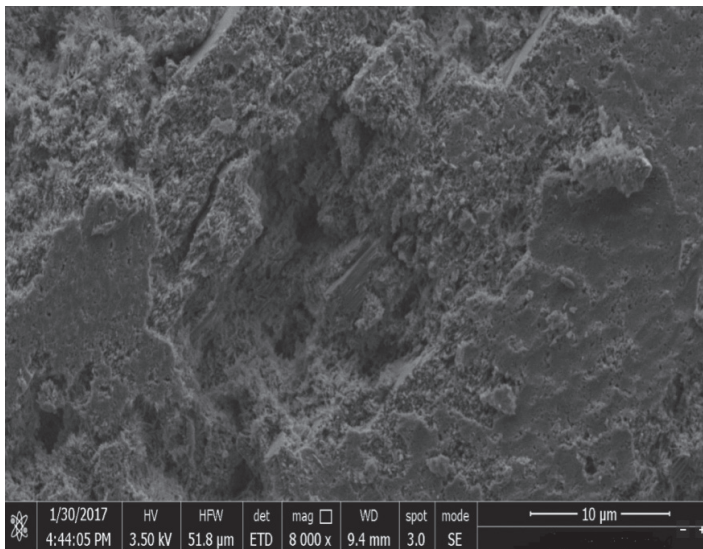


Fig. 4. SEM photos of breakthroughs of samples made using a recycling mortar, visible phase C-S-H

## Summary

The article presents the possibility of effective utilization of recycling mortar in cement composites.

The presented results of tests have confirmed that after specific suitable thermal processing the tested recycling material reveals the pozzolana properties

in composites and improves compression strength values. The optimum strength parameters and the highest level of pozzolana activity index have been obtained for the baking temperature of 650°C. Increasing the processing temperature by 150°C (to 800°C) deteriorates of strength and pozzolana parameters. The suitability of tested material as an active additive is also significantly influenced by the milling degree, close to specific surface of cement.

In realized tests the assumed of baking temperature of recycling material had high influence on the composite strength properties. As the tests results show, the recycling material produced in such way may be successfully used as an alternative for cement or in the future as fillers or other type II additives for cementitious composites.

## References

- BOŁTRYK M., KALINOWSKA-WICHROWSKA K. 2016. *The cement composites with modified recycled addition*. Budownictwo i Inżynieria Środowiska, 7(1): 7–10.
- BRAGA M., DE BRITO J., VEIGA R. 2012. *Incorporation of fine concrete aggregates in mortars*. Construction and Building Materials, 36: 960–968.
- DUAN Z.H., POON C.S. 2014. *Properties of recycled aggregate concrete made with recycled aggregates with different amounts of old adhered mortars*. Materials and Design, 58: 19–29.
- Eurostat. Your key to European statistic. 2016. <http://ec.europa.eu/eurostat> (access: 26.04.2016).
- JIN R., CHEN Q. 2015. *Investigation of concrete recycling in the U.S. construction industry*. Procedia Engineering, 118: 894–901.
- KALINOWSKA-WICHROWSKA K. 2017a. *Stosowanie spoiwa recyklingowego jako przykład redukcji CO<sub>2</sub>*. Budownictwo i Inżynieria Środowiska, 8(1): 41–46.
- KALINOWSKA-WICHROWSKA K. 2017b. *Use of recycling blender as an example of reduction cement in cement composites*. In: *Aktual'nye problemy issledovaniâ materialov, konstrukcij, tehnologij i organizacii stroitel'stva v transgraničnom aspekte*. Sbornik statej II Meždunarodnoj naučnoj konferencii. Izdatel'stvo Brestskij Gosudarstvennyj Tehničeskij Universitet, Brest, p. 67–70.
- KRZYWOBŁOCKA-LAURÓW R. 1998. *Badania składu fazowego betonu*. Instrukcja 357/98. Instytut Techniki Budowlanej, Warszawa.
- PN-EN 196-1:2006. *Metody badania cementu – Część 1: Oznaczanie wytrzymałości*.
- PN-EN 196-7: 2009. *Metody badania cementu – Część 7: Metody pobierania i przygotowania próbek cementu*.
- PN-EN 197-1. *Cement – Część 1: Skład, wymagania i kryteria zgodności dotyczące cementów powszechnego użytku*.
- PN-EN 450-1:2009. *Popiół lotny do betonu. Część 1: Definicje, specyfikacje i kryteria zgodności*.
- Rola cementu w niskoemisyjnej gospodarce do 2050 roku*. 2016. Stowarzyszenie Producentów Cementu. [lowcarboneyconomy.cembureau.eu](http://lowcarboneyconomy.cembureau.eu) (access: 26.04.2016).
- ZAJĄC B., GOŁĘBIOWSKA I. 2014. *Zagospodarowanie odpadów budowlanych*. Inżynieria i Aparatura Chemiczna, 53(6): 393–395.
- ZENGFENG Z., REMOND S., DAMIDOT D., WEIYA X. 2015. *Influence of fine recycled concrete aggregates on properties of mortars*. Construction and Building Materials, 81: 179–186.



Quarterly peer-reviewed scientific journal

ISSN 1505-4675  
e-ISSN 2083-4527

**TECHNICAL SCIENCES**

Homepage: [www.uwm.edu.pl/techsci/](http://www.uwm.edu.pl/techsci/)



## DESIGN OF MODERN TOOLS FOR DIGITAL OUTPUT RASTER SCANNING

***Oleg Yushchuk***<sup>1</sup>, ***Bogdana Havrysh***<sup>1</sup>, ***Oleksandr Tymchenko***<sup>2</sup>,  
***Karolina Szturo***<sup>2</sup>

<sup>1</sup>Department of Prepress Technologies  
Ukrainian Academy of Printing, Lviv

<sup>2</sup>Department of Safety Engineering  
University of Warmia and Mazury

**Key words:** test-object, resolution, output scanning device.

### Abstract

Quality control at all stages of the polygraphic process will allow to establish a feedback between technological processes of printing. The validity of the selected criteria, technological effectiveness and objectivity of the quality assessment methods will allow to organise technically accurate modelling of the processes as well as to promptly interfere with the production process if necessary. The tendency of the development of technologies and control tools as well as computer expansion are the reasons why the objectivity and impartiality of the assessment become the main criteria for the choice of method for quality assessment of the polygraphic product. Methodological purpose of the quality control is to make the polygraphic process technologically driven and stable, and the quality of the received print – more predictable.

### Introduction

Current international standards and regulatory materials governing the operations of quality control, thus achieved the necessary quality printing products. Today, the printing market increasingly prevalent technology of making printing plates by digital image output to the forming material, known as Computer-to-plate-technology, which differs from the traditional lack of stage separations getting (TIKHONOV 2000).

---

Correspondence: Oleksandr Tymchenko, Katedra Inżynierii Bezpieczeństwa, Uniwersytet Warmińsko-Mazurski w Olsztynie, ul. Oczapowskiego 11, 10-719 Olsztyn, phone: 89 524 61 25.

Improving Computer-to-plate-technology promotes the development of digital monitoring forms. Typically, PostScript-file that allows you to verify the accuracy of the output of digital systems, including printing plates, generating elements that contain a variety of test objects that can measure the exposure resolution.

In today's competitive environment one of the key issues is ensuring consistently high quality printing products while minimizing costs. Modern printing companies realize the need for certification as an important factor in achieving this goal. Standardization is particularly relevant in light of current trends to reduce the circulation of orders because it promotes the competitiveness of offset printing (HAVRYSH, YUSCHYK 2015).

For the evaluation of the quality of offset printing plates appropriate measuring control strips have been developed and new types of measuring devices are also created (GNAWALI et al., 2013, *Control of CtP...* 2015).

## Quality control tools

The control processes have become more computerized and automatized; due to this automatic measurement tools as well as network digital control systems (complexes) are more actively implemented in the production process, which allows to carry out overall control at all stages and phases of the process. Implementation of electronic complexes gives the opportunity to promptly interfere with the production process at a particular point.

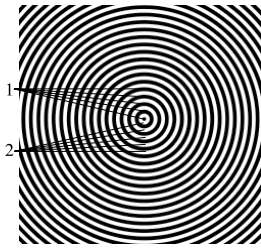
The objective of the invention is to work out a scale for the resolution control of output scanning devices by means of software synthesis of the control elements of the scale which will allow to visually assess the actual resolution of a raster output scanning device, such as laser and inkjet printers, system "Computer-to-film", "Computer-to-plate", "Computer-to-press" and digital printing machines.

This is possible as the scale for resolution control of the output scanning devices, that is composed of the elements for resolution assessment of fast, slow and 45° angled scan directions, gives the possibility to assess the actual resolution of these devices.

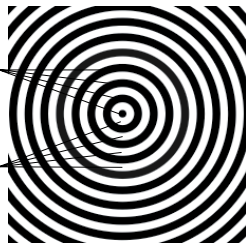
## Development of the scale for resolution control

The structural scheme of the scale for resolution control of the output scanning devices is given at Figure 1; it consists of four functional groups that, in turn, are composed of thin annular and straight lines of equal thickness (2.6458, 5.2917, 10.58, 21.17, 42.3, 84.7 μm) (HAVRYSH, YUSCHYK 2015).

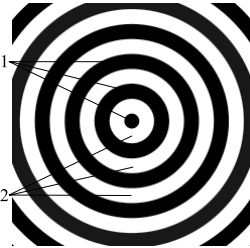




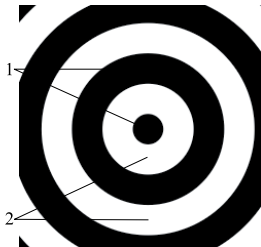
unit 1 Fig. 1 (9,600 dpi)



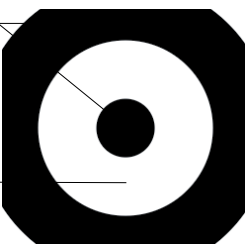
unit 2 Fig. 1 (4,800 dpi)



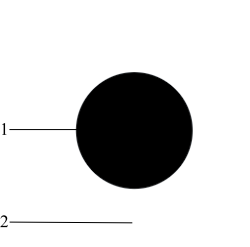
unit 3 Fig. 1 (2,400 dpi)



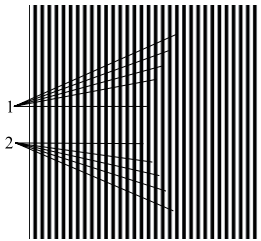
unit 4 Fig. 1 (1,200 dpi)



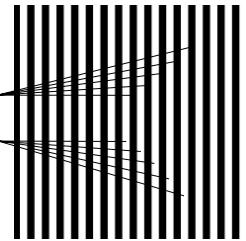
unit 5 Fig. 1 (600 dpi)



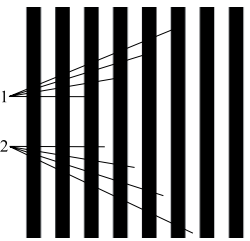
unit 6 Fig. 1 (300 dpi)



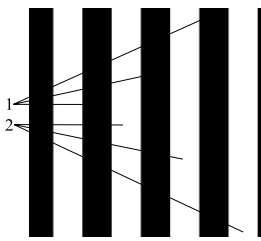
unit 7 Fig. 1 (9,600 dpi)



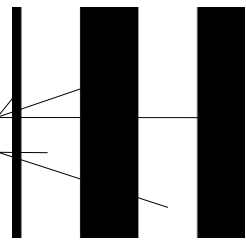
unit 8 Fig. 1 (4,800 dpi)



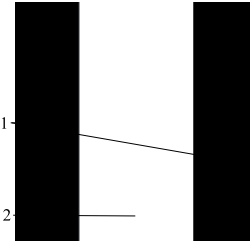
unit 9 Fig. 1 (2,400 dpi)



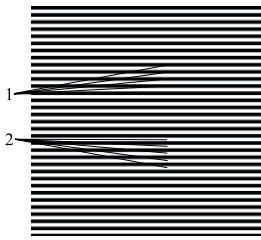
unit 10 Fig. 1 (1,200 dpi)



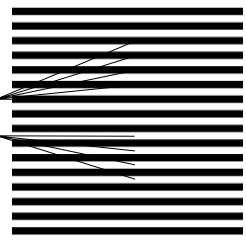
unit 11 Fig. 1 (600 dpi)



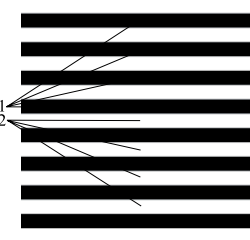
unit 12 Fig. 1 (300 dpi)



unit 13 Fig. 1 (9,600 dpi)



unit 14 Fig. 1 (4,800 dpi)



unit 15 Fig. 1 (2,400 dpi)

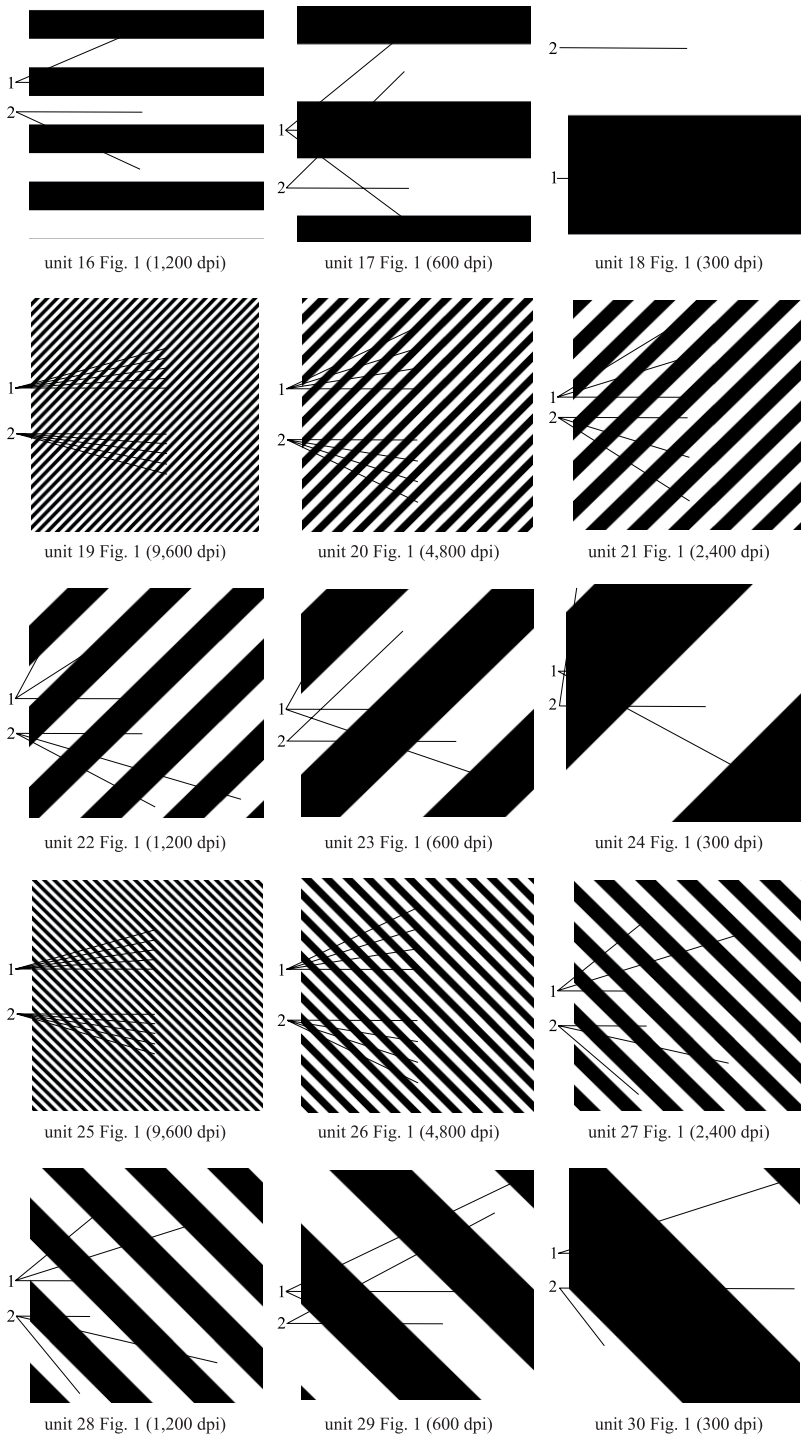


Fig. 2. Enlarged test scale fields for different resolution values (enlargement 37,000%:  
1 – line, 2 – gap between lines)

The working scheme of the scale for resolution control of the output scanning devices is as follows: the program file with the control scale is transferred to a sheet, photo material or multimetal plate by means of the raster scanning device (Fig. 1), and the resolution value at which the control elements are reflected without distortions is visually set (Fig. 2). Then, for correctly reflected resolution fields, the measurement of integral optical density value is carried out (SHCHADENKO 2009, NAGORNOV 2004); it shall ideally amount to 0.3 for 50% line gauge. On the basis of the deviation from this value the conclusion regarding the accuracy of the settings of the raster output scanning device is made.

The given scale for the resolution control of the output scanning devices allows to assess the accuracy of the main settings of raster output scanning devices (HAVRYSH, YUSCHYK 2015).

The given test-object refers to the scales for prompt resolution control of the output scanning devices, such as laser and inkjet printers, laser photo-exposing printers, computer-to-plate systems, computer-to-printing machine systems, and digital printing machines.

The test-object for the resolution control of the output scanning devices allows to assess the accuracy of the main settings of the raster output scanning devices.

The test-object for the resolution assessment of the output scanning devices given at Figure 1 is composed of four functional groups, each of which has 6 elements of 9,600, 4,800, 2,400, 1,200, 600, 300 dpi resolution.

Functional group I contains thin annular lines (elements 1–6), functional group II – thin straight vertical lines (elements 7–12), functional group III – thin straight horizontal lines (elements 13–18), functional group IV – thin straight 45° angled lines (elements 19–24) and thin straight 135° angled lines (elements 25–30) (HAVRYSH, YUSCHYK 2015). In the bottom part there are elements that are identical to the elements of the upper, left and right parts.

The test-object for the resolution assessment of the output scanning devices is used as follows: the test-object is transferred to a sheet, photo material or multimetal plate by means of the raster scanning device, and the resolution value at which the control elements are reflected without distortions is visually set. Then, for correctly reflected resolution fields, the measurement of integral optical density value is carried out (SHCHADENKO 2009); it shall ideally amount to 0.3 for 50% line gauge (LINSLEY 1980). On the basis of the deviation from this value the conclusion regarding the accuracy of the settings of the raster output scanning device is made.

Figure 2 shows elements of blocks of circular, vertical, horizontal and 45° and 135° angles with a resolution of 9,600, 4,800, 2,400, 1,200, 600, and 300 dpi with an increase of 37,000%.

## Conclusions

It is developed the technique of estimating the accuracy of reproduction of information by raster scanning devices of output on the reproduction of raster and dashed elements of control scales.

For real images, in the case of degradation of resolution (mismatch of the raster scanning output device), it is necessary to apply image processing using recovery methods with the automatic selection of parameters, which will allow clear images of test object fields with high resolution (higher than 1,200 dpi).

## Acknowledgment

The authors are appreciative to colleagues for their support and appropriate suggestions, which allowed to improve the materials of the article.

## References

- Control of CtP Plates After Their Development Offset printing technology*. Offset Lithography. Online: <http://www.offsetprintingtechnology.com> (access: 26 Apr, 2017).
- GNAWALI O., FONSECA R., JAMIESON K., LEVIS P. 2013. *CTP: An efficient, robust, and reliable collection tree protocol for wireless sensor networks*. ACM Transactions on Sensor Networks (TOSN), 10(1): 16.
- HAVRYSH B., YUSCHYK O. 2015. *The patent for utility model „Test facility to control the resolution of raster output scanners”*. The patent for utility model No. 98879.
- LINSLEY D. 1980. *Recording materials and use of lasers in small format imaging*. SPIE Seminar Proceedings, 223: 7–10.
- NAGORNOV I. 2004. *Development control elements for computer-to-plate-systems*. Successes of Natural Science, M., 7: 104–105.
- SHCHADENKO A. 2009. *Adapty rastrer polygraphic transformation in technology*. Doctoral dissertation, St. Petersburg.
- TIKHONOV V. 2000. *Preparation image of information for polygraphic*. Kompyu Art., 9.

## Guide for Authors

### Introduction

Technical Sciences is a peer-reviewed research Journal published in English by the Publishing House of the University of Warmia and Mazury in Olsztyn (Poland). Journal is published continually since 1998. Until 2010 Journal was published as a yearbook, in 2011 and 2012 it was published semiyearly. From 2013, the Journal is published quarterly in the spring, summer, fall, and winter.

The Journal covers basic and applied researches in the field of engineering and the physical sciences that represent advances in understanding or modeling of the performance of technical and/or biological systems. The Journal covers most branches of engineering science including biosystems engineering, civil engineering, environmental engineering, food engineering, geodesy and cartography, information technology, mechanical engineering, materials science, production engineering etc.

Papers may report the results of experiments, theoretical analyses, design of machines and mechanization systems, processes or processing methods, new materials, new measurements methods or new ideas in information technology.

The submitted manuscripts should have clear science content in methodology, results and discussion. Appropriate scientific and statistically sound experimental designs must be included in methodology and statistics must be employed in analyzing data to discuss the impact of test variables. Moreover there should be clear evidence provided on how the given results advance the area of engineering science. Mere confirmation of existing published data is not acceptable. Manuscripts should present results of completed works.

There are three types of papers: a) research papers (full length articles); b) short communications; c) review papers.

The Journal is published in the printed and electronic version. The electronic version is published on the website ahead of printed version of Technical Sciences.

**Technical Sciences does not charge submission or page fees.**

### Types of paper

The following articles are accepted for publication:

### Reviews

Reviews should present a focused aspect on a topic of current interest in the area of biosystems engineering, civil engineering, environmental engineering, food engineering, geodesy and cartography, information technology, mechanical engineering, materials science, production engineering etc. They should include all major findings and bring together reports from a number of sources. These critical reviews should draw out comparisons and conflicts between work, and provide an overview of the 'state of the art'. They should give objective assessments of the topic by citing relevant published work, and not merely present the opinions of individual authors or summarize only work carried out by the authors or by those with whom the authors agree. Undue speculations should also be avoided. Reviews generally should not exceed 6,000 words.

### Research Papers

Research Papers are reports of complete, scientifically sound, original research which contributes new knowledge to its field. Papers should not exceed 5,000 words, including figures and tables.

### **Short Communications**

Short Communications are research papers constituting a concise description of a limited investigation. They should be completely documented, both by reference list, and description of the experimental procedures. Short Communications should not occupy more than 2,000 words, including figures and tables.

### **Letters to the Editor**

Letters to the Editor should concern with issues raised by articles recently published in scientific journals or by recent developments in the engineering area.

### **Contact details for submission**

The paper should be sent to the Editorial Office, as a Microsoft Word file, by e-mail: techsci@uwm.edu.pl

### **Referees**

Author/authors should suggest, the names, addresses and e-mail addresses of at least three potential referees. The editor retains the sole right to decide whether or not the suggested reviewers are used.

### **Submission declaration**

After final acceptance of the manuscript, the corresponding author should send to the Editorial Office the author's declaration. Submission of an article implies that the work has not been published previously (except in the form of an abstract or as part of a published lecture or academic thesis or as an electronic preprint), that it is not under consideration for publication elsewhere, that publication is approved by all authors and tacitly or explicitly by the responsible authorities where the work was carried out, and that, if accepted, it will not be published elsewhere in the same form, in English or in any other language.

To prevent cases of ghostwriting and guest authorship, the author/authors of manuscripts is/are obliged to: (i) disclose the input of each author to the text (specifying their affiliations and contributions, i.e. who is the author of the concept, assumptions, methods, protocol, etc. used during the preparation of the text); (ii) disclose information about the funding sources for the article, the contribution of research institutions, associations and other entities.

### **Language**

Authors should prepare the full manuscript i.e. title, abstract and the main text in English (American or British usage is accepted). Polish version of the manuscript is not required.

### **The file type**

Text should be prepared in a word processor and saved in doc or docx file (MS Office).

### **Article structure**

Suggested structure of the manuscript is as follows:

- Title
- Authors and affiliations
- Corresponding author
- Abstract
- Keywords
- Introduction
- Material and Methods
- Results and Discussion
- Conclusions

Acknowledgements (optional)  
References  
Tables  
Figures

### **Subdivision – numbered sections**

Text should be organized into clearly defined and numbered sections and subsections (optionally). Sections and subsections should be numbered as 1. 2. 3. then 1.1 1.2 1.3 (then 1.1.1, 1.1.2, ...). The abstract should not be included in numbering section. A brief heading may be given to any subsection. Each heading should appear on its own separate line. A single line should separate paragraphs. Indentation should be used in each paragraph.

Font guidelines are as follows:

- Title: 14 pt. Times New Roman, bold, centered, with caps
- Author names and affiliations: 12 pt. Times New Roman, bold, centered, italic, two blank line above
- Abstract: 10 pt. Times New Roman, full justified, one and a half space. Abstract should begin with the word Abstract immediately following the title block with one blank line in between. The word Abstract: 10 pt. Times New Roman, centered, indentation should be used
- Section Headings: Not numbered, 12 pt. Times New Roman, bold, centered; one blank line above
- Section Sub-headings: Numbered, 12 pt. Times New Roman, bold, italic, centered; one blank line above
- Regular text: 12 pt. Times New Roman, one and a half space, full justified, indentation should be used in each paragraph

### **Title page information**

The following information should be placed at the first page:

#### **Title**

Concise and informative. If possible, authors should not use abbreviations and formulae.

#### **Authors and affiliations**

Author/authors' names should be presented below the title. The authors' affiliation addresses (department or college; university or company; city, state and zip code, country) should be placed below the names. Authors with the same affiliation must be grouped together on the same line with affiliation information following in a single block. Authors should indicate all affiliations with a lower-case superscript letter immediately after the author's name and in front of the appropriate address.

#### **Corresponding author**

It should be clearly indicated who will handle correspondence at all stages of refereeing and publication, also post-publication process. The e-mail address should be provided (footer, first page). Contact details must be kept up to date by the corresponding author.

#### **Abstract**

The abstract should have up to 100-150 words in length. A concise abstract is required. The abstract should state briefly the aim of the research, the principal results and major conclusions. Abstract must be able to stand alone. Only abbreviations firmly established in the field may be eligible. Non-standard or uncommon abbreviations should be avoided, but if essential they must be defined at their first mention in the abstract itself.

## **Keywords**

Immediately after the abstract, author/authors should provide a maximum of 6 keywords avoiding general, plural terms and multiple concepts (avoid, for example, 'and', 'of'). Author/authors should be sparing with abbreviations: only abbreviations firmly established in the field may be eligible.

## **Abbreviations**

Author/authors should define abbreviations that are not standard in this field. Abbreviations must be defined at their first mention there. Author/authors should ensure consistency of abbreviations throughout the article.

## **Units**

All units used in the paper should be consistent with the SI system of measurement. If other units are mentioned, author/authors should give their equivalent in SI.

## **Introduction**

Literature sources should be appropriately selected and cited. A literature review should discuss published information in a particular subject area. Introduction should identify, describe and analyze related research that has already been done and summarize the state of art in the topic area. Author/authors should state clearly the objectives of the work and provide an adequate background.

## **Material and Methods**

Author/authors should provide sufficient details to allow the work to be reproduced by other researchers. Methods already published should be indicated by a reference. A theory should extend, not repeat, the background to the article already dealt within the Introduction and lay the foundation for further work. Calculations should represent a practical development from a theoretical basis.

## **Results and Discussion**

Results should be clear and concise. Discussion should explore the significance of the results of the work, not repeat them. A combined Results and Discussion section is often appropriate.

## **Conclusions**

The main conclusions of the study may be presented in a Conclusions section, which may stand alone or form a subsection of a Results and Discussion section.

## **Acknowledgements**

Author/authors should include acknowledgements in a separate section at the end of the manuscript before the references. Author/authors should not include them on the title page, as a footnote to the title or otherwise. Individuals who provided help during the research study should be listed in this section.

## **Artwork**

### **General points**

- Make sure you use uniform lettering and sizing of your original artwork
- Embed the used fonts if the application provides that option
- Aim to use the following fonts in your illustrations: Arial, Courier, Times New Roman, Symbol
- Number equations, tables and figures according to their sequence in the text
- Size the illustrations close to the desired dimensions of the printed version

## **Formats**

If your electronic artwork is created in a Microsoft Office application (Word, PowerPoint, Excel) then please supply 'as is' in the native document format

Regardless of the application used other than Microsoft Office, when your electronic artwork is finalized, please 'Save as' or convert the images to one of the following formats (note the resolution requirements given below):

EPS (or PDF): Vector drawings, embed all used fonts

JPEG: Color or grayscale photographs (halftones), keep to a minimum of 300 dpi

JPEG: Bitmapped (pure black & white pixels) line drawings, keep to a minimum of 1000 dpi or combinations bitmapped line/half-tone (color or grayscale), keep to a minimum of 500 dpi

### **Please do not:**

- Supply files that are optimized for screen use (e.g., GIF, BMP, PICT, WPG); these typically have a low number of pixels and limited set of colors
- Supply files that are too low in resolution
- Submit graphics that are disproportionately large for the content

## **Color artwork**

Author/authors should make sure that artwork files are in an acceptable format (JPEG, EPS PDF, or MS Office files) and with the correct resolution. If, together with manuscript, author/authors submit color figures then Technical Sciences will ensure that these figures will appear in color on the web as well as in the printed version at no additional charge.

## **Tables, figures, and equations**

Tables, figures, and equations/formulae should be identified and numbered consecutively in accordance with their appearance in the text.

Equations/mathematical and physical formulae should be presented in the main text, while tables and figures should be presented at the end of file (after References section). Mathematical and physical formulae should be presented in the MS Word formula editor.

All types of figures can be black/white or color. Author/authors should ensure that each figure is numbered and has a caption. A caption should be placed below the figure. Figure must be able to stand alone (explanation of all symbols and abbreviations used in figure is required). Units must be always included. It is noted that figure and table numbering should be independent.

Tables should be numbered consecutively in accordance with their appearance in the text. Table caption should be placed above the table. Footnotes to tables should be placed below the table body and indicated with superscript lowercase letters. Vertical rules should be avoided. Author/authors should ensure that the data presented in tables do not duplicate results described in figures, diagrams, schemes, etc. Table must be able to stand alone (explanation of all symbols and abbreviations used in table is required). Units must be always included. As above, figure and table numbering should be independent.

## **References**

References: All publications cited in the text should be presented in a list of references following the text of the manuscript. The manuscript should be carefully checked to ensure that the spelling of authors' names and dates of publications are exactly the same in the text as in the reference list. Authors should ensure that each reference cited in the text is also present in the reference list (and vice versa).

Citations may be made directly (or parenthetically). All citations in the text should refer to:

1. Single author

The author's name (without initials, with caps, unless there is ambiguity) and the year of publication should appear in the text

2. Two authors

Both authors' names (without initials, with caps) and the year of publication should appear in the text

3. Three or more authors

First author's name followed by et al. and the year of publication should appear in the text

Groups of references should be listed first alphabetically, then chronologically.

*Examples:*

"... have been reported recently (ALLAN, 1996a, 1996b, 1999; ALLAN and JONES, 1995). KRAMER et al. (2000) have recently shown..."

The list of references should be arranged alphabetically by authors' names, then further sorted chronologically if necessary. More than once reference from the same author(s) in the same year must be identified by the letters "a", "b", "c" etc., placed after the year of publication.

References should be given in the following form:

KUMBHAR B.K., AGARVAL R.S., DAS K. 1981. Thermal properties of fresh and frozen fish. *International Journal of Refrigeration*, 4(3), 143–146.

MACHADO M.F., OLIVEIRA F.A.R., GEKAS V. 1997. Modelling water uptake and soluble solids losses by puffed breakfast cereal immersed in water or milk. In *Proceedings of the Seventh International Congress on Engineering and Food*, Brighton, UK.

NETER J., KUTNER M.H., NACHTSCHEIM C.J., WASSERMAN W. 1966. *Applied linear statistical models* (4th ed., pp. 1289–1293). Irwin, Chicago.

THOMSON F.M. 1984. Storage of particulate solids. In M. E. Fayed, L. Otten (Eds.), *Handbook of Powder Science and Technology* (pp. 365–463). Van Nostrand Reinhold, New York.

Citation of a reference as 'in press' implies that the item has been accepted for publication.

Note that the full names of Journals should appear in reference list.

### **Submission checklist**

The following list will be useful during the final checking of an article prior to the submission. Before sending the manuscript to the Journal for review, author/authors should ensure that the following items are present:

- Text is prepared with a word processor and saved in DOC or DOCX file (MS Office).
- One author has been designated as the corresponding author with contact details: e-mail address
- Manuscript has been 'spell-checked' and 'grammar-checked'
- References are in the correct format for this Journal
- All references mentioned in the Reference list are cited in the text, and vice versa
- Author/authors does/do not supply files that are too low in resolution
- Author/authors does/do not submit graphics that are disproportionately large for the content